# Nonlinear Dynamics and Systems Theory

## An International Journal of Research and Surveys

**InforMath Publishing Group**
**http://www.e-ndst.kiev.ua**

---

NONLINEAR DYNAMICS AND SYSTEMS THEORY

An International Journal of Research and Surveys

Volume 21          Number 5          2021

## CONTENTS

NONLINEAR DYNAMICS & SYSTEMS THEORY

Volume 21,  No. 5,  2021

## INSTRUCTIONS FOR CONTRIBUTORS

**(1) General.** Nonlinear Dynamics and Systems Theory (ND&ST) is an international journal devoted to publishing peer-refereed, high quality, original papers, brief notes and review articles focusing on nonlinear dynamics and systems theory and their practical applications in engineering, physical and life sciences. Submission of a manuscript is a representation that the submission has been approved by all of the authors and by the institution where the work was carried out. It also represents that the manuscript has not been previously published, has not been copyrighted, is not being submitted for publication elsewhere, and that the authors have agreed that the copyright in the article shall be assigned exclusively to InforMath Publishing Group by signing a transfer of copyright form. Before submission, the authors should visit the website:

**http://www.e-ndst.kiev.ua**

for information on the preparation of accepted manuscripts. Please download the archive Sample_NDST.zip  containing example of article file (you can edit only the file Samplefilename.tex).

**(2) Manuscript and Correspondence.** Manuscripts should be in English and must meet common standards of usage and grammar. To submit a paper, send by e-mail a file in PDF format directly to

*Professor A.A. Martynyuk,* Institute of Mechanics,
Nesterov str.3, 03057, MSP 680, Kiev-57, Ukraine
e-mail:  journalndst@gmail.com

or to one of the Regional Editors or to a member of the Editorial Board. Final version of the manuscript must typeset using LaTex program which is prepared in accordance with the style file of the Journal. Manuscript texts should contain the title of the article, name(s) of the author(s) and complete affiliations. Each article requires an abstract not exceeding 150 words. Formulas and citations should not be included in the abstract. AMS subject classifications and key words must be included in all accepted papers. Each article requires a running head (abbreviated form of the title) of no more than 30 characters. The sizes for regular papers, survey articles, brief notes, letters to editors and book reviews are: (i) 10-14 pages for regular papers, (ii) up to 24 pages for survey articles, and (iii) 2-3 pages for brief notes, letters to the editor and book reviews.

**(3)  Tables, Graphs and Illustrations.** Each figure must be of a quality suitable for direct reproduction and must include a caption. Drawings should include all relevant details and should be drawn professionally in black ink on plain white drawing paper. In addition to a hard copy of the artwork, it is necessary to attach the electronic file of the artwork (preferably in PCX format).

**(4)  References.** Each entry must be cited in the text by author(s) and number or by number alone. All references should be listed in their alphabetic order. Use please the following style:

Journal: [1] H. Poincare, Title of the article. *Title of the Journal* **volume**
(issue) (year) pages. [Language]

Book: [2] A.M. Lyapunov, *Title of the Book.* Name of the Publishers, Town, year.

Proceeding: [3] R. Bellman, Title of the article. In: *Title of the Book.* (Eds.).
Name of the Publishers, Town, year, pages. [Language]

**(5)  Proofs and Sample Copy.** Proofs sent to authors should be returned to the Editorial Office with corrections within three days after receipt. The corresponding author will receive a sample copy of the issue of the Journal for which his/her paper is published.

**(6)  Editorial Policy.** Every submission will undergo a stringent peer review process. An editor will be assigned to handle the review process of the paper. He/she will secure at least two reviewers' reports. The decision on acceptance, rejection or acceptance subject to revision will be made based on these reviewers' reports and the editor's own reading of the paper.

## CONTENTS

# NONLINEAR DYNAMICS AND SYSTEMS THEORY

## An International Journal of Research and Surveys

**Nonlinear Dynamics and Systems Theory** (ISSN 1562–8353 (Print), ISSN 1813–7385 (Online)) is an international journal published under the auspices of the S.P. Timoshenko Institute of Mechanics of National Academy of Sciences of Ukraine and Curtin University of Technology (Perth, Australia). It aims to publish high quality original scientific papers and surveys in areas of nonlinear dynamics and systems theory and their real world applications.

## AIMS AND SCOPE

**Nonlinear Dynamics and Systems Theory** is a multidisciplinary journal. It publishes papers focusing on proofs of important theorems as well as papers presenting new ideas and new theory, conjectures, numerical algorithms and physical experiments in areas related to nonlinear dynamics and systems theory. Papers that deal with theoretical aspects of nonlinear dynamics and/or systems theory should contain significant mathematical results with an indication of their possible applications. Papers that emphasize applications should contain new mathematical models of real world phenomena and/or description of engineering problems. They should include rigorous analysis of data used and results obtained. Papers that integrate and interrelate ideas and methods of nonlinear dynamics and systems theory will be particularly welcomed. This journal and the individual contributions published therein are protected under the copyright by International InforMath Publishing Group.

## PUBLICATION AND SUBSCRIPTION INFORMATION

**Nonlinear Dynamics and Systems Theory** will have 5 issues in 2022, printed in hard copy (ISSN 1562–8353) and available online (ISSN 1813–7385), by InforMath Publishing Group, Nesterov str., 3, Institute of Mechanics, Kiev, MSP 680, Ukraine, 03057. Subscription prices are available upon request from the Publisher, EBSCO Information Services (`mailto:journals@ebsco.com`), or website of the Journal: `http://e-ndst.kiev.ua`. Subscriptions are accepted on a calendar year basis. Issues are sent by airmail to all countries of the world. Claims for missing issues should be made within six months of the date of dispatch.

## ABSTRACTING AND INDEXING SERVICES

Papers published in this journal are indexed or abstracted in: Mathematical Reviews / MathSciNet, Zentralblatt MATH / Mathematics Abstracts, PASCAL database (INIST–CNRS) and SCOPUS.

# Delay-Independent Stability Conditions
# for a Class of Nonlinear Mechanical Systems

A. Yu. Aleksandrov *

*Saint Petersburg State University, 7–9 Universitetskaya Nab., St. Petersburg, 199034, Russia*

**Abstract:** A mechanical system with linear gyroscopic forces and nonlinear homogeneous dissipative and positional forces is studied. The case is considered where there is a time-varying delay in positional forces. With the aid of the decomposition method and the Razumikhin approach, conditions are obtained ensuring that the trivial equilibrium position of the system under investigation is asymptotically stable for any nonnegative, continuous and bounded delay. Estimates for the convergence rate of motions are derived. The developed approach is used in a problem of stabilization of mechanical systems via controls with delay in a feedback law. An example is given to demonstrate the effectiveness of the obtained results.

**Keywords:** *mechanical system; nonlinear forces; stability; time-varying delay; decomposition; stabilization.*

**Mathematics Subject Classification (2010):** 34K20, 93D30.

## 1 Introduction

Systems of high-dimensional second-order differential equations are widely used as mathematical models of gyroscopic devices [1–3]. An effective approach to the analysis of stability and other dynamic properties of such models consists of the decomposition of the complete system into first-order precession and nutation subsystems.

The justification of the correctness of such a decomposition for linear stationary gyroscopic systems was given in [1, 2] by the Lyapunov first method via the expansion of the roots of the characteristic equations in series with respect to negative powers of a large parameter. It was proved that, for sufficiently large values of the parameter, the asymptotic stability of the isolated nutation and precession subsystems implies the same property for the complete system.

---

* Corresponding author: `mailto:a.u.aleksandrov@spbu.ru`

Another approach to the justification of decomposition of gyroscopic systems into precession and nutation subsystems was proposed in [4]. This approach is based on the Lyapunov direct method. Therefore, its application turned out to be effective not only for linear time-invariant systems, but also for some classes of nonlinear and time-varying systems (see [5–9]).

In particular, in [7], it was used for the stability analysis of mechanical systems with linear gyroscopic forces and nonlinear homogeneous dissipative and positional forces. A special form of decomposition was constructed and new conditions of the asymptotic stability of equilibrium positions were found.

In the present paper, we will consider the same class of nonlinear mechanical systems as in [7] under the additional assumption that there is a time-varying delay in positional forces. Our objective is to study the impact of delay on the stability of equilibrium positions. It is well known (see, for instance, [10–12]) that an introduction of a delay might destroy stability. With the aid of the decomposition method and a special technique for the application of the Razumikhin theorem to nonlinear time-delay systems developed in [13, 14], we will obtain conditions providing the asymptotic stability of equilibrium positions for any nonnegative, continuous and bounded delay. In addition, we will derive estimates for the convergence rate of motions. Moreover, we will show that the obtained results can be effectively used for the stabilization of mechanical systems via controls with delay in a feedback law.

## 2   Background and Problem Formulation

In this paper, $\mathbb{R}$ denotes the field of real numbers, $\mathbb{R}^n$ is the $n$-dimensional Euclidean space with the associated norm $\|\cdot\|$ of a vector, the notation $\mathbb{R}^{n\times n}$ is used for the vector space of $n \times n$ matrices.

**Definition 2.1** (see [15, 16]) A function $f(x) : \mathbb{R}^n \mapsto \mathbb{R}$ is called homogeneous of the order $\lambda \in \mathbb{R}$ if $f(cx) = c^\lambda f(x)$ for any $c > 0$ and $x \in \mathbb{R}^n$.

**Remark 2.1** In the present contribution, the homogeneity with respect to the standard dilation is considered [16, 17].

Let motions of a mechanical system be modeled by the equations

$$A\ddot{q}(t) + (B(\dot{q}(t)) + G)\dot{q}(t) + Q(q(t)) = 0. \tag{1}$$

Here $q(t), \dot{q}(t) \in \mathbb{R}^n$ are the vectors of generalized coordinates and velocities, respectively, $A, G \in \mathbb{R}^{n\times n}$ are constant matrices, the entries of the matrix $B(\dot{q}) \in \mathbb{R}^{n\times n}$ are continuous for $\dot{q} \in \mathbb{R}^n$ homogeneous functions of the order $\nu > 0$, the components of the vector $Q(q) \in \mathbb{R}^n$ are continuously differentiable for $q \in \mathbb{R}^n$ homogeneous functions of the order $\mu > 1$.

The system (1) has the trivial equilibrium position

$$q = \dot{q} = 0. \tag{2}$$

Stability of this equilibrium position was studied in [7] with the aid of the decomposition method. The auxiliary isolated subsystems

$$G\dot{y}(t) = -Q(y(t)), \tag{3}$$

$$A\dot{z}(t) = -(B(z(t)) + G)z(t) \tag{4}$$

were constructed, and the following constraints were imposed on the equations under consideration.

**Assumption 2.1** The inequality $\mu > \nu + 1$ holds.

**Assumption 2.2** The matrix $A$ is symmetric and positive definite, while the matrix $G$ is skew-symmetric and nonsingular.

**Assumption 2.3** The function $\dot{q}^\top B(\dot{q})\dot{q}$ is positive definite.

**Assumption 2.4** There exists a continuously differentiable homogeneous of the order $\nu + 1$ vector function $w(z) \in \mathbb{R}^n$ such that

$$\frac{\partial w(z)}{\partial z} A^{-1} G z = B(z)z$$

for $z \in \mathbb{R}^n$.

**Assumption 2.5** The zero solution of the subsystem (3) is asymptotically stable.

**Remark 2.2** Assumptions 2.2 and 2.3 imply that the system (1) is under the action of linear gyroscopic forces $-G\dot{q}$, nonlinear homogeneous dissipative forces $-B(\dot{q})\dot{q}$ and nonlinear homogeneous positional forces $-Q(q)$.

Let us note that nonlinear homogeneous forces are widely used in mathematical models of mechanical systems (see, e.g., [18–23]). Such forces can be related to both physical configurations and purely nonlinear material properties. Moreover, nonlinear homogeneous functions provide smooth approximations of non-smooth forces [24].

**Remark 2.3** From the conditions imposed on the matrix $G$, it follows that $n$ should be an even number.

**Remark 2.4** A criterion for the fulfilment of Assumption 2.4 was obtained in [7].

In [7], it was proved that, under Assumptions 2.1–2.5, the equilibrium position (2) of the system (1) is asymptotically stable.

**Remark 2.5** It is known [7] that Assumption 2.1 cannot be relaxed.

The objective of this paper is to study the impact of delay in positional forces on the stability of the equilibrium position. We consider the system

$$A\ddot{q}(t) + (B(\dot{q}(t)) + G)\dot{q}(t) + Q(q(t)) + D(q(t - \tau(t)) = 0, \tag{5}$$

where the components of the vector $D(q) \in \mathbb{R}^n$ are continuously differentiable for $q \in \mathbb{R}^n$ homogeneous functions of the order $\mu$, $\tau(t)$ is a nonnegative, continuous and bounded for $t \geq 0$ delay, and the remaining notation is the same as for (1).

For a given delay $\tau(t)$, denote $h = \sup_{t \geq 0} \tau(t)$. Let the initial functions for the solutions of (5) belong to the space $C^1([-h, 0], \mathbb{R}^n)$ of continuously differentiable functions $\varphi(\theta) : [-h, 0] \mapsto \mathbb{R}^n$ with the uniform norm

$$\|\varphi\|_h = \max_{\theta \in [-h, 0]} (\|\varphi(\theta)\| + \|\dot{\varphi}(\theta)\|).$$

We will look for conditions ensuring the delay-independent asymptotic stability of the equilibrium position (2) of the system (5).

## 3   Stability Analysis

Instead of (3), construct a new isolated subsystem in the form

$$G\dot{y}(t) = -Q(y(t)) - D(y(t)). \tag{6}$$

**Assumption 3.1** The zero solution of the subsystem (6) is asymptotically stable.

**Theorem 3.1** *Let Assumptions 2.1–2.4 and 3.1 be fulfilled. Then the equilibrium position (2) of the system (5) is asymptotically stable for any nonnegative, continuous and bounded for $t \geq 0$ delay $\tau(t)$.*

***Proof.*** Define new variables by the formulae

$$z(t) = \dot{q}(t), \quad Gy(t) + w(z(t)) = A\dot{q}(t) + Gq(t),$$

where the vector function $w(z)$ satisfies the conditions of Assumption 2.4.

We obtain the system

$$
\begin{aligned}
G\dot{y}(t) = & -Q(y(t)) - D(y(t)) + \Big(Q(y(t)) - Q\big(y(t) - G^{-1}Az(t) + G^{-1}w(z(t))\big)\Big) \\
& + \Big(D(y(t)) - D\big(y(t-\tau(t)) - G^{-1}Az(t-\tau(t)) + G^{-1}w(z(t-\tau(t)))\big)\Big) \\
& + \frac{\partial w(z(t))}{\partial z}A^{-1}\Big(B(z(t))z(t) + Q\big(y(t) - G^{-1}Az(t) + G^{-1}w(z(t))\big)\Big) \\
& + \frac{\partial w(z(t))}{\partial z}A^{-1}D\big(y(t-\tau(t)) - G^{-1}Az(t-\tau(t)) + G^{-1}w(z(t-\tau(t)))\big),
\end{aligned}
\tag{7}
$$

$$
\begin{aligned}
A\dot{z}(t) = & -(B(z(t)) + G)z(t) - Q\big(y(t) - G^{-1}Az(t) + G^{-1}w(z(t))\big) \\
& - D\big(y(t-\tau(t)) - G^{-1}Az(t-\tau(t)) + G^{-1}w(z(t-\tau(t)))\big).
\end{aligned}
$$

For a solution $(y^\top(t), z^\top(t))^\top$ of (7), denote by $(y_t^\top, z_t^\top)^\top$ the restriction of the solution to the segment $[t-h, t]$, i.e., $(y_t^\top, z_t^\top)^\top : \theta \mapsto (y^\top(t+\theta), z^\top(t+\theta))^\top$, $\theta \in [-h, 0]$. Let

$$\|(y_t^\top, z_t^\top)^\top\|_h = \max_{\theta \in [-h, 0]} \|(y^\top(t+\theta), z^\top(t+\theta))^\top\|.$$

The system (6) is homogeneous. Therefore, from Assumption 3.1 it follows (see [15,16]) that, for any number $\gamma_1 > \mu$, there exists a continuously differentiable for $y \in \mathbb{R}^n$ homogeneous of the order $\gamma_1 - \mu + 1$ Lyapunov function $V_1(y)$ such that the inequalities

$$a_1\|y\|^{\gamma_1 - \mu + 1} \leq V_1(y) \leq a_2\|y\|^{\gamma_1 - \mu + 1}, \tag{8}$$

$$\left\|\frac{\partial V_1(y)}{\partial y}\right\| \leq a_3\|y\|^{\gamma_1 - \mu}, \quad \dot{V}_1\big|_{(6)} \leq -a_4\|y\|^{\gamma_1}$$

are valid for $y \in \mathbb{R}^n$. Here $a_i > 0$, $i = 1, 2, 3, 4$.

Furthermore, it should be noted that the zero solution of (4) is asymptotically stable, and a Lyapunov function for this subsystem can be chosen as follows:

$$V_2(z) = \left(z^\top Az\right)^{(\gamma_2 - \nu)/2},$$

where $\gamma_2 > \nu + 1$.

Next, construct the function

$$V(y, z) = V_1(y) + \eta V_2(z), \tag{9}$$

where $\eta$ is a positive parameter. The function (9) is positive definite and satisfies the estimates

$$a_1 \|y\|^{\gamma_1 - \mu + 1} + \eta a_5 \|z\|^{\gamma_2 - \nu} \le V(y, z) \le a_2 \|y\|^{\gamma_1 - \mu + 1} + \eta a_6 \|z\|^{\gamma_2 - \nu}$$

for $y, z \in \mathbb{R}^n$, where $a_5, a_6$ are positive coefficients.

Consider its derivative along the solutions of (7). We obtain that there exists a number $\delta > 0$ such that

$$\dot{V}\big|_{(7)} \le -a_4 \|y(t)\|^{\gamma_1} - \eta b_1 \|z(t)\|^{\gamma_2}$$

$$+ b_2 \Big( \eta \|y(t)\|^{\mu} \|z(t)\|^{\gamma_2 - \nu - 1} + \|y(t)\|^{\gamma_1 - 1} \|z(t)\|$$

$$+ \|y(t)\|^{\gamma_1 - \mu} \|z(t)\|^{\mu} + \|y(t)\|^{\gamma_1 - \mu} \|z(t)\|^{2\nu + 1} \Big)$$

$$+ b_3 \left( \|y(t)\|^{\gamma_1 - \mu} + \eta \|z(t)\|^{\gamma_2 - \nu - 1} \right) \Big\| D \left( y(t) - G^{-1} A z(t) + G^{-1} w(z(t)) \right)$$

$$- D \left( y(t - \tau(t)) - G^{-1} A z(t - \tau(t)) + G^{-1} w(z(t - \tau(t))) \right) \Big\|$$

for $\|(y_t^\top, z_t^\top)^\top\|_h < \delta$. Here $b_1, b_2, b_3$ are positive constants.

With the aid of the Young inequality, it can be verified that if $\delta$ and $\eta$ are sufficiently small and

$$\max\left\{ 1; \frac{\mu}{2\nu + 1} \right\} < \frac{\gamma_1}{\gamma_2} \le \frac{\mu}{\nu + 1},$$

then

$$\dot{V}\big|_{(7)} \le -\frac{1}{2} a_4 \|y(t)\|^{\gamma_1} - \frac{1}{2} \eta b_1 \|z(t)\|^{\gamma_2}$$

$$+ b_3 \left( \|y(t)\|^{\gamma_1 - \mu} + \eta \|z(t)\|^{\gamma_2 - \nu - 1} \right) \Big\| D \left( y(t) - G^{-1} A z(t) + G^{-1} w(z(t)) \right)$$

$$- D \left( y(t - \tau(t)) - G^{-1} A z(t - \tau(t)) + G^{-1} w(z(t - \tau(t))) \right) \Big\|$$

for $\|(y_t^\top, z_t^\top)^\top\|_h < \delta$.

Assume that the following conditions are fulfilled for a solution $(y^\top(t), z^\top(t))^\top$ of (7):
(i) $\|(y_t^\top, z_t^\top)^\top\|_h < \delta$,
(ii) $V(y(\theta), z(\theta)) \le 2V(y(t), z(t))$ for $\theta \in [t - h, t]$.
Using (ii) and the estimates (8), we arrive at the inequalities

$$\|y(\theta)\| \le c_1 \left( \|y(t)\| + \|z(t)\|^{\frac{\gamma_2 - \nu}{\gamma_1 - \mu + 1}} \right), \tag{10}$$

$$\|z(\theta)\| \le c_2 \left( \|y(t)\|^{\frac{\gamma_1 - \mu + 1}{\gamma_2 - \nu}} + \|z(t)\| \right) \tag{11}$$

for $\theta \in [t - h, t]$, where $c_1$ and $c_2$ are positive constants.

Let $\gamma_1 = \gamma_2 \mu / (\nu + 1)$. Then $\gamma_1 - \mu + 1 > \gamma_2 - \nu$. With the aid of (10), (11) and the mean value theorem, it can be shown (see [13, 14]) that

$$\left\| D\left(y(t) - G^{-1}Az(t) + G^{-1}w(z(t))\right) \right.$$

$$\left. -D\left(y(t - \tau(t)) - G^{-1}Az(t - \tau(t)) + G^{-1}w(z(t - \tau(t)))\right) \right\|$$

$$\leq \tilde{c}\left(\|y(t)\|^{\gamma_1 - \mu + 1} + \|z(t)\|^{\gamma_2 - \nu}\right)^{\frac{\mu - 1}{\gamma_1 - \mu + 1} + \frac{1}{\gamma_2 - \nu}},$$

where $\tilde{c} = \mathrm{const} > 0$.

Applying the Young inequality once again, we obtain that, for an appropriate choice of $\delta$, the estimate

$$\dot{V}\Big|_{(7)} \leq -\frac{1}{3}a_4\|y(t)\|^{\gamma_1} - \frac{1}{3}\eta b_1\|z(t)\|^{\gamma_2} \tag{12}$$

holds. Hence the Lyapunov function (9) satisfies the conditions of the Razumikhin theorem (see [10]). Therefore, the zero solution of (7) is asymptotically stable for any nonnegative, continuous and bounded delay. From the relationship between the variables $y(t), z(t)$ and $q(t), \dot{q}(t)$, it follows that the equilibrium position (2) of the system (5) possesses the same property.

## 4   Estimates of Motions

In this section, we will show that, with the aid of the Lyapunov function (9) and the differential inequalities method (see [25,26]), estimates for the convergence rate of motions of (5) to the equilibrium position (2) can be derived.

Let Assumptions 2.1–2.4 and 3.1 be fulfilled. Consider the function (9) with $\gamma_1 = \gamma_2 \mu / (\nu + 1)$. According to the proof of Theorem 3.1, for an appropriate choice of $\eta$ and $\delta$, the fulfilment of (i) and (ii) implies that (12) holds.

Using inequalities (8) and (12), we obtain

$$\dot{V}\Big|_{(7)} \leq -dV^{\frac{\gamma_1}{\gamma_1 - \mu + 1}}(y(t), z(t)),$$

where $d = \mathrm{const} > 0$.

Applying the approach developed in [14], one can verify the existence of positive numbers $\Delta, \alpha_1, \alpha_2$ such that if the initial conditions of a solution $(y^\top(t), z^\top(t))^\top$ of (7) satisfy the inequalities $t_0 \geq 0$, $\|(y_{t_0}^\top, z_{t_0}^\top)^\top\|_h < \Delta$, then

$$\|y(t)\| \leq \alpha_1(t - t_0 + 1)^{-\frac{1}{\mu - 1}},$$

$$\|z(t)\| \leq \alpha_2(t - t_0 + 1)^{-\omega} \tag{13}$$

for $t \geq t_0$, where

$$\omega = \frac{1}{(\mu - 1)(\nu + 1)}\left(\mu - \frac{\mu - \nu - 1}{\gamma_2 - \nu}\right). \tag{14}$$

It is worth noting that, to obtain more precise estimate (13) in the sense of minimization of the exponent, one should pass to the limit in (14) as $\gamma_2 \to \infty$.

Taking into account the relationship between the variables $y(t), z(t)$ and $q(t), \dot{q}(t)$, we arrive at the following theorem.

**Theorem 4.1** *Let Assumptions 2.1–2.4 and 3.1 be fulfilled. Then, for any $\rho \in (0, 1)$ and any nonnegative, continuous and bounded for $t \geq 0$ delay $\tau(t)$, there exist positive numbers $\tilde{\Delta}, \beta_1, \beta_2$ such that if for a solution $q(t)$ of (5) the inequalities $t_0 \geq 0$, $\|q_{t_0}\|_h < \tilde{\Delta}$ hold, then*

$$\|q(t)\| \leq \beta_1 (t - t_0 + 1)^{-\frac{1}{\mu-1}}, \qquad \|\dot{q}(t)\| \leq \beta_2 (t - t_0 + 1)^{-\frac{\rho\mu}{(\mu-1)(\nu+1)}}$$

*for $t \geq t_0$.*

## 5  Control Synthesis

Let the system (1) be of the form

$$A\ddot{q}(t) + (B(\dot{q}(t)) + G)\dot{q}(t) + \frac{\partial \Pi(q(t))}{\partial q} = 0. \tag{15}$$

Here $\Pi(q)$ is a twice continuously differentiable for $q \in \mathbb{R}^n$ homogeneous of the order $\mu + 1$ function. Thus, the positional forces in (15) are potential.

We will suppose that the potential energy $\Pi(q)$ is a negative definite function. Then, under Assumptions 2.2, 2.3, the equilibrium position (2) of (15) is unstable (see [2, 26]).

Next, consider the corresponding control system

$$A\ddot{q}(t) + (B(\dot{q}(t)) + G)\dot{q}(t) + \frac{\partial \Pi(q(t))}{\partial q} = U, \tag{16}$$

where $U$ is a control vector. Our objective is to design a feedback control law stabilizing the equilibrium position under the constraint that there exists a delay in the control scheme.

Let

$$U = -\varepsilon \|q(t - \tau(t))\|^{\mu-1} G q(t - \tau(t)). \tag{17}$$

Here $\varepsilon$ is a positive parameter.

**Theorem 5.1** *If Assumptions 2.1–2.4 are fulfilled, then the equilibrium position (2) of the system (16) closed by the control (17) is asymptotically stable for any $\varepsilon > 0$ and any continuous, nonnegative and bounded for $t \geq 0$ delay.*

**Proof.** To prove the theorem, it is sufficient to show the fulfilment of Assumption 3.1.

The corresponding subsystem (6) takes the form

$$\dot{y}(t) = -G^{-1}\frac{\partial \Pi(y(t))}{\partial y} - \varepsilon \|y(t)\|^{\mu-1} y(t). \tag{18}$$

Consider the Lyapunov function

$$V_1(y) = -\Pi(y). \tag{19}$$

This function is positive definite. Differentiating (19) along the solutions of (18), we obtain

$$\dot{V}_1\big|_{(18)} = \varepsilon(\mu + 1)\|y(t)\|^{\mu-1}\Pi(y(t)) \leq -\tilde{a}\varepsilon\|y(t)\|^{2\mu},$$

where $\tilde{a}$ is a positive constant. Thus, the zero solution of (18) is asymptotically stable.

The application of Theorem 3.1 completes the proof.

**Remark 5.1** Theorem 5.1 guarantees the asymptotic stability of the equilibrium position for any value of parameter $\varepsilon$. Hence, the control forces (17) may be arbitrary small compared with the destabilizing potential forces.

## 6 Example

Consider the control system

$$\ddot{q}(t) + b\|\dot{q}(t)\|^{\nu}\dot{q}(t) + G\dot{q}(t) - \|q(t)\|^2 q(t) = U, \tag{20}$$

where $n = 2$, $q(t) = (q_1(t), q_2(t))^{\top}$,

$$G = \begin{pmatrix} 0 & g \\ -g & 0 \end{pmatrix},$$

$b, g$ and $\nu$ are positive parameters, $U = (u_1, u_2)^{\top}$ is a control vector.

It should be noted that from the results of [7] it follows that Assumption 2.4 is fulfilled for the system (20), and the vector function $w(z)$ can be defined by the formula

$$w(z) = b\|z\|^{\nu}G^{-1}z.$$

Applying Theorem 5.1, we obtain that, under the condition $\nu < 2$, the control law

$$U = -\varepsilon\|q(t - \tau(t))\|^2 G q(t - \tau(t))$$

stabilizes the equilibrium position $q = \dot{q} = 0$ of (20) for any positive values of $b, g, \varepsilon$ and any continuous, nonnegative and bounded for $t \geq 0$ delay $\tau(t)$.

## 7 Conclusion

In the present paper, an approach to the decomposition of stability problem for a class of nonlinear mechanical systems is developed. Instead of the stability analysis for the original time-delay second order system (5), it is proposed to study stability for simpler delay-free first order isolated subsystems (4) and (6). It is worth noting that, unlike the classical decomposition conditions for linear gyroscopic systems [1, 2], to justify the decomposition of (5), Theorem 3.1 does not require the presence of a large parameter in the equations under study. It is shown that with the aid of the Lyapunov function constructed in the proof of the theorem, estimates of convergence rate of motions can be derived. An application of the developed approach to the control design for a mechanical system is presented. An interesting direction for further research is an extension of the obtained results to nonlinear mechanical systems with delay and switched force fields.

### Acknowledgment

## References

[1] V. I. Zubov. *Analytical Dynamics of Gyroscopic Systems.* Sudostroenie, Leningrad, 1970. [Russian]

[2] D. R. Merkin. *Gyroscopic Systems.* Moscow: Nauka, 1974. [Russian]

[3] V. M. Matrosov. *The Method of Vector Lyapunov Functions: Analysis of Dynamical Properties of Nonlinear Systems.* Moscow: Fizmatlit, 2001. [Russian]

[4] A. A. Kosov. Stability investigation of singular systems by means of the Lyapunov vector functions method. *Vestnik St. Petersburg University. Ser. 10* (4) (2005) 123–129. [Russian]

[5] A. Yu. Aleksandrov, Y. Chen, A. A. Kosov, and L. Zhang. Stability of hybrid mechanical systems with switching linear force fields. *Nonlinear Dynamics and Systems Theory* **11** (1) (2011) 53–64.

[6] A. Yu. Aleksandrov, A. A. Kosov, and Y. Chen. Stability and stabilization of mechanical systems with switching. *Autom. Remote Control* **72** (6) (2011) 1143–1154.

[7] A. Y. Aleksandrov, A. P. Zhabko, and A. A. Kosov. Analysis of stability and stabilization of nonlinear systems via decomposition. *Siberian Math. J.* **56** (6) (2015) 968–981.

[8] A. Y. Aleksandrov and E. B. Aleksandrova. Asymptotic stability conditions for a class of hybrid mechanical systems with switched nonlinear positional forces. *Nonlinear Dynamics* **83** (4) (2016) 2427–2434.

[9] A. Y. Aleksandrov. Stability analysis and synthesis of stabilizing controls for a class of nonlinear mechanical systems. *Nonlinear Dynamics* **100** (4) (2020) 3109–3119.

[10] J. K. Hale and S. M. Verduyn Lunel. *Introduction to Functional Differential Equations.* Springer, New York, 1993.

[11] H. Y. Hu and Z. H. Wang. *Dynamics of Controlled Mechanical Systems with Delayed Feedback.* Springer, Berlin, 2002.

[12] V. Yu. Slyusarchuk. Absolutely unstable differential equations with aftereffect. *Nonlinear Dynamics and Systems Theory* **20** (3) (2020) 327–332.

[13] A. Y. Aleksandrov and A. P. Zhabko. On the stability of the solutions of a class of nonlinear delay systems. *Autom. Remote Control* **67** (9) (2006) 1355–1365.

[14] A. Y. Aleksandrov and A. P. Zhabko. On the asymptotic stability of solutions of nonlinear systems with delay. *Siberian Math. J.* **53** (3) (2012) 393–403.

[15] V. I. Zubov. *Methods of A.M. Lyapunov and Their Applications.* P. Noordhoff Ltd, Groningen, 1964.

[16] L. Rosier. Homogeneous Lyapunov function for homogeneous continuous vector field. *Systems Control Lett.* **19** (1992) 467–473.

[17] A. Polyakov. *Generalized Homogeneity in Systems and Control.* Springer, Cham, 2020.

[18] I. Kovacic. Forced vibrations of oscillators with a purely nonlinear power-form restoring force. *J. Sound Vib.* **330** (2011) 4313–4327.

[19] G. M. Moatimid, F. M. F. Elsabaa, and M. H. Zekry. Approximate solutions of coupled nonlinear oscillations: Stability analysis. *J. Appl. Comput. Mech.* **7** (2) (2021) 382–395.

[20] H. M. Sedighi and F. Daneshmand. Nonlinear transversely vibrating beams by the homotopy perturbation method. *J. Appl. Comput. Mech.* **1** (1) (2015) 1–9.

[21] O. Baiz and H. Benaissa. Analysis of dynamic frictional contact problem for electro-elastic materials. *Nonlinear Dynamics and Systems Theory* **21** (2) (2021) 150–165.

[22] Md. Maqbul. Almost periodic solutions for a class of nonlinear duffing system with time-varying coefficients and stepanov-almost periodic forcing terms. *Nonlinear Dynamics and Systems Theory* **20** (5) (2020) 512–522.

[23] P. Hagedorn. On the destabilizing effect of non-linear damping in non-conservative systems with follower forces. *Int. J. Non-Linear Mechanics* **5** (1970) 341–358.

[24] I. Kovacic and M. Zukovic. Coupled purely nonlinear oscillators: normal modes and exact solutions for free and forced responses. *Nonlinear Dynamics* **87** (2017) 713–726.

[25] V. Lakshmikantham, S. Leela, and A. A. Martynyuk. *Stability Analysis of Nonlinear Systems.* Marcel Dekker, New York, 1989.

[26] N. Rouche, P. Habets, and M. Laloy. *Stability Theory by Lyapunov's Direct Method.* Springer, New York, 1977.

# Adaptive Sliding Mode Control Based on Fuzzy Systems Applied to the Permanent Magnet Synchronous Machine

S. Bentouati [1*], A. Tlemçani [2], N. Henini [3] and H. Nouri [4]

[1] *Laboratory of Mechanics, Physics, Mathematical Modeling (LMP2M), University of Medea, Medea 26000, Algeria.*
[2] *Laboratory of Research in Electrotechnics and Automation (LREA) University of Medea, 26000, Algeria.*
[3] *Laboratory of Renewable Energies and Materials (LREM), University of Medea, 26000, Algeria.*
[4] *Power Systems Electronics and Control Research Group, Department of Engineering Design and Mathematics, Bristol, U.K., BS16 1QY.*

**Abstract:** This paper develops an adaptive sliding mode control based on fuzzy systems. In this control technique, the possibilities offered by Sugeno type fuzzy systems, in terms of their ability to approximate continuous nonlinear functions, are exploited, and the Lyapunov theory is used to establish a parametric adaptation law ensuring the global stability of the system. In addition, the control law includes a sliding mode term, which has the role of compensating the effects of the reconstruction errors. This technique is applied to control a permanent magnet synchronous machine. The results obtained show the effectiveness of the proposed method.

* Corresponding author: mailto:bentouati.smain@gmail.com

## 1   Introduction

The use of classical control techniques (proportional, integral and/or derivative actions control) requires knowing the system parameters in order to set the appropriate control parameters which permit reaching the desired goal. Thus, errors and inaccuracies might well happen during the process. Moreover, the control is hard due to the existing coupling between the variables of the system (interaction between the variables to be controlled). Yet nevertheless, using the so-called robust control methods including adaptive control can help solve the problem. Recent contributions in adaptive control, both theoretical and practical, have allowed to better understand adaptive systems [1–4]. The main purpose of adaptive control is the synthesis of adaptation laws to automatically adjust regulators of the control loops in order to achieve or maintain a given level of performance, when the parameters of the process to be controlled are unknown or little known [5–9]. Indeed, a large research effort is invested in understanding the structural and functional aspects of biological systems and in particular the processes of the human brain. This led to try new ways which integrate the non-linearities and uncertainties inherent in the real system. The fuzzy systems approach seems to be practical, and studies have shown that certain classes have the quality of being universal function approximators [10–16]. This important property has opened a new way to use fuzzy systems in the field of control [1–4]. Hence, several works are oriented towards combining fuzzy systems with control techniques such as adaptive control. In these control schemes, fuzzy systems are used to approximate non-linear functions. In this paper, an adaptive control based on fuzzy systems is developed. Fuzzy systems are used to approximate the model of the system to be controlled, and in order to compensate the effects of reconstruction errors, we introduce a sliding mode term in the control law. The approximation theory and the Lyapunov theory are used to establish a parametric adaptation law ensuring the boundedness of all the signals of the system and the error of the fuzzy system parameters.

## 2   Description of The Sugeno Type Fuzzy System

The fuzzy system in its design consists of four main modules [17–20]: 1) the fuzzy rule base, or knowledge base, contains the fuzzy rules describing the behavior of the system; 2) the fuzzy inference engine transforms, with the help of fuzzy reasoning techniques, the fuzzy part resulting from the fuzzification into a new fuzzy part; 3) the fuzzification transforms the physical input quantity into a fuzzy quantity; 4) the defuzzification transforms the fuzzy quantity resulting from the inference into a physical quantity. There is a great number of possibilities of realization of fuzzy systems with a multitude of choices for each, and each combination of choices generates a class of fuzzy systems. In our work, we are interested in the Sugeno type fuzzy system, initially developed by Sugeno and Takagi for modeling of systems from numerical data [21]. In this case the consequences of the rules are numerical functions, which depend on the current values of the input variables. In this way, the defuzzification step required by other fuzzy systems is skipped. As our goal is to develop a law of adaptation of the parameters of the fuzzy system, it is therefore essential to give the analytical expression of the output of Sugeno's fuzzy system, to approximate any nonlinear function from numerical data.

Let us denote by $x_{sf_1}, \ldots, x_{sf_n}$ the inputs of Sugeno's fuzzy system, and by $y_{sf}$ its output. For each variable $x_{sf_i}$ is associated $m_i$ fuzzy sets $F_i^j$ in universe of discourse $U_i$ such that for any $x_{sf_i}$ in $U_i$, there exists at least one degree of membership. $\mu_{F_i^j}(x_{sf_i}) \neq 0$,

where $i = 1, 2, ..., n$ and $j = 1, 2, ..., m_i$. The rule base of the fuzzy system includes $M = \prod_{i=1}^{n} m_i$ rules such as

$$R_l : if \ x_{sf_1} \ isF_1^{l1} and...and \ x_{sf_i} is \ F_i^{li} \ and...and \ x_{sf_n} \ isF_n^{ln} \ then \ y_{sf_1}(x) = a_0^l + ... + a_n^l x_{f_n}. \tag{1}$$

Each fuzzy rule $R_l$ corresponds to a combination of $(F_1^{l1}, ..., F_i^{li}, ..., F_n^{ln})$ fuzzy sets. In fact, the knowledge base contains all possible combinations of the fuzzy sets of the input variables. In this case, the consequences of the rules are numerical functions, which depend on the current values of the observation variables $(x_{sf})_{i=1,...n}$. From the previous set of rules, the expression for the final output is given by the following relationship [16, 18, 22]:

$$y_{s_f} = \frac{\sum_{l=1}^{M} \mu_l y_{sf_l}}{\sum_{l=1}^{M} \mu_l} \tag{2}$$

with

$$\mu_l = \prod_{i=1}^{n} \mu_{F_i^{li}} x_i \ , \quad 1 \le l_i \le m_i. \tag{3}$$

This represents the degree of confidence or activation of the rule $R_l$. Since each rule has a numerical conclusion, the total output of the fuzzy system is obtained by calculating a weighted average, and in this way, the time consumed by the defuzzification procedure is avoided. The membership functions characterizing the fuzzy sets $F_i^j$ are chosen based on Gaussian functions defined by the following relation:

$$\mu_{F_i^j}(x_{sf_i}) = exp(-0.5(v_i^j(x_{sf_i} - c_i^j))), \tag{4}$$

where $c$ is the mean, $v$ is the inverse of the variance. In the case where the parameters of the premises are a priori fixed, the only adjustable parameters will be those of the conclusion. Thus, the final output can be written in the following form:

$$y_{s_f} = W(x_{s_f})A, \tag{5}$$

where A is a vector of parameters $a_i^j$, and $W(x_{s_f})$ is a vector of fuzzy basis functions, $l = 1, ..., M; i = 1, ..., n;$ and $1 \le l_i \le m_i$.

## 3 Adaptive Control Based on Fuzzy Systems

### 3.1 Formulation of the problem

Let us define a nonlinear system by the collection of m differential equations of order n such as

$$u_i = F_i(X)x_i^{(n)} + G_i(X), \tag{6}$$

$y_i = x_i; \quad i = 1, ..., m, \quad X = [x^{(n-1)}, ..., x]^T, \quad x = [x_1, ..., x_m]^T, \quad u = [u_1, ..., u_m]^T,$ and $y = [y_1, ..., y_m]^T$ are, respectively, the state vector, the input vector and the output vector. Moreover, we assume that the time derivative of $F_i(X)$ verifies the following condition:

$$|F_i(X)| \le F_{i0}\|X\|, \tag{7}$$

where $F_{i0}$ is a known positive constant. To help establishing the control law, we introduce the following definitions:

– The tracking error vector $e_i = [e_i \quad \dot{e}_i \, ... \, e_i^{(n-1)}]^T \ \in \mathcal{R}^m \ $ with $e_i = x_{id} - x_i$.
– The filtered tracking error

$$s_i = (\frac{\partial}{\partial t} + \lambda)^{(n-1)} e_i \qquad (8)$$

can be written as $\ s_i = C_i \, e_{i0}$, where $C_i = [\lambda^{(n-1)} \quad (n-1)\lambda^{n-2} \quad ... \, 1]$.
– The reference signal

$$y_{ir}^{(n)} = x_{id}^{(n)} + C_{ir} \, e_i \qquad (9)$$

with $C_{ir} = [0 \quad \lambda^{(n-1)} \quad (n-1)\lambda^{(n-2)} \quad ...(n-1)\lambda]$ and $x_{id}^{(n)}$ being the $n^{th}$ derivative of the reference $x_{id}$.

To synthesize the control law, the functions $F_i(X)$ and $G_i(X)$ are replaced by two Sugeno fuzzy systems of the form $W(X)\theta$ such as

$$F_i(X) = W_{f_i}(X)\theta_{fi} + \varepsilon_{f_i} \qquad (10)$$

$$G_i(X) = W_{g_i}(X)\theta_{g_i} + \varepsilon_{gi}, \qquad (11)$$

where $\varepsilon_{f_i}$ and $\varepsilon_{g_i}$ are the reconstruction errors of functions $F_i(X)$ and $G_i(X)$ such that [4]

$$|\varepsilon_{f_i}| \le \bar{\varepsilon}_{f_i} \qquad (12)$$

$$|\varepsilon_{g_i}| \le \bar{\varepsilon}_{g_i}. \qquad (13)$$

We denote the estimate of the function $F_i(X)$ by $\hat{F}_i(X)$ and $G_i(X)$ by $\hat{G}_i(X)$ such that

$$\hat{F}_i(X) = W_{f_i}(X)\hat{\theta}_{f_i} \qquad (14)$$

$$\hat{G}_i(X) = W_{g_i}(X)\hat{\theta}_{g_i}. \qquad (15)$$

The adaptive fuzzy control problem is posed as follows. For the nonlinear system defined by equation (6), determine the adjustment laws of the parameters of the two fuzzy systems that allow to estimate, online, the functions $F_i(X)$ *and* $G_i(X)$ as well as the adequate control $u_i$ such that the tracking error converges asymptotically to zero.

## 3.2   Synthesis of the control law

Our goal is to design a control such that the tracking error converges asymptotically to zero. Thus, this control is given by

$$u_i = k_{id}s_i + \frac{1}{2}F_{i0}\,\|X\|\,s_i + W_{f_i}(X)\hat{\theta}_{f_i}y_{ir}^{(n)} + W_{gi}(X)\hat{\theta}_{g_i} + K_i sign(s_i), \qquad (16)$$

where $K_i$ is the sliding mode term, it is given by

$$K_i = \bar{\varepsilon}_{f_i}|y_{ir}^{(n)}| + \bar{\varepsilon}_{g_i}. \qquad (17)$$

The parameters of the fuzzy systems are adjusted by the following adaptation laws:

$$\dot{\hat{\theta}}_{f_i} = \eta_{f_i}W_{f_i}^T(X)s_i y_{ir}^{(n)}, \qquad (18)$$

$$\dot{\hat{\theta}}_{g_i} = \eta_{f_i}W_{g_i}^T(X)s_i. \qquad (19)$$

The schematic diagram of adaptive control based on fuzzy systems is shown in Figure 1.
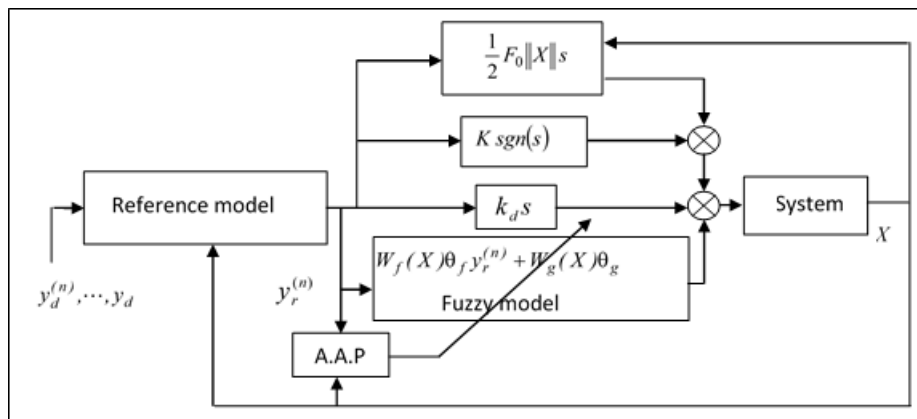
**Figure 1**: Structure of adaptive control based on fuzzy systems.

## 4  Study of the Stability

Using the control law (16) and the dynamic model of the nonlinear system (6), and knowing that $y_{ir}^{(n)} = y_i^{(n)} + \dot{s}_i$, the dynamics of the error is given by

$$F_i \dot{s}_i = -k_{id} s_i - \frac{1}{2} F_{i0} \|X\| s_i - W_{f_i}(X)\tilde{\theta}_{f_i} y_{ir}^{(n)} - W_{g_i}(X)\tilde{\theta}_{g_i} - k_i sign(s_i) + \varepsilon_{f_i} y_{ir}^{(n)} + \varepsilon_{g_i}, \quad (20)$$

where $\tilde{\theta}_{f_i}$ and $\tilde{\theta}_{g_i}$ are the parametric errors, they are given by $\tilde{\theta}_{f_i} = \hat{\theta}_{f_i} - \bar{\theta}_{f_i}$ and $\tilde{\theta}_{g_i} = \hat{\theta}_{g_i} - \bar{\theta}_{g_i}$ with $\bar{\theta}_{f_i}$ and $\tilde{\theta}_{g_i}$ being the parameter vectors for the reconstruction errors to be zero.

Let the following Lyapunov function:

$$V = \frac{1}{2} s_i^2 F_i + \frac{1}{2}(\tilde{\theta}_{f_i}^T \eta_{f_i}^{-1} \tilde{\theta}_{f_i}) + \frac{1}{2}(\tilde{\theta}_{g_i}^T \eta_{g_i}^{-1} \tilde{\theta}_{g_i}). \quad (21)$$

By deriving (21) with respect to time, we obtain

$$\dot{V} = \frac{1}{2} s_i^2 F_i + s_i F_i \dot{s}_i + \tilde{\theta}_{f_i}^T \eta_{f_i}^{-1} \dot{\hat{\theta}}_{f_i} + \tilde{\theta}_{g_i}^T \eta_{g_i}^{-1} \dot{\hat{\theta}}_{g_i}. \quad (22)$$

Replacing (20) in (22), we have

$$\begin{aligned}
\dot{V} =& \frac{1}{2} s_i^2 \dot{F}_i - s_i^2 k_{id} - \frac{1}{2} s_i^2 F_{i0} \|X\| - s_i W_{f_i}(X)\tilde{\theta}_{f_i} y_{ir}^{(n)} - s_i W_{g_i}(X)\tilde{\theta}_{g_i} \\
&+ \tilde{\theta}_{f_i}^T \eta_{f_i}^{-1} \dot{\hat{\theta}}_{f_i} + \tilde{\theta}_{g_i}^T \eta_{g_i}^{-1} \dot{\hat{\theta}}_{g_i} + s_i \varepsilon_{f_i} y_{ir}^{(n)} + s_i \varepsilon_{g_i} - s_i K_i sign(s_i).
\end{aligned} \quad (23)$$

To facilitate the demonstration, we make the following decomposition:
$\dot{V}_1 = -s_i^2 k_{id},$
$\dot{V}_2 = \frac{1}{2} s_i^2 \dot{F}_i - \frac{1}{2} s_i^2 F_{i0} \|X\|,$
$\dot{V}_3 = s_i W_{f_i}(X)\tilde{\theta}_{f_i} y_{ir}^{(n)} + \tilde{\theta}_{f_i}^T \eta_{f_i}^{-1} \dot{\hat{\theta}}_{f_i} - s_i W_{g_i}(X)\tilde{\theta}_{g_i} + \tilde{\theta}_{g_i}^T \eta_{g_i}^{-1} \dot{\hat{\theta}}_{g_i}.$

Thus, the expression of $\dot{V}$ is put in the following form:
$\dot{V}_4 = s_i \varepsilon_{f_i} y_{ir}^{(n)} + s_i \varepsilon_{g_i} - s_i K_i sign(s_i),$
$\dot{V} = \dot{V}_1 + \dot{V}_2 + \dot{V}_3 + \dot{V}_4.$

Knowing that $k_d$ is a positive constant, we get $\dot{V}_1 \leq 0$. Using condition (7), we have $\dot{V}_2 \leq 0$.

Following the adaptation laws in (18), and (19), we obtain $\dot{V}_3 \leq 0$. According to the expression of the slip mode term (16), it comes $\dot{V}_4 \leq 0$. Hence, the time derivative of the Lyapunov function verifies

$$\dot{V} \leq 0. \tag{24}$$

The inequality (24) implies that s converges asymptotically to zero and that all signals in the system are bounded.

## 4.1 Application to the permanent magnet synchronous machine

The machine model is established by considering the commonly accepted simplifying assumptions that the machine is of symmetric, unsaturated construction and that the iron losses and space harmonics of the magnetic field are negligible. The dynamics of the machine is represented by its rotor-related PARK model [23–25] so that the electrical quantities appear in a continuous form, easy to process by the control algorithm. Thus, this model is given by

$$\begin{cases} v_d &= R_s i_d + L_d \frac{di_d}{dt} - pL_q \Omega i_q, \\ v_q &= R_s i_q + L_q \frac{di_q}{dt} + pL_d \Omega i_d + p\Omega \Phi_f, \\ j\frac{d\Omega}{dt} &= T_{em} - T_r - F_c \Omega, \\ T_{em} &= \frac{3}{2} p(\Phi_f i_q + (L_d - L_q)i_d i_q), \end{cases} \tag{25}$$

where $\Phi_f$ is the total permanent magnet flux, $(L_d, L_q)$ are the forward and quadrature inductances, $(i_d, i_q)$ are the stator current components, $(v_d, v_q)$ are the stator voltage components, $R_s$ is the stator resistance, $\Omega$ is the rotational speed, $F_c$ is the strongly viscous coefficient, $j$ is the moment of inertia, $T_r$ is the resistive torque and $p$ is the number of pole pairs.

## 4.2 Speed control

In the case of a permanent magnet synchronous machine without salience $(L_d = L_q)$ and without dampers, the electromagnetic torque depends only on the q-axis current component. The power input is optimized for a given torque if the disturbance current $i_d = 0$, [26]. The control must maintain zero and adjust the torque with. Physically, this strategy amounts to maintaining the armature reaction flux in quadrature with the rotor flux produced by the system. The overall structure of this command is shown in Figure 2. A coordinate transformation ($dq$-abc) is used to calculate the reference stator currents. These currents are compared to the actual measured currents to set the control of each inverter arm. Using the equilibrium equation between the driving torque and the torque opposed by the mechanical part of the system, we can write

$$i_q = F(\Omega)\frac{d\Omega}{dt} + G(\Omega). \tag{26}$$

The implementation of this command requires the approximation of the functions $F(\Omega)$ and $G(\Omega)$ by the fuzzy systems, thus, this approximation is given by

$$F(\Omega) = W_f(\Omega)\theta_f + \varepsilon_{f_\Omega}, \tag{27}$$

$$G(\Omega) = W_g(\Omega)\theta_g + \varepsilon_{g_\Omega} \tag{28}$$
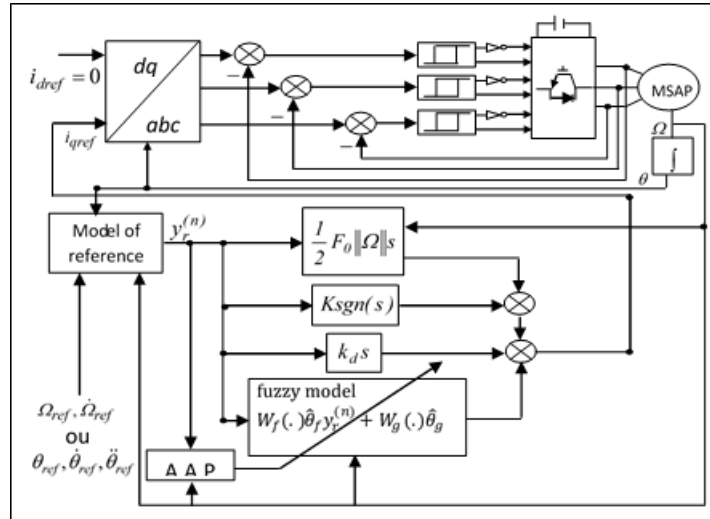
**Figure 2**: Speed/position control structure by the adaptive control method based on fuzzy systems.

with $\varepsilon_{f_\Omega}$ and $\varepsilon_{g_\Omega}$ being the reconstruction errors of functions $F_i(\Omega)$ and $G_i(\Omega)$ such that $|\varepsilon_{f\Omega}| \leq \bar{\varepsilon}_{f\Omega}$, $|\varepsilon_{g\Omega}| \leq \bar{\varepsilon}_{g\Omega}$.

In this approximation, we choose two Sugeno fuzzy systems of order one having the input. Three membership functions are associated to this input. Thus, we have three rules for each fuzzy system.

The estimated functions generated by the fuzzy systems are given by

$$\hat{F}(\Omega) = W_f(\Omega)\hat{\theta}_f, \tag{29}$$

$$\hat{G}(\Omega) = W_g(\Omega)\hat{\theta}_g, \tag{30}$$

where $\hat{\theta}_f$ and $\hat{\theta}_g$ are the internal parameters of the fuzzy systems, they are adjusted by the following adaptation law:

$$\dot{\hat{\theta}}_f = \eta_{f_\Omega} W_f^T(\Omega) s \dot{y}_r, \tag{31}$$

$$\dot{\hat{\theta}}_g = \eta_{g_\Omega} W_g^T(\Omega) s, \tag{32}$$

where $\eta_{f_\Omega}$ and $\eta_{g_\Omega}$ are positive constants, $s$ and $\dot{y}_r$ are, respectively, the error and the reference signal, their expressions are given by $s = \Omega_{ref} - \Omega$, $\dot{y}_r = \dot{\Omega}_{ref}$.

From the estimated fuzzy functions, the law control has the following form:

$$i_{q_{ref}} = k_{d\Omega} s + \frac{1}{2} F_{0\Omega} \|\Omega\| s + W_f(\Omega)\hat{\theta}_f \dot{y}_r + W_g(\Omega)\hat{\theta}_g + k_\Omega sign(s), \tag{33}$$

where $k_\Omega$ is the gain of the slip mode term, its expression is given by $k_\Omega = \bar{\varepsilon}_{f\Omega}|\dot{y}_r| + \bar{\varepsilon}_{g\Omega}$.

### 4.3   Position control

The schematic diagram of this control is shown in Figure 2. Through fuzzy systems, the functions $F(\dot{\theta})$ and $G(\dot{\theta})$ in equation (26) are approximated as follows:

$$F(\dot{\theta}) = W_f(\dot{\theta})\theta_f + \varepsilon_{f_\theta}, \tag{34}$$

$$G(\dot{\theta}) = W_g(\dot{\theta})\theta_g + \varepsilon_{g_\theta}, \tag{35}$$

with $\varepsilon_{f_\theta}$ and $\varepsilon_{g_\theta}$ being the reconstruction errors of functions $F(\dot{\theta})$ and $G(\dot{\theta})$ such that $|\varepsilon_{f\theta}| \leq \bar{\varepsilon}_{f\theta}$, $|\varepsilon_{g\theta}| \leq \bar{\varepsilon}_{g\theta}$.

In our application, two Sugeno fuzzy systems of order one with three fuzzy rules are used to approximate the functions $F(\dot{\theta})$ and $G(\dot{\theta})$. The fuzzy systems generate the estimated functions $\hat{F}(\dot{\theta})$ and $\hat{G}(\dot{\theta})$ such that

$$\hat{F}(\dot{\Omega}) = W_f(\dot{\Omega})\hat{\theta}_f, \tag{36}$$

$$\hat{G}(\dot{\Omega}) = W_g(\dot{\Omega})\hat{\theta}_g, \tag{37}$$

where $\hat{\theta}_f$ and $\hat{\theta}_g$ are the internal parameters of the fuzzy systems, they are adjusted by the following adaptation law:

$$\dot{\theta}_f = \eta_{f_\theta} W_f^T(\theta) s \ddot{y}_r, \tag{38}$$

$$\dot{\theta}_g = \eta_{g_\theta} W_g^T(\theta) s, \tag{39}$$

where $s$ and $\ddot{y}_r$ are, respectively, the filtered error and the reference signal, they are given by $s = \dot{\theta}_{ref} - \dot{\theta} + \lambda(\theta_{ref} - \theta)$, $\ddot{y}_r = \ddot{\theta}_{ref} + \lambda(\dot{\theta}_{ref} - \dot{\theta})$, whereas $\eta_{f_\theta}$ and $\eta_{g_\theta}$ are positive constants. Based on the estimated fuzzy functions, the adaptive controller provides the command $i_{qref}$, which is given by

$$i_{q_{ref}} = k_{d\theta} s + \frac{1}{2} F_{0\theta} \left\| \dot{\theta} \right\| s + W_f(\dot{\theta})\hat{\theta}_f \ddot{y}_r + W_g(\dot{\theta})\hat{\theta}_g + k_\theta sign(s), \tag{40}$$

where $K_\theta$ is the gain of the slip mode term, it is given by $K_\theta = \bar{\varepsilon}_{f_\theta}|\ddot{y}_r| + \bar{\varepsilon}_{g_\theta}$.

## 5   Numerical Simulation

In this section, we present the results obtained from the simulation of the adaptive control technique based on fuzzy systems applied to the permanent magnet synchronous machine. The values of the tuning coefficients, imposing the desired dynamics, are gathered in Tables 1 and 2.

| $\eta_{f\Omega}$ | $\eta_{g\Omega}$ | $k_{d\Omega}$ | $F_{0\Omega}$ | $\bar{\varepsilon}_{f\Omega}$ | $\bar{\varepsilon}_{g\Omega}$ |
|---|---|---|---|---|---|
| 0.05 | 0.05 | 1 | 0.05 | 0.01 | 0.01 |

**Table 1**: Speed adjustment coefficients.

| $\eta_{f\theta}$ | $\eta_{g\theta}$ | $k_{d\theta}$ | $F_{0\theta}$ | $\bar{\bar{\varepsilon}}_{f\theta}$ | $\bar{\bar{\varepsilon}}_{g\theta}$ | $\lambda$ |
|------|------|------|------|------|------|------|
| 50.1 | 50.1 | 10 | 10 | 0.1 | 0.1 | 70.8 |

**Table 2**: Position adjustment coefficients.
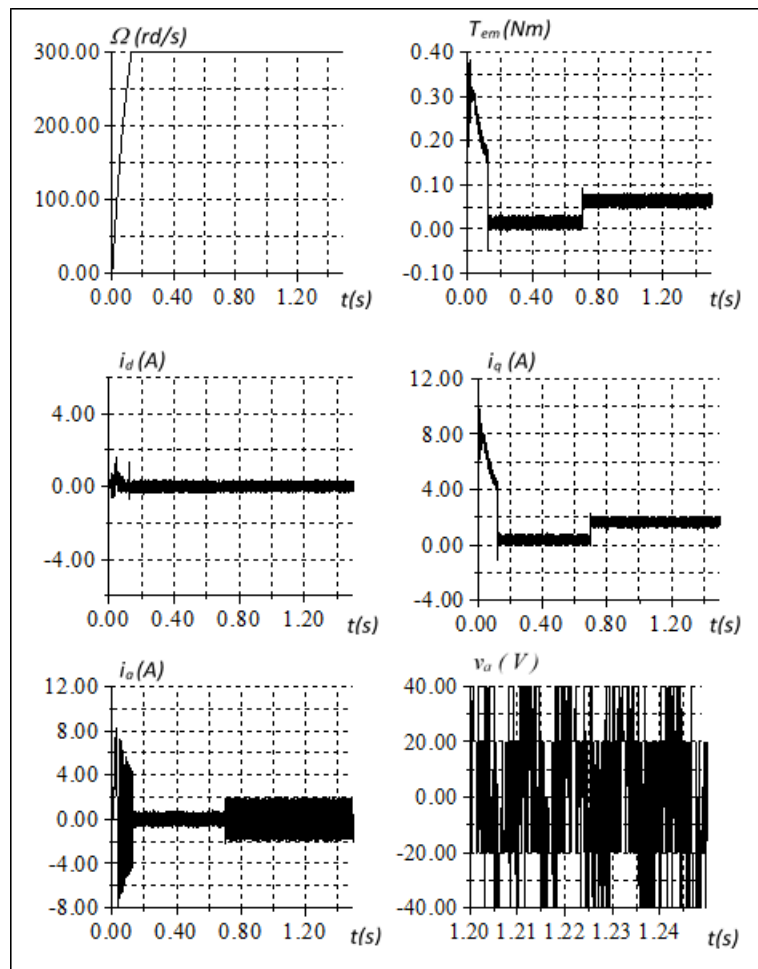


**Figure 3**: Dynamic behavior of the MSAP during a start-up with load variation at time t = 0.7 s.
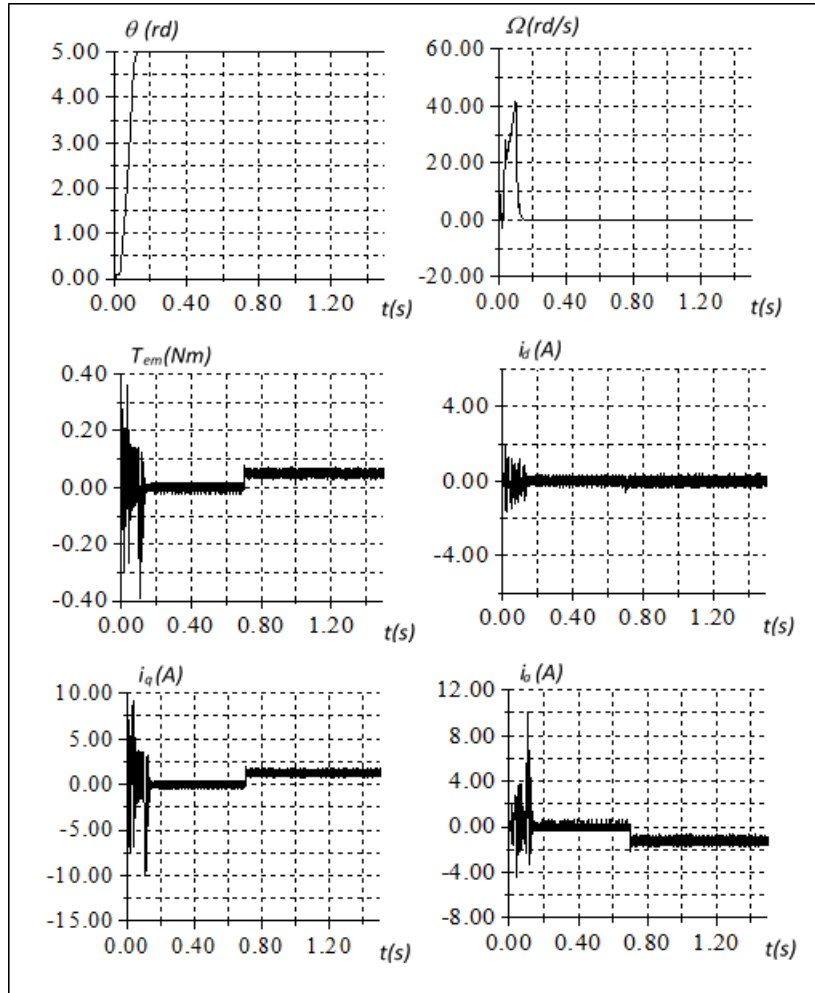
**Figure 4**: Dynamic behavior of the MSAP during positioning with load variation at time t = 0.7 s.
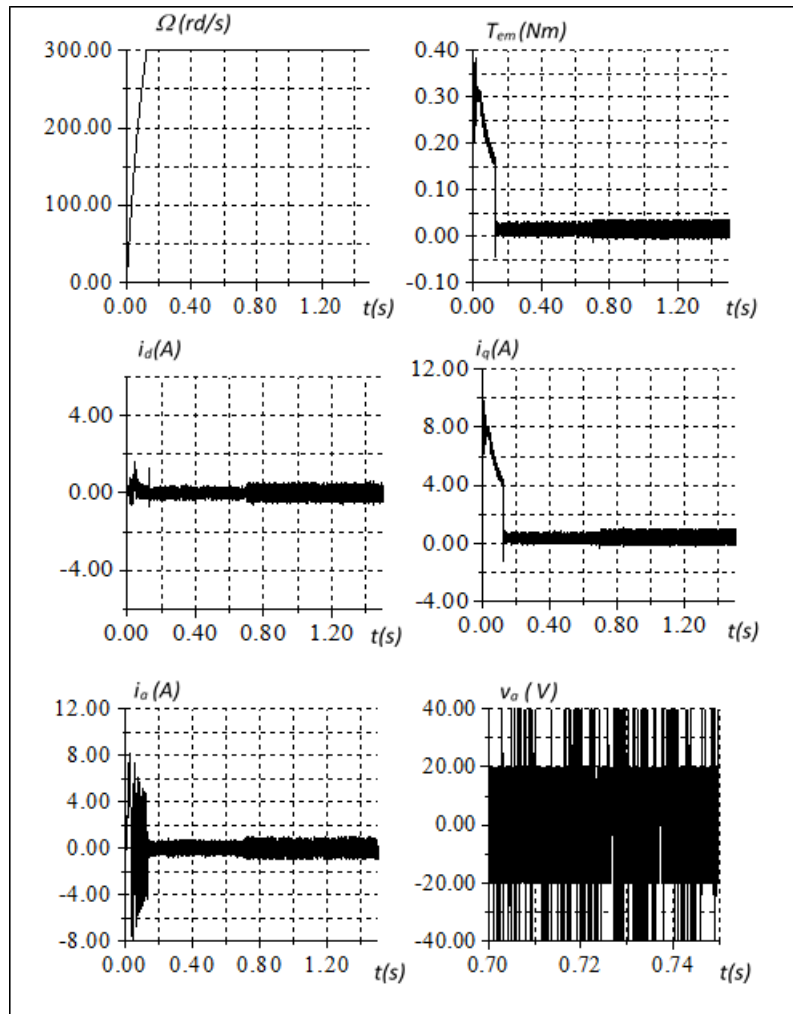
**Figure 5**: Dynamic behavior of the MSAP during a start-up with parametric variations at time t = 0.8 s.
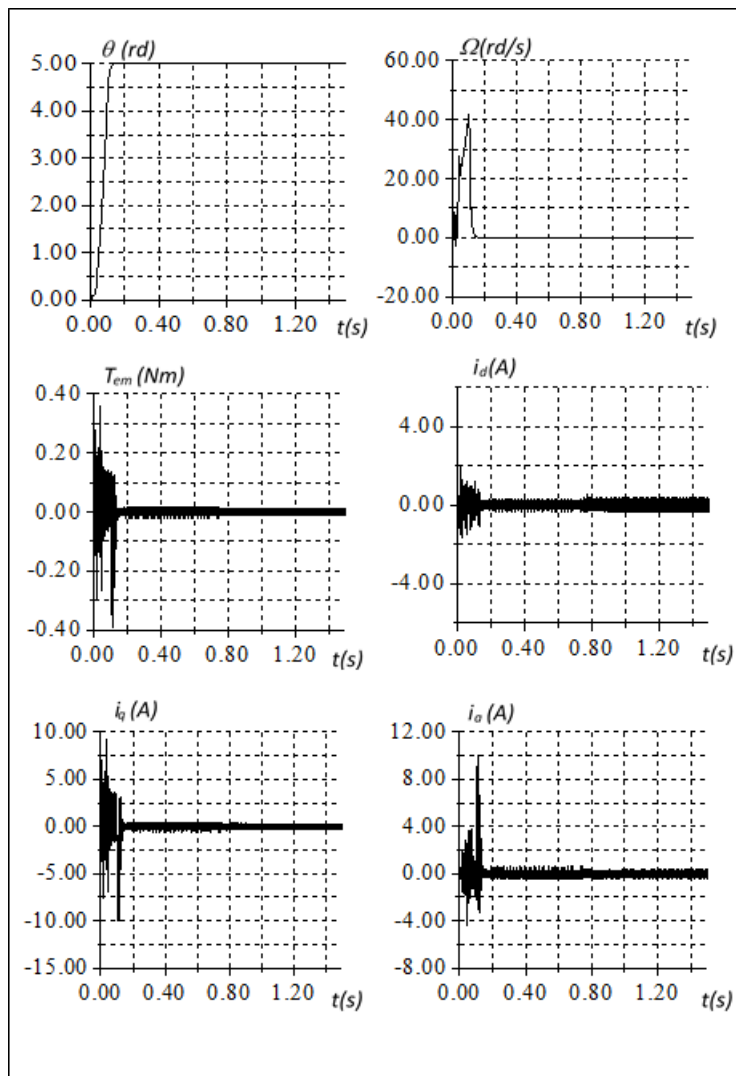
**Figure 6**: Dynamic behavior of the MSAP during positioning with parametric variations at time t = 0.8 s.

Figure 3 shows the responses obtained during a start-up for a speed setpoint of 300 rd/s with load variation. Figure 4 gives the responses obtained during positioning. We note very interesting dynamic and static performances, the disturbance rejection is effective, the decoupling of the $d$-$q$ axes is not affected by the severe regime applied to the machine. The speed and position drops are of the order of 0.076 and 0.03, respectively. The times required to compensate for these are equal to 0.002s and 0.016s, respectively. To evaluate the performance of this control scheme with respect to parametric variations, we have tested the influence of parametric variations on the performance of the speed and position control. We consider variations on the stator resistance, on the inductances as well as on the magnet flux. The stator resistance is varied by 100, the inductances

are varied by –50, and the magnet flux by –10. The obtained responses are shown in Figures 5 and 6. From these results, we notice that the adaptive control based on fuzzy systems presents a strong robustness towards parametric variations, which proves the effectiveness of this control technique.

## 6    Conclusion

In this paper, we have presented and applied a new approach of adaptive control based on fuzzy systems, in order to control the speed and position of the permanent magnet synchronous machine. The fuzzy systems are used to approximate the non-linear functions, which are determined by a self-learning or self-tuning according to a law that ensures the global stability of the system. In the light of the recorded responses, the proposed adaptive control based on fuzzy systems presents good performances. Indeed, the tests carried out on the model of the synchronous machine with permanent magnets, allowed us to judge positively the stability and the effectiveness of this algorithm.

## Acknowledgment

## References

[1] C. Y. Su and Y. Stephanenko. Adaptive control of a classe of non linear systems with fuzzy logic. *IEEE Tran. on Fuzzy Systems* **2** (2) (1994) 285–294.

[2] Y. T. Kim and Z. Bien. Robust Indirect Adaptive Fuzzy Control. *Proc. IEEE Int. Conf. on Fuzzy Systems. Seoul, Korea* (1999) 1293–1298.

[3] Y. W. Cho, Y. H. Yee and M. Park. An Indirect Model Reference adaptive Fuzzy Control for SISO Takagi-Sugeno Model. *Proc. IEEE Int. Conf. on Fuzzy Systems. Seoul, Korea* (1999) 474–479.

[4] L. X. Wang. Stable Adaptive Fuzzy Control of Nonlinear Systems. *IEEE Tran. On Fuzzy Systems* **1** (1) (1993) 146–155.

[5] M. Ming, W. Liang, Z. Feng, J. Ling, A. Mamun and X. Xiao. PID-type sliding mode-based adaptive motion control of a 2-DOF piezoelectric ultrasonic motor driven stage. *Mecatronics* **76** (2021) 102543.

[6] Z. Ning, B. Cai, R. Weng, L. Zhang and S. F. Su. Stability and control of Fuzzy Semi-Markov Jump Systems Under Unknown Semi-Markov Kernel. *IEEE Transactions on Fuzzy Systems* (2021).

[7] R. P. Noronha. Diversity Control in the Hybridization GA-PSO with Fuzzy Adaptive Inertial Weight. *5th International Conference on Intelligent Computing and Control Systems (ICICCS) IEEE* (2021) 1055–1062.

[8] Q. Shi, H. K. Lam, C. Xuan and M. Chen. Adaptive neuro-fuzzy PID controller based on twin delayed deep deterministic policy gradient algorithm. *Neurocomputing* **402** (2020) 183–194.

[9] T. S. Mohamed, and E. Miler. Daniel. Adaptive Control of a class of discret-time nonlineaar systems yielding linear-like behavior. *Automatica, Elsevier* **130** (2021) 109691.

[10] F. Hamidia, A. Abbadi, A. Tlemçani and M. S. Boucherit. Dual star induction motor supplied with double photovoltaic panels based on fuzzy logic tupe-2. *Nonlinear Dynamics and Systems Theory* **18** (4) (2018) 359–371.

[11] A. Morceli, A. Tlemçani and M. S. Boucherit. Shunt Active Power Filter Based Harmonics Compensation of Low-Voltage Network Using Fuzzy Logic System. *Nonlinear Dynamics and Systems Theory* **17** (1) (2018) 70–85.

[12] X. Zeng and M. G. Singh. Approximation theory of fuzzy systems-MIMO case. *IEEE Transaction on Fuzzy Systems* **3** (2) (1995) 219–235.

[13] X. Zeng and M. G. Singh. Approximation accuracy analysis of fuzzy systems as function approximators. *IEEE Transactions on Fuzzy Systems* **4** (1) (1996) 44–63.

[14] A. Shmilovici and O. Z. Maimon. Fuzzy systems approximation by frames-SISO case. In: *Proc. of 1995 IEEE Intern. Conf. on Fuzzy Systems*, 1995, vol. 4, 2057–2062.

[15] H. Ying. General SISO Takagi-Sugeno fuzzy systems with linear rule consequent are universal approximators. *IEEE Transactions on Fuzzy Systems* **6** (4) (1998) 582–587.

[16] B. Kosko. Neural *Networks and Fuzzy Systems: A Dynamical Approach to Machine Intelligence*. Prentice Hall, 1992.

[17] J. M. Mendel. Fuzzy logic systems for engineering: a tutorial. *Proceeding of the IEEE* **83** (3) (1995) 345–377.

[18] J. S. Jang and C. T. Sun. Neuro-fuzzy modeling and control. *Proceeding of the IEEE* **83** (3) (1995) 378–406.

[19] H. *Le Reglage Par Logique Floue*. Presses Polytechniques Romandes, 1994.

[20] J. J. Buckley and H. Ying. Fuzzy Controller theory: Limit theorems for linear fuzzy control rules. *Automatica* **25** (3) (1989) 469–472.

[21] M. Sugeno and G. T. Kang. Structure Identification of Fuzzy Model. *Fuzzy sets and systems* **28** (1) (1988) 15–33.

[22] F.H.F. Leung and P. K. S. Tam. Fuzzy model controller for inverted pendulum. *Electronics Letters* **32** (2) (1996) 1683–1685.

[23] P. Pillay and R. Krishnan. Modeling, simulation and analysis of permanent magnet motor drives. *IEEE Trans. on Industry Applications* **25** (2) (1989) 265–273.

[24] P. Pillay and R. Krishnan. Modeling of permanent magnet motor drive. *IEEE Trans. on Industrial Electronics* **35** (4) (1988).

[25] T. H. Liu, C. M. Young and C. H. Liu. Microprocessor-based controller design and simulation for a permanent magnet synchronous motor drive. *IEEE Trans. on Industrial Electronics* **35** (4) (1988) 516–523.

[26] J. M. Thomas. Motion Control With Permanent Magnet AC Machine. *Proc. of the IEEE* **82** (8) (1994) 1241–1252.

# Dynamics of Nonlinearly Damped Duffing-Van Der Pol Oscillator Driven by Frequency Modulated Signal

B. Bhuvaneshwari [1], S. Valli Priyatharsini [1], V. Chinnathambi [1,*] and S. Rajasekar [2]

[1] *Department of Physics, Sadakathullah Appa College, Tirunelveli 627 011, Tamil Nadu, India.*
[2] *School of Physics, Bharathidasan University, Tiruchirapalli 620 024, Tamilnadu, India.*

**Abstract:** The dynamics of a nonlinearly damped Duffing-Van der Pol (DVP) oscillator driven by a frequency modulated (FM) signal is numerically investigated as a function of the amplitude ($g$) and frequency ($\Omega$) of the high-frequency signal and damping exponent ($P$). FM signals are basically classified into two types, namely, Narrow-Band FM (NBFM) and Wide-Band FM (WBFM). We considered both signals to study the dynamics of the system. As the amplitude $g$ and frequency $\Omega$ of the high-frequency signal are varied, with other parameters at a constant value, a variety of features such as different routes to chaos, periodic windows, period-doubling and reverse period-doubling bifurcations, periodic bubbles, hysteresis and vibrational resonance are found to occur due to the signals. Our results show many striking departures from the behaviour of a linearly damped system with the FM signal. A bifurcation diagram, phase portrait, Poincaré map, resonance plot are also plotted to show the manifestation of periodic and chaotic orbits and resonance phenomenon.

**Keywords:** *DVP oscillator; nonlinear damping; FM signal; hysteresis; chaos; vibrational resonance.*

**Mathematics Subject Classification (2010):** 34C55, 34C25, 37D45, 37G35, 70K30.

---

* Corresponding author: mailto:veerchinnathambi@gmail.com

## 1   Introduction

There have been enormous contributions to the study of the dynamical behaviours in linearly damped and driven dynamical systems, including various routes to chaos, crises and resonance phenomenon [1–4]. However, there is a need for research on various dynamical behaviours in nonlinearly damped driven dynamical systems. Exploring the features of various dynamics in systems with different types of setup of the external force is of great importance. Recently, Cheib et al. [5] studied the dynamics of a two-degree-of-freedom nonlinear mechanical system under the action of harmonic excitation. Khachnaoni [6] investigated the existence of homoclinic orbits for damped vibration system with small forcing terms and Kyziol and Okninski [7] found the periodic steady-state solutions of the periodically driven Duffing-Van der Pol oscillator using the Krylov-Bogoliubov-Mitropolsky approach. It is of considerable interest to study the system under the influence of FM signal. The study of such signal will be helpful in creating and controlling nonlinear dynamical behaviours [8–10]. The nonlinear damping term is taken to be proportional to the power of the velocity in the form $\gamma \dot{x} \mid \dot{x} \mid^{P-1}$. A similar nonlinear damping term was used previously by researchers [3, 11–13].

The FM signal is basically classified into two types, namely, Narrow Band FM (NBFM) and Wide Band FM (WBFM) or Broad band FM. An NBFM signal is the FM signal with a smaller bandwidth. The modulation index $(M_f)$ of the NBFM signal is small as compared to one radian. Hence the spectrum of the NBFM signal consists of the carrier and upper and lower side-bands. The NBFM signal can be expressed mathematically as

$$S_1(t) = f(\cos \omega t - g \sin \Omega t \sin \omega t), \ \Omega >> \omega, \tag{1a}$$

where the amplitude $f$ of the low-frequency ($\omega$) periodic signal is modulated by the high-frequency ($\Omega$) periodic signal with amplitude $g$. With the use of the formula $\sin \Omega t \sin \omega t = \frac{1}{2}[\cos(\Omega - \omega) - \cos(\Omega + \omega)]$, it takes the form

$$S_1(t) = f \cos \omega t + \frac{fg}{2} \left[ \cos(\Omega + \omega)t - \cos(\Omega - \omega)t \right], \ \Omega >> \omega. \tag{1b}$$

When $\Omega >> \omega$, the frequency modulated signal can also be treated as consisting of a low-frequency signal $f \cos \omega t$ and two high-frequency signals with frequencies $(\Omega + \omega)$ and $(\Omega - \omega)$. This signal is used in FM mobile communications such as police wireless, ambulances, taxicabs, etc. For large value of the modulation index, the FM signal ideally contains the carrier and an infinite number of side bands located symmetrically around the carrier. Such an FM signal has infinite bandwidths and is called the Wide Band FM (WBFM) signal. The modulation index of the WBFM is higher than 1. This signal is used in the entertainment broadcasting applications such as FM radio, TV etc. The expression for the WBFM signal is complex since it is sine of sine function. The only way to solve this equation is by using the Bessels function. The mathematical expression for the WBFM signal is

$$S_2(t) = f \sin(\omega t + g \sin \Omega t), \ \Omega >> \omega. \tag{2}$$

The equation of motion of a nonlinearly damped DVP oscillator with the NBFM signal is given by

$$\ddot{x} + \gamma \dot{x}(1 - x^2) \mid \dot{x} \mid^{P-1} -\alpha^2 x + \beta x^3 = S_1(t) \tag{3}$$

and with the WBFM signal is given by

$$\ddot{x} + \gamma\dot{x}(1 - x^2) \mid \dot{x} \mid^{P-1} -\alpha^2 x + \beta x^3 = S_2(t), \tag{4}$$

where $\alpha$ is the natural frequency, $\beta$ is the constant parameter which plays the role of a nonlinear parameter, $\gamma > 0$ is the damping parameter of the system, $P$ is the damping exponent, $S_1(t)$ and $S_2(t)$ are the NBFM and WBFM signals. Recently, many researchers used these signals to analyze the dynamical behaviours of various dynamical systems [8–10]. In the present study, we wish to numerically analyze the dynamical behaviours in a nonlinearly damped DVP oscillator driven by the NBFM and WBFM signals.

The paper is structured as follows. Section 2 gives the dynamical behaviours of a nonlinearly damped DVP oscillator subjected to the NBFM signal. We show the occurrence of various dynamical behaviours such as bifurcations and chaos, hysteresis and vibrational resonance phenomena due to the presence of the NBFM signal. We take up the system with the WBFM signal in Section 3. Finally, the conclusion of the research work is given in Section 4.

## 2 Dynamical Behaviours of the System with NBFM Signal

### 2.1 Bifurcations and chaos

The aim of this section is to seek numerically the dynamical behaviours of the system (Eq.(3)) when the control parameter $g$ evolves for different values of the damping exponent $P$. When the control parameter $g$ is varied and a bifurcation takes place, a qualitative change of the system happens.

Eq.(3) and Eq.(4) are solved by the fourth-order Runge-Kutta method with the time step size $\Delta t = (2\pi/\omega)/1000$. The initial conditions in the numerical calculations are fixed at $x(0) = 0.1$ and $\dot{x}(0) = 0.0$. Numerical solutions corresponding to first 500 drive cycles are left as transient. We analysed the behaviour of the systems (Eq.(3) and Eq.(4)) by varying the amplitude $g$ of the signals with the fixed values of $f, \omega$ and $\Omega$. The numerical results are demonstrated through the bifurcation diagram, phase portrait, Poincaré map and response amplitude. For our numerical computation, we fix the parameters at $\alpha$=1.0, $\beta$=5.0, $\gamma$=0.4, $\omega$=0.1,$\Omega$=5.0, $P$=1.0,1.5 and 2.0 and the signal amplitudes $f$ and $g$ are varied from small values. From our numerical analysis, we find the following.

First, we show the effect of the control parameter $g$ with the fixed value of $f$=0.2 and $P$=1.0,1.5 and 2.0. Fig.1 shows the bifurcation diagram of the system (Eq.(3)) with $f$=0.2 and $P$=1.0,1.5 and 2.0. In Fig.1(a), for $P$=1.0 no chaotic behaviour is observed. But for $P$=1.5 and 2.0 various dynamical behaviours such as a period-doubling bifurcation leading to chaotic behaviour, periodic windows and a reverse period-doubling bifurcation occur, which is clearly evident in Fig.1(b) and Fig.1(c). Magnification of a part of the bifurcation diagram of Fig.1(c) is shown in Fig.1(d). Fig.1(d) shows the bifurcation diagram where $f$ is set to 0.2 and $P$=2.0, while $g$ is varied. For small values of $g$ the coexistence of two limit cycle orbits occurs. As the parameter $g$ is increased, both the orbits exhibit a transcritical bifurcation and a cascade of period-doubling bifurcation leading to chaotic motion. A transcritical bifurcation occurs at $g$=2.3174. The period-1,2,4,8 and 16 orbits are found in the intervals (0-2.4055), (2.4055-2.4481), (2.4481-2.4588), (2.4588-2.4603) and (2.4603-2.4626), respectively. The onset of chaos is found at $f$=2.4632. An example of the chaotic orbit at $g = 2.95$ and the corresponding Poincaré map are shown
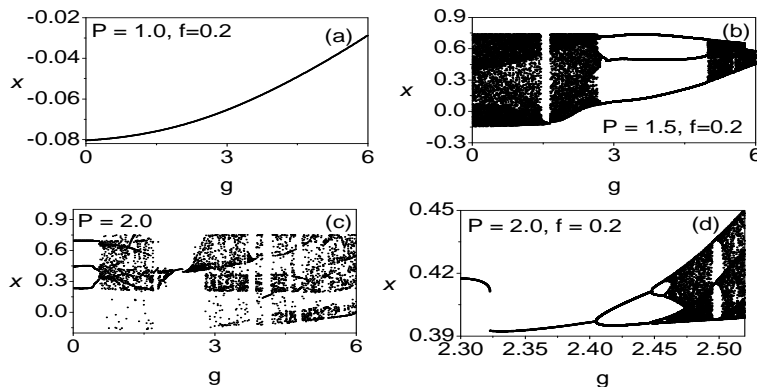
**Figure 1**: (a-c) Bifurcation diagrams for few values of $P$ with $f = 0.2$. (d) Magnification of a part of the bifurcation diagram of Fig.1(c). The other parameter values are $\alpha = 1.0$, $\beta = 5.0$, $\gamma = 0.4$, $\Omega = 5.0$ and $\omega = 0.1$.
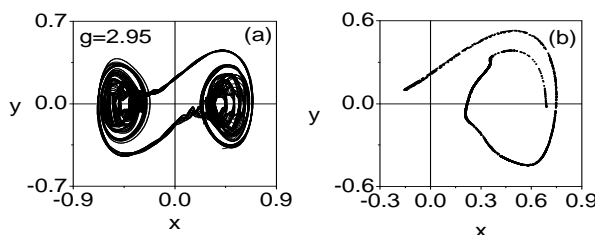


**Figure 2**: (a) Chaotic orbit for $g = 2.95$ and (b) the corresponding Poincaré map.

in Fig.2. A feature of the chaotic regime is the presence of windows of periodic solutions interspersed throughout the range of their existence. The period-3 window occurs for $g \in (2.495, 2.498)$, in which there is no chaotic behaviour. It is interesting, as the control parameter $g$ is increased in the range $g \in (2.44, 2.48)$. In Fig.1(d), we also observe that the two bands of the chaotic attractor merge into a single band when the amplitude $g$ is gradually increased beyond $g$=2.4632. In Fig.1(d), we can see that for fixed $f$=0.2, when $g$ is increased through $g$=2.4750, the chaotic bands start to merge into a large one. Another type of bifurcation which is seen in Fig.1(d) is the occurrence of sudden widening or sudden increase in the size of the attractor at $g$=2.8012.

Fig.3(a) shows the bifurcation phenomenon for $g \in [2.490, 2.500]$. We see that just above $g_c = 2.49462$, there is a stable period-$3T$, while just below $g_c$ there is chaos. We have observed that the system (Eq.(3)) also admits the intermittency route to chaos for suitable range of parameters. For example, we have observed that for $f$=0.2 and $P$=2.0, and $g$ in the range $g \in (2.49462, 2.49458)$, the type-I intermittency occurs through a transition from the period-3 window to chaos via the intermittency (type-I) across the saddle node boundary ($g = 2.49462$). The intermittency signature is shown in Fig.3(b) and Fig.3(c) where the periodic oscillations are interrupted by intermittent amplitude bursts in the range $g \in (2.49462, 2.49458)$ as g is decreased, with further decrease in the amplitude $g$, the system gives birth to fully developed chaos which is shown in Fig.3(d).
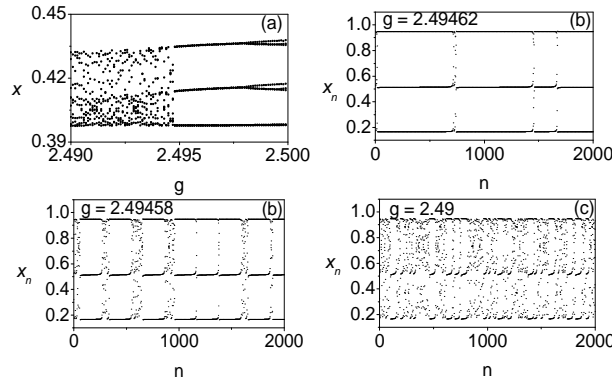
**Figure 3**: (a) Bifurcation diagram of the system (Eq.(3)) in the intermittency region. (b-d) $x(n)$ versus $n$, illustrating the intermittency route to chaos.

## 2.2 Hysteresis

In this section, we numerically analyze the occurrence of another dynamical behaviour such as the hysteresis phenomenon, that is, the possibility of jumping through the co-existence of attractors in a way that is not reversible when we fix a parameter back to its original value. It is present in the mechanical system, electromagnetism, chemical kinetics, astrochemical cloud models and nonlinear optics. In particular, the hysteresis phenomenon is observed in the generalized Ueda oscillator [14], modified Chua's circuit model [15], classical Morse oscillator [16] and the experimental study of Colpitt's oscillator [17]. The system (Eq.(3)) is found to show hysteresis for several ranges of values of the parameters. We give an example, with $f$=0.2, $P$=2.0 and $g$=1.0,$P$=2.0. Fig.4(a) shows the bifurcation behaviour for $g \in [1.5, 3.0]$ where $g$ is varied from 1.5 in the forward direction. Fig.4(b) is obtained by varying $g$ in the reverse direction from the value 3.0. Different bifurcation patterns are followed in Fig.4(a) and Fig.4(b). That is, the system (Eq.(3)) exhibits the hysteresis behaviour when the control parameter $g$ is varied smoother from a small to a larger and then to a small value. In a similar manner, we can observe the hysteresis phenomenon, when $g$ is fixed at 1.0, $P$=2.0, while $f$ is varied from a small value. Hysteresis is realized when $f$ is varied in the forward and reverse directions in the interval $f \in [0.8, 1.2]$, which is shown in Fig.4(c) and Fig.4(d). As shown in Fig.4, the presence of hysteresis and the coexistence of multiple attractors allow us to change the behaviour of the system (Eq.(3)) from chaos to regular by increasing the amplitudes $f$ and $g$ from a small to larger value to a smaller value. The suppression and enhancement of chaos are also observed which is clearly evident in Fig.4(a-d).

## 2.3 Vibrational resonance (VR)

In a nonlinear dynamical system driven by a biharmonic signal consisting of the low- and high-frequencies $\omega$ and $\Omega$ with $\Omega >> \omega$, when the amplitude $g$ or frequency $\Omega$ of the high-frequency signal is varied, the response amplitude at the low-frequency $\omega$ exhibits a resonance. This high-frequency induced resonance is called the Vibrational Resonance (VR). Landa and McClintock [18] first reported the VR in a bistable system. Later on, a theoretical treatment for analyzing the VR has been proposed by Gitterman [19].
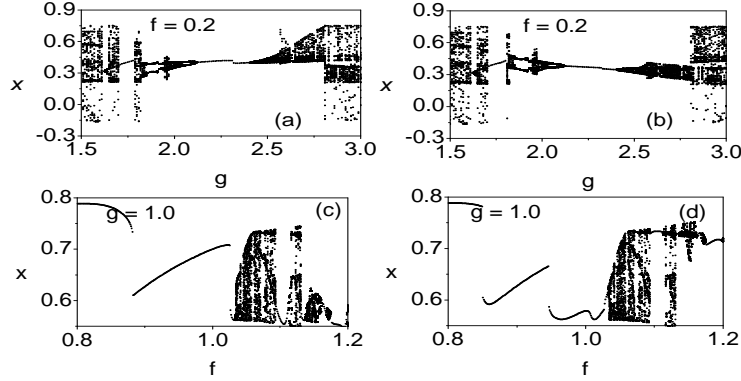
**Figure 4**: Bifurcation diagrams: (a) $g$ is varied in the forward direction from zero with $f = 0.2$. (b) $g$ is varied in the reverse direction from 3.0 with $f = 0.2$. Bifurcation diagrams: (c) $f$ is varied in the forward direction from zero with $g = 1.0$. (d) $f$ is varied in the reverse direction from 1.2 with $g = 1.0$. The values of the other parameters in Eq.(3) are $P = 2.0, \alpha = 1.0, \beta = 5.0, \omega = 0.1, \Omega = 5.0$ and $\gamma = 0.4$.

After these seminal works, the features of this resonance have been studied theoretically, numerically and experimentally in a variety of systems [20, 21].

In addition to the hysteresis behaviour, the system described by Eq.(3) also exhibits the phenomenon of VR, when the amplitude $g$ and frequency $\Omega$ of the high-frequency signal are varied. To quantify the occurrence of the VR, we use response amplitude ($Q$) of the system (Eq.(3)) at the signal frequency $\omega$. The system (Eq.(3)) can be numerically integrated using the fourth-order Runge-Kutta method with the time step size $T = (2\pi/\omega)/1000$. The first $10^3$ drive cycles are left as transient and the values of $x(t)$ correspond to the response amplitude ($Q$). From the numerical solution of $x(t)$, the response amplitude is computed through with $T = 2\pi/\omega$ being the period of the response and $n$ taken as 500.

$$Q = \sqrt{Q_s^2 + Q_c^2}/f, \tag{5a}$$

where

$$Q_s = \frac{2}{nT} \int_0^{nT} x(t) \sin(\omega t) dt, \tag{5b}$$

$$Q_c = \frac{2}{nT} \int_0^{nT} x(t) \cos(\omega t) dt. \tag{5c}$$

First, we show the occurrence of the VR due to the control parameter $g$ for a few values of the damping exponent $P$ with $f = 0.2$. The variation of numerically computed $Q$ against the control parameter $g$ for three fixed values of $P$, namely, $P = 0.9, 1.0$ and $1.1$ is shown in Fig.5(a). The values of other parameters are fixed as $\alpha = 1.0, \beta = 5.0, \gamma = 0.4$, $\omega = 0.1, \Omega = 5.0$ and $f = 0.2$. In Fig.5(a), for $P = 0.9, 1.0$ and $1.1$, the response amplitude $Q$ is found to be maximum at $g = 9.5, 8.95$ and $8.0$, respectively. The first striking result is that the maximum of the resonance curve increases as $P$ increases and at the same time, its location is shifted towards a lower value of the high-frequency amplitude $g$. Fig.5(b) shows the variation of numerically computed $Q$ against the control parameter
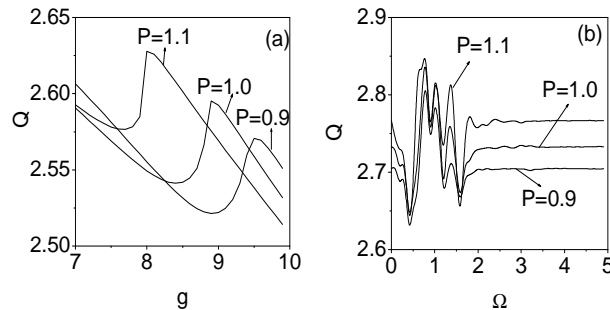
**Figure 5**: (a) Response amplitude $Q$ versus $g$ with $f = 0.2$. (b) Response amplitude $Q$ versus $\Omega$ with $f = 0.2$ for three values of $P$, namely, $P = 0.9, 1.0, 1.1$. The other parameters values are $\alpha = 1.0, \beta = 5.0, \gamma = 0.4, \omega = 0.1$ and $\Omega = 5.0$.

$\Omega$ for three values of $P = 0.9, 1.0, 1.1$, respectively. For all the values of $P$, multiple resonances take place in the intervals $0.5 < \Omega < 2.0$ and no resonance is observed in the intervals $0 < \Omega < 0.5$ and $2.0 < \Omega < 5.0$, which is clearly evident in Fig.5(b). At $\Omega = 0.975$, the maximum value of the response amplitude $Q$ occurs for all the values of $P$.

## 3 Dynamical Behaviours of the System with WBFM Signal

### 3.1 Bifurcations and chaos

For our numerical simulations, we fix the same parametric values as those previously used in the system (Eq.(3)). Fig.6 shows the bifurcation diagram for three fixed values of $P$, namely, $P$=1.0,1.5 and 2.0 with $f$=0.2. Fig.6(a) shows the bifurcation pattern where $f$ is fixed at $f$=0.2 and $P$=1.0, while $g$ is varied. As $g$ is increased from zero, a stable period-$T(= (2\pi/\omega))$ orbit occurs which persists up to $g$=0.76231 and then it loses its stability giving birth to a chaotic orbit. At $f$=0.86275, the chaotic orbit suddenly disappears and the long-time motion settles to a periodic orbit. Fig.6(b) corresponds to $P$=1.5 and $f$=0.2 when the control parameter $g$ is smoothly varied, the system (Eq.(4)) starts with a chaotic motion followed by the reverse period-doubling and periodic windows. The periodic behaviour is observed for $0.7625 < g < 0.86275$. When the parameter $g$ is further increased from $g$=0.86275 one finds that the chaotic orbits persist for a range of $g$ values. At $g$=0.96472, the chaotic motion suddenly disappears and the long-time motion settles to a periodic behaviour. The bifurcation diagram corresponding to $P$=2.0 and $g \in [0, 2]$ with $f$=0.2 is shown in Fig.6(c). When the control parameter $g$ is smoothly varied, the system (Eq.(4)) starts with period-$3T$ orbit followed by a chaotic orbit, periodic bubble orbit and reverse period-doubling bifurcation. At $g$=0.96472, the chaotic motion disappears and the long-time motion settles to a periodic behaviour. Magnification of a part of the bifurcation diagram of Fig.6(c) is shown in Fig.6(d). This figure clearly shows the reverse period-doubling bifurcation, periodic bubble orbit, and chaotic orbit. For clarity, the chaotic orbit in the $(x - \dot{x})$ plane and the strange attractor in the Poincaré map of the system driven by the WBFM signal is presented in Fig.7. It is important to note that no hysteresis behaviour has been detected while checking all the bifurcation diagrams (Fig.6) in the system (Eq.(4)). But these bifurcation diagrams show
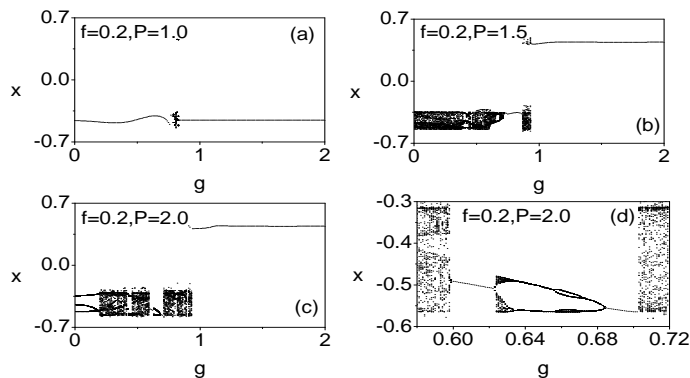
**Figure 6**: (a-c) Bifurcation diagrams for a few values of $P$ with $f = 0.2$. (d) Magnification of a part of the bifurcation diagram of Fig.6(c). The other parameters values are $\alpha = 1.0$, $\beta = 5.0$, $\gamma = 0.4$, $\Omega = 5.0$ and $\omega = 0.1$.

a great number of coexisting attractors (chaotic domain) intermingled with imbricated windows made up of periodic windows of different periodicity, period doubling of both types, periodic bubbles, reverse period doubling and sudden chaos.
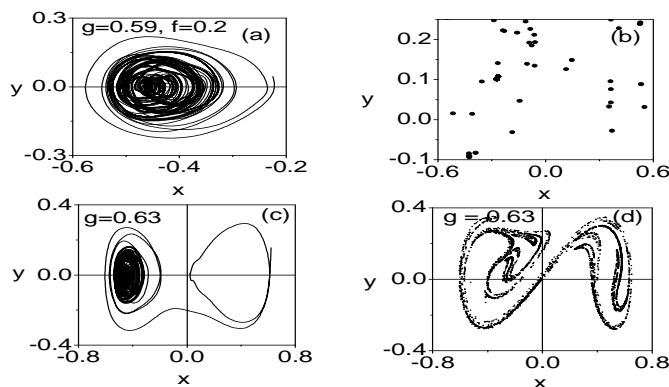


**Figure 7**: (a) One band chaotic orbit at $g = 0.59$ and (b) the double band chaotic orbit at $g = 0.63$. Ths corresponding Poincaré maps are shown in Figs.7(b) and 7(d).

### 3.2    Vibrational resonance

In order to analyze the occurrence of the VR in the system (Eq.(4)) we treat $g$ and $\Omega$ as the control parameters. The response amplitude ($Q$) is calculated from the Eq.(5a).

When the system is driven by the WBFM signal, the variation of numerically computed $Q$ with $g$ and $\Omega$ is shown in Fig.8. Fig.8(a) shows the variation of numerically computed $Q$ against the control parameter $g$ for $f=0.1$ and $P=0.1$, 0.5 and 1.0. For all the values of $P$, as $g$ increases from 0, the value of $Q$ increases and reaches a maximum value at $g = g_{VR} = 6.05$ and then decreases with further increase in $g$. For $P = 0.1$, 0.5

and 1.0, the single resonance is observed at $g = 6.05$ with different $Q_{max} = 0.541$, 0.495 and 0.5. Fig.8(b) illustrates the variation of numerically computed $Q$ with $\Omega$ for a few values of $P$. The maximum value of peak is detected at three places for $P = 0.1$ and two places at $P = 1.0$ and multiple peaks are observed for $P = 0.5$, which are clearly evident in Fig.8(b).
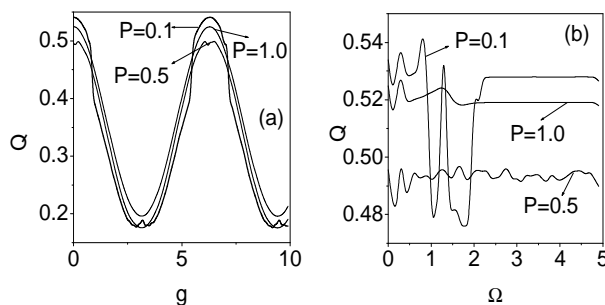


**Figure 8**: (a) Response amplitude $Q$ versus $g$ with $f = 0.1$. (b) Response amplitude $Q$ versus $\Omega$ with $f = 0.1$ for three values of $P$, namely, $P = 0.1$, 0.5, 1.0. The other parameter values are $\alpha = 1.0$, $\beta = 5.0$, $\gamma = 0.4$, $\omega = 0.1$ and $\Omega = 5.0$.

## 4    Conclusions

This paper reports the dynamics of a nonlinearly damped Duffing-Van der Pol oscillator driven by a frequency modulated signal as a function of the amplitudes of the signal and damping exponent. We considered both signals such as NBFM and WBFM to study the dynamics of the system numerically. We demonstrated the effect of the amplitudes $f$ and $g$ on the dynamics of the system with other parameters at a constant value. With the variation of the amplitudes of the signal, the system exhibits period-doubling and reverse period-doubling bifurcations, periodic windows, period bubbles, hysteresis, vibrational resonance and chaotic orbits. Our results reveal many striking departures from the behaviour of a linearly damped system with the FM signal. It is also found that the FM signal suppresses the critical chaotic behaviour in some parameter ranges. The basic properties of the dynamics of the system are analyzed by the bifurcation diagram, phase portrait, Poincaré map and resonance plot. The additional features of the system in terms of coherence resonance, parametric resonance, Ghost vibrational resonance etc, deserve further study.

## References

[1] J. Guckenheimer and P. Holmes. *Nonlinear Oscillations, Dynamical Systems and Bifurcation of Vector Fields.* Springer, New York, 1983.

[2] M. Lakshmanan and S. Rajasekar. *Nonlinear Dynamics, Integrability, Chaos and Patterns.* Springer, Berlin 2003.

[3] M. V. Sethu Meenakshi, S. Athisayanathan, V. Chinnathambi and S. Rajasekar. Horseshoe Dynamics in Fractionally Damped DVP Oscillator Driven by Nonsinusoidal forces. *Int. J. Nonlinear Science* **27** (2019) 81–94.

[4] S. Mukhopadhyay, B. Demircioglu and A. Chatterjee. Quantum Dynamics of a Nonlinear Kicked Oscillator. *Nonlinear Dynamics and Systems Theory* **11** (2) (2011) 173–182.

[5] A. K. Cheib, V. E. Puzyrov and N. V. Savchenko. Analysis of the Dynamics of a Two-degree-of-Freedom Nonlinear Mechanical System Under Harmonic Excitation. *Nonlinear Dynamics and Systems Theory* **20** (2) (2020) 168–178.

[6] K. Khachnaoni. Homoclinic Orbits For Damped Vibration System With Small Forcing Terms. *Nonlinear Dynamics and Systems Theory* **18** (1) (2018) 80–91.

[7] J. Kyziol and A. Okninski. The Duffing-Van der Pol Equation: Metamorphoses of Resonance Curves. *Nonlinear Dynamics and Systems Theory* **15** (1) (2015) 25–31.

[8] S. Gurubaran, B. R. D. Nayagam, V. Ravichandran, V. Chinnathambi and S. Rajasekar. Vibrational Resonance in the Classical Morse oscillator driven by Narrow-band and Wide-band frequency modulated signal. *J. Pure. App. Chem. Res.* **5** (3) (2016) 131–141.

[9] M. V. Sethu Meenakshi, S. Athisayanathan, V. Chinnathambi and S. Rajasekar. Effect of Narrow Band Frequency Modulated Signal on Horseshoe Chaos in Nonlinearly Damped Duffing-vander Pol Oscillator. *Annual Review of Chaos theory, Bifurcation and Dynamical Systems* **7** (2017) 41–55.

[10] V. Balashunmuga Jothi, B. Bhuvaneshwari, S. Kavitha and V. Chinnathambi. Vibrational Resonance in Two-coupled DVP oscillator Driven by FM signal. *Sadakath research journal* **6** (2019) 23–30.

[11] J. P. Baltanas, J. L. Trueba and M. A. F. Sanjuan. Energy Dissipation in a Nonlinearly Damped Duffing Oscillator. *Physica D* **159** (2001) 22–34.

[12] M. V. Sethu Meenakshi, S. Athisayanathan, V. Chinnathambi, and S. Rajasekar. Effect of Fractional Damping in Double-well DVP oscillator Driven by Different Sinusoidal Forces. DE GRUYTER, http://doi.org/10.1515/ijnsns-2016-0165, *Int. J. Nonlinear Science and Numerical Simulation* (2019) 1–10.

[13] M. Borowice, G. Litak and A. Syta. Vibration of Duffing Oscillator: Effect of Fractional Damping. *Shock vibration* **14** (2007) 29–36.

[14] K. Sun, A. Di-li Duo Li-Kun, Y. Dong, H. Wang and K. Zhong. Multiple Coexisting Attractors and Hysteresis in the Generalized Ueda Oscillator. *Mathematical Problems in Engineering* Article ID.256092, (2013) [DOI:10.1155/2013/256092].

[15] K. Abirami, S. Rajasekar, M. A. F. Sanjuan. Vibrational and Ghost Vibrational Resonance in a Modified Chua's Circuit Model Equation. *Int. J. Bifur. Chaos* **24** (2014) 1430031.

[16] S. Guruparan, V. Ravichandran, S. Selvaraj, V. Chinnathambi and S. Rajasekar. Coexistence of Multiple Attractors, Hysteresis and VR in the Classical Morse Oscillator Driven by an AM Signal. *Ukraine J. of Physics* **62** (1) (2017) 51–59.

[17] O. de Feo and G. Mario Maggio. Bifurcations in the Colpitts Oscillator from Theory to Practice. *Int. J. Bifur. Chaos* **13** (2003) 2917–2934.

[18] P. S. Landa and P. V. E. McClintock. Vibrational Resonance. *J. Phys. Math. Gen.* **33** (2000) L433–L438.

[19] M. Gitterman. A Bistable Oscillator Driven by Two Periodic Fields. *J. Phys. A: Math. Gen.* **34** (2001) L355–L358.

[20] S. Jeyakumari, V. Chinnathambi, S. Rajasekar and M. A. F. Sanjuan. Vibrational Resonance in an asymmetric Duffing Oscillator. *Int. J. Bifur. Chaos* **21** (2011) 275–286.

[21] K. Abirami, S. Rajasekar and M. A. F. Sanjuan. Vibrational Resonance in a Harmonically Trapped Potential System. *Commun. Nonlinear Sci. Numer. Simulat* **47** (2017) 370–378.

# Optimal Estimation of Unknown Data of Cauchy Problem for First Order Linear Impulsive Systems of Ordinary Differential Equations from Indirect Noisy Observations of Their Solutions

O. G. Nakonechnyi and Yu. K. Podlipenko *

*Taras Shevchenko National University of Kyiv, Kyiv, Ukraine*

**Abstract:** This paper is concerned with Cauchy problems for first-order systems of impulsive linear ordinary differential equations with unknown right-hand sides, initial conditions, and jumps of solutions at impulse points entering into the statement of these problems which are assumed to be subjected to some quadratic restrictions. From indirect noisy observations of their solutions on a finite system of intervals, optimal, in a certain sense, estimates of images of unknown data under linear continuous operators are obtained. It is shown how to apply the obtained results for finding the guaranteed estimates of unknown coefficients of the nonlinear Gompers equation which is widely used in population dynamics.

**Keywords:** *optimal estimate; guaranteed estimate; noisy observations; impulsive ordinary differential equations.*

**Mathematics Subject Classification (2010):** 34A30, 34A37, 34A55.

## 1 Introduction

In this paper, for Cauchy problems for systems of linear impulsive ordinary differential equations, we propose a novel technique of finding optimal estimates of images of their data under linear continuous operators. We assume that the right-hand sides of equations, initial conditions, and jumps of solutions at impulse points entering into the statement of these problems are unknown and belong to certain ellipsoids in the corresponding function spaces.

---

* Corresponding author: `mailto:youripodlipenko@gmail.com`

For solving such estimation problems, we need supplementary data (observations of solutions of the above Cauchy problems). By observations of unknown solutions we mean functions that are linear transformations of the same solutions distorted by additive random noises. Such a kind of observations is motivated by the fact that unknown solutions often cannot be observed directly. Here we use indirect noisy observations of solutions on a finite system of intervals.

Under the condition that unknown correlation functions of noises in observations belong to some special sets, it is established that such estimates and estimation errors are expressed explicitly via solutions of special uniquely solvable systems of linear impulsive ordinary differential equations.

For this, we first solve the problem of guaranteed (minimax) estimation of values of linear functionals from the above-mentioned right-hand sides and obtain the boundary value problems, not depending on the specific form of linear functionals, that generate the guaranteed estimates. Further, we apply these results for obtaining the optimal estimates.

Notice that this work is a continuation of our earlier studies set forth in [3] and [4], where we elaborate the guaranteed (minimax) estimation method for the case of the problem of estimation of linear functionals from unknown solutions and right-hand sides of first order linear periodic systems of ordinary differential equations.

## 2  Preliminaries and Auxiliary Results

Let $\mathbb{C}$ denote the field of complex numbers, $\Lambda^*$ denote the matrix complex conjugate and transpose of a matrix $\Lambda$. Let $[t_0, T]$ be a closed interval of $\mathbb{R}$, and $\{t_i\}$ be a given strictly increasing sequence of impulse points in $(t_0, T)$ such that $t_0 < t_1 < \cdots < t_q < t_{q+1} := T$.

A Cauchy problem for a system of first order linear impulsive differential equations on $[t_0, T]$ is a problem of the form

$$\frac{dx(t)}{dt} = A(t)x(t) + B(t)f(t) \quad \text{for a.e.} \quad t \in (t_0, T], \tag{1}$$

$$\Delta x \mid_{t=t_i} = B_i x(t_i) + C_i g_i, \quad i = 1, \ldots, q, \quad x(t_0) = Cx_0, \tag{2}$$

where $A(t) = [a_{ij}(t)]$ is an $n \times n$-matrix with $a_{ij}(\cdot) \in L^2(t_0, T)$, $B(t) = [b_{ij}(t)]$ is an $n \times r$-matrix with $b_{ij}(\cdot)$ being piecewise continuous on $[0, T]$, $f(t)$ is a vector-function such that $f(t) \in \mathbb{C}^r$ and $f \in (L^2(t_0, T))^r$, $B_i$, $C_i$, $g_i$, $C$ and $x_0$ are $n \times n$, $n \times k$, $k \times 1$, $n \times m$, and $m \times 1$ constant matrices, respectively, $\Delta x(t) \mid_{t=t_i} = x(t_i^+) - x(t_i)$ denotes the jumps of $x(t)$ at the points of impulses $t_i$, with $x(t_i^+) = \lim_{t \to t_i+} x(t)$.

By a solution of this problem, we mean a function $x(t) \in \mathcal{A}$ that is left continuous, satisfies the equation (1) almost everywhere (a.e.) on $(t_0, T]$, and the conditions (2), where by $\mathcal{A}$ we denote a class of left continuous functions $y(t) \in \mathbb{C}^n$ defined on $[t_0, T]$ such that $y(\cdot) \mid_{(t_{i-1}, t_i)} \in (W_2^1(t_{i-1}, t_i))^n$, $i = 1, \ldots, q+1$. Here $W_2^1(a, b) = \{u(t) \in L^2(a, b) \text{ such that } \frac{du(t)}{dt} \in L^2(a, b)\}$.

Further we will assume that the following conditions are valid:

$$\det(E + B_i) \neq 0, \quad i = 1, \ldots, q. \tag{3}$$

Under the conditions (3), the problem (1), (2) as well as the problem

$$-\frac{dz(t; u)}{dt} = A^*(t)z(t; u) + g(t) \quad \text{for a.e.} \quad t \in [t_0, T),$$

$$\Delta z(t)\mid_{t=t_i} = -(E + B_i^*)^{-1} B_i^* z(t_i) + g_i', \quad i = 1, \ldots, q, \quad z(T) = z_0,$$

that is adjoint of nonhomogeneous problem (1), (2), are uniquely solvable for any vector-functions $f(t) \in \mathbb{C}^r$, $g(t) \in \mathbb{C}^n$ such that $f \in (L^2(t_0, T))^r$, $g \in (L^2(t_0, T))^n$ and for any vectors $g_i \in \mathbb{C}^k$, $g_i' \in \mathbb{C}^n$ $x_0 \in \mathbb{C}^m$, $z_0 \in \mathbb{C}^n$.

These assertions follow from the results contained in [6], [2], [5].

## 3  Statement of the Problem of Guaranteed Estimation of Linear Functionals Defined on Unknown Cauchy Data

Let us give the definition of guaranteed estimates of linear functionals defined on solutions to the problem (1), (2) from observations of these solutions on a finite system of intervals.

Let $\Omega_j^i$, $j = 1, \ldots, M_i$, be a given system of subintervals of $(t_{i-1}, t_i)$, $F := (f, g_1, \ldots, g_q, x_0) \in \mathcal{H} := (L^2(t_0, T))^r \times \mathbb{C}^{kq} \times \mathbb{C}^m$.

The problem is to estimate the expression

$$l(F) = \int_{t_0}^{T} (f(t), l_0(t))_r \, dt + \sum_{i=1}^{q} (g_i, a_i)_k + (x_0, a)_m \tag{4}$$

from observations of the form

$$y_j^i(t) = H_j^i(t) x(t) + \xi_j^i(t), \quad t \in \Omega_j^i, \quad j = 1, \ldots, M_i, \quad i = 1, \ldots, q+1, \tag{5}$$

in the class of estimates

$$\widehat{l(F)} = \sum_{i=1}^{q+1} \sum_{j=1}^{M_i} \int_{\Omega_j^i} (y_j^i(t), u_j^i(t))_l \, dt + c, \tag{6}$$

linear with respect to observations (5); here $x(t)$ is the state of a system described by problem (1), (2), $l_0 \in (L^2(t_0, T)^r$, $a_i \in \mathbb{C}^k$, $a \in \mathbb{C}^m$, $H_j^i(t)$ are $l \times n$ matrices with the entries that are piecewise continuous complex-valued functions on $\bar{\Omega}_j^i$, $u_j^i(t)$ are vector-functions belonging to $(L^2(\Omega_j^i))^l$, $c \in \mathbb{C}$, and by $(\cdot, \cdot)_d$ we denote the inner product in $\mathbb{C}^d$.

We suppose that the vector-function $f$ and vectors $g_1, \ldots, g_q, x_0$ are unknown and the element $F = (f, g_1, \ldots, g_q, x_0)$ belongs to the set $G_1$, where

$$G_1 = \Big\{ F \in \mathcal{H} : f \in (L^2(t_0, T))^r, g_i \in \mathbb{C}^k, x_0 \in \mathbb{C}^m,$$

$$\sum_{i=1}^{q} (Q_i(g_i - g_i^0), g_i - g_i^0)_k + (Q_0(x_0 - x_0^0), x_0 - x_0^0)_m$$

$$+ \int_{t_0}^{T} (Q(t)(f(t) - f_0(t)), f(t) - f_0(t))_r \, dt \leq 1 \Big\},$$

$\xi := (\xi_1^1(\cdot), \ldots, \xi_{M_1}^1(\cdot), \ldots, \xi_1^{q+1}(\cdot), \ldots, \xi_{M_{q+1}}^{q+1}(\cdot)) \in G_2$, where $\xi_j^i(\cdot)$ are observation errors in (5), that are realizations of random vector-functions $\xi_j^i(t) = \xi_j^i(\omega, t) \in \mathbb{C}^l$, and $G_2$ denotes the set of random elements $\xi$, whose components have zero means, $\mathbb{E}\xi_j^i(\cdot) =$

0, with Lebesgue square integrable second moments on $\Omega_j^i$, and unknown correlation matrices $R_j^i(t,s) = \mathbb{E}\xi_j^i(t)(\xi_j^i)^*(s)$ satisfying the condition

$$\sum_{i=1}^{q+1}\sum_{j=1}^{M_i}\int_{\Omega_j^i}\operatorname{Tr}\left[D_j^i(t)R_j^i(t,t)\right]dt \le 1, \tag{7}$$

where $f_0 \in (L^2(t_0,T))^r$ is a prescribed vector-function, $g_1^0,\dots,g_q^0 \in \mathbb{C}^k$ and $x_0^0 \in \mathbb{C}^m$ are prescribed vectors, $D_j^i(t)$ and $Q(t)$ are known Hermitian positive definite $l \times l$ and $r \times r$-matrices with entries which are complex-valued continuous functions on $\bar{\Omega}_j^i$ and $[t_0,T]$, correspondingly, $Q_i$, $i = 0,1,\dots,q$, are Hermitian positive definite matrices with constant elements for which there exist their inverse matrices $(D_j^i)^{-1}(t)$, $Q^{-1}(t)$, and $Q_i^{-1}$, $\operatorname{Tr} D := \sum_{i=1}^{l} d_{ii}$ denotes the trace of the matrix $D = \{d_{ij}\}_{i,j=1}^{l}$.

Set $u := (u_1^1(\cdot),\dots,u_{M_1}^1(\cdot),\dots,u_1^{q+1}(\cdot),\dots,u_{M_{q+1}}^{q+1}(\cdot)) \in H$, where $H := (L^2(\Omega_1^1))^l \times \cdots \times (L^2(\Omega_{M_1}^1))^l \times \dots, \times (L^2(\Omega_1^{q+1}))^l \times \cdots \times (L^2(\Omega_{M_{q+1}}^{q+1}))^l$. The norm in space $H$ is defined by

$$\|u\|_H = \left\{\sum_{i=1}^{q+1}\sum_{j=1}^{M_i}\|u_j^i(\cdot)\|_{(L^2(\Omega_j^i))^l}\right\}^{1/2}.$$

**Definition 3.1** The estimate

$$\widehat{\widehat{l(F)}} = \sum_{i=1}^{q+1}\sum_{j=1}^{M_i}\int_{\Omega_j^i}(y_j^i(t),\hat{u}_j^i(t))_l\,dt + \hat{c},$$

in which vector-functions $\hat{u}_j^i(\cdot)$, and a number $\hat{c}$ are determined from the condition

$$\inf_{u \in H, c \in \mathbb{C}}\sigma(u,c) = \sigma(\hat{u},\hat{c}),$$

where

$$\sigma(u,c) = \sup_{F \in G_1,\,\xi \in G_2}\mathbb{E}|l(F) - \widehat{l(F)}|^2,$$

will be called the guaranteed (minimax) estimate of expression (4). The quantity

$$\sigma := \{\sigma(\hat{u},\hat{c})\}^{1/2}$$

will be called the error of the guaranteed estimation of $l(F)$.

Thus, a guaranteed estimate is an estimate minimizing the maximal mean-square estimation error calculated for the worst-case realization of the perturbations.

## 4   Representations for Guaranteed Estimates and Estimation Errors of $l(F)$

In this section we deduce equations that generate the minimax estimates.

For any fixed $u \in H$, introduce the vector-function $z(t;u)$ as a unique solution to the problem

$$-\frac{dz(t;u)}{dt} = A^*(t)z(t;u) - \sum_{i=1}^{q+1}\sum_{j=1}^{M_i}\chi_{\Omega_j^i}(t)(H_j^i)^*(t)u_j^i(t) \quad \text{for a.e.} \quad t \in [t_0,T), \tag{8}$$

$$\Delta z(t;u)\,|_{t=t_i} = -(E + B_i^*)^{-1} B_i^* z(t_i;u), \quad i = 1, \ldots, q, \quad z(T;u) = 0, \qquad (9)$$

where

$$\chi_\Omega(t) = \begin{cases} 1 & \text{if } t \in \Omega, \\ 0 & \text{if } t \notin \Omega \end{cases}$$

is a characteristic function of the set $\Omega$.

The unique solvability of this problem follows from condition (3).

**Lemma 4.1** *Finding the minimax estimate of functional $l(F)$ is equivalent to the problem of optimal control of the system (8), (9) with the cost function*

$$I(u) = \int_{t_0}^T (Q^{-1}(t)(B^*(t)z(t;u) + l_0(t)), B^*(t)z(t;u) + l_0(t))_r dt$$

$$+ \sum_{i=1}^q (Q_i^{-1}(C_i^*(E + B_i^*)^{-1} z(t_i;u) + a_i), C_i^*(E + B_i^*)^{-1} z(t_i;u) + a_i)_k$$

$$+ (Q_0^{-1}(a + C^* z(t_0;u)), a + C^* z(t_0;u))_m$$

$$+ \sum_{i=1}^{q+1} \sum_{j=1}^{M_i} \int_{\Omega_j^i} ((D_j^i)^{-1}(t)u_j^i(t), u_j^i(t))_l dt \to \inf_{u \in H}. \quad (10)$$

***Proof.*** Let $x$ be a solution to problem (1), (2). From (4)$-$(6), we obtain

$$\widehat{l(F)} = \sum_{i=1}^{q+1} \sum_{j=1}^{M_i} \int_{\Omega_j^i} (y_j^i(t), u_j^i(t))_l dt + c$$

$$= \sum_{i=1}^{q+1} \int_{t_{i-1}}^{t_i} (x(t), \sum_{j=1}^{M_i} \chi_{\Omega_j^i}(t)(H_j^i)^*(t)u_j^i(t))_n dt + \sum_{i=1}^{q+1} \sum_{j=1}^{M_i} \int_{\Omega_j^i} (\xi_j^i(t), u_j(t))_l dt + c.$$

Transform the first term in the right-hand side of this equality. Applying the integration by parts formula, we have

$$\sum_{i=1}^{q+1} \int_{t_{i-1}}^{t_i} (x(t), \sum_{j=1}^{M_i} \chi_{\Omega_j^i}(t)(H_j^i)^*(t)u_j^i(t))_n dt = -\sum_{i=1}^{q+1} \int_{t_{i-1}}^{t_i} \left(x(t), -\frac{dz(t;u)}{dt} - A^*(t)z(t;u)\right)_n dt$$

$$= -\sum_{i=1}^{q+1} \left((x(t_{i-1}^+), z(t_{i-1}^+;u))_n - (x(t_i), z(t_i;u))_n\right) - \sum_{i=1}^{N+1} \int_{t_{i-1}}^{t_i} \left(\frac{dx(t)}{dt} - A(t)x(t), z(t;u)\right)_n dt$$

$$= -(x(t_0), z(t_0;u))_n$$

$$- \sum_{i=1}^q (C_i g_i, (E + B_i^*)^{-1} z(t_i))_n - \sum_{i=1}^{q+1} \int_{t_{i-1}}^{t_i} \left(B(t)f(t), z(t;u)\right)_n dt.$$

Here we have used the fact that

$$\sum_{i=1}^{q+1} \left((x(t_{i-1}^+), z(t_{i-1}^+;u))_n - (x(t_i), z(t_i;u))_n\right)$$

$$= (x(t_0), z(t_0; u))_n + \sum_{i=1}^{q} \Big( (x(t_i^+), z(t_i^+; u))_n - (x(t_i), z(t_i; u))_n \Big)$$

and

$$\sum_{i=1}^{q} \Big( (x(t_i^+), z(t_i^+; u))_n - (x(t_i), z(t_i; u))_n \Big)$$

$$= \sum_{i=1}^{q} \Big( ((E + B_i)x(t_i) + C_i g_i, (E - (E + B_i^*)^{-1} B_i^*) z(t_i; u))_n - (x(t_i), z(t_i; u))_n \Big)$$

$$= \sum_{i=1}^{q} \Big( ((E + B_i)x(t_i), (E - (E + B_i^*)^{-1} B_i^*) z(t_i; u))_n - (x(t_i), z(t_i; u))_n \Big)$$

$$+ \sum_{i=1}^{q} (C_i g_i, (E - (E + B_i^*)^{-1} B_i^*) z(t_i; u))_n$$

$$= \sum_{i=1}^{q} \Big( ((E + B_i)x(t_i), (E + B_i^*)^{-1} z(t_i; u))_n - (x(t_i), z(t_i; u))_n \Big)$$

$$+ \sum_{i=1}^{q} (C_i g_i, (E + B_i^*)^{-1} z(t_i; u))_n = \sum_{i=1}^{q} (g_i, C_i^*(E + B_i^*)^{-1} z(t_i; u))_k.$$

Since

$$l(F) = \int_{t_0}^{T} (f(t), l_0(t))_r dt + \sum_{i=1}^{q} (g_i, a_i)_k + (x_0, a)_m,$$

we get

$$l(F) - \widehat{l(F)} = \int_{t_0}^{T} (f(t), l_0(t) + B^*(t)z(t; u))_r dt + \sum_{i=1}^{q} (g_i, a_i + C_i^*(E + B_i^*)^{-1} z(t_i; u))_k$$

$$+ (x_0, a + C^* z(t_0; u))_m - \sum_{i=1}^{q+1} \sum_{j=1}^{M_i} \int_{\Omega_j^i} (\xi_j^i(t), u_j(t))_l dt - c.$$

The latter equality yields

$$\mathbb{E}[l(F) - \widehat{l(F)}] = \int_{t_0}^{T} (f(t), l_0(t) + B^*(t)z(t; u))_r dt$$

$$+ \sum_{i=1}^{q} (g_i, a_i + C_i^*(E + B_i^*)^{-1} z(t_i; u))_k + (x_0, a + C^* z(t_0; u))_m - c.$$

From here on, we apply the same reasoning as in the proof of Lemma in [4] to obtain

$$\inf_{c \in \mathbb{C}} \sup_{F \in G_1, \xi \in G_2} \mathbb{E}|l(F) - \widehat{l(F)}|^2 = I(u),$$

where $I(u)$ is determined by formula (10) and the infimum over $c$ is attained at

$$c = \int_{t_0}^{T} \left( f_0(t), l_0(t) + B^*(t)z(t;u))_r dt \right)_r dt$$

$$+ \sum_{i=1}^{q} (g_i^0, a_i + C_i^*(E + B_i^*)^{-1}z(t_i;u))_k + (x_0^0, a + C^*z(t_0;u))_m. \quad (11)$$

The proof is complete.

Further in the proof of Theorem 4.1 stated below, it will be shown that solving the optimal control problem $(8)-(10)$ is reduced to solving some system of impulsive periodic differential equations.

**Theorem 4.1** *The minimax estimate $\widehat{\widehat{l(F)}}$ of the expression $l(F)$ has the form*

$$\widehat{\widehat{l(F)}} = \sum_{i=1}^{q+1} \sum_{j=1}^{M_i} \int_{\Omega_j^i} (y_j^i(t), \hat{u}_j^i(t))_l dt + \hat{c} = l(\hat{\hat{F}}),$$

*where*

$$\hat{u}_j^i(t) = D_j^i(t)H_j^i(t)p(t), \quad i = 1,\ldots,q+1, \quad j = 1,\ldots,M_i, \quad (12)$$

$$\hat{c} = \int_{t_0}^{T} \left( f_0(t), l_0(t) + B^*(t)\hat{z}(t))_r dt \right)_r dt$$

$$+ \sum_{i=1}^{q} (g_i^0, a_i + C_i^*(E + B_i^*)^{-1}\hat{z}(t_i))_k + (x_0^0, a + C^*\hat{z}(t_0))_m,$$

$\hat{\hat{F}} := (\hat{f}, \hat{g}_1, \ldots, \hat{g}_q, \hat{x}_0)$ *with*

$$\hat{f}(t) = f_0(t) + Q^{-1}(t)B^*(t)\hat{p}(t), \quad \hat{g}_i = g_i^0 + Q_i^{-1}C_i^*(E + B_i^*)^{-1}\hat{p}(t_i), \quad i = 1\ldots,q,$$

$$\hat{x}_0 = x_0^0 + Q_0^{-1}(t)C^*\hat{p}(t_0), \quad (13)$$

$p(t)$, $\hat{z}(t)$, *and* $\hat{p}(t)$ *are determined from the solution of the systems of equations*

$$-\frac{d\hat{z}(t)}{dt} = A^*(t)\hat{z}(t) - \sum_{i=1}^{q+1} \sum_{j=1}^{M_i} \chi_{\Omega_j^i}(t)(H_j^i)^*(t)D_j^i(t)H_j^i(t)p(t) \quad \text{for a.e.} \quad t \in [t_0, T), \quad (14)$$

$$\Delta\hat{z}(t) \mid_{t=t_i} = -(E + B_i^*)^{-1}B_i^*\hat{z}(t_i), \quad i = 1,\ldots,q, \quad \hat{z}(T) = 0, \quad (15)$$

$$\frac{dp(t)}{dt} = A(t)p(t) + B(t)Q^{-1}(t)(B^*\hat{z}(t) + l_0(t)) \quad \text{for a.e.} \quad t \in (t_0, T], \quad (16)$$

$$\Delta p(t) \mid_{t=t_i} = B_i p(t_i) + C_i Q_i^{-1}(C_i^*(E + B_i^*)^{-1}\hat{z}(t_i) + a_i),$$

$$i = 1,\ldots,q, \quad p(t_0) = CQ_0^{-1}(C^*\hat{z}(t_0) + a) \quad (17)$$

*and*

$$-\frac{d\hat{p}(t)}{dt} = A^*(t)\hat{p}(t) - \sum_{i=1}^{q+1}\sum_{j=1}^{M_i}\chi_{\Omega_j^i}(t)(H_j^i)^*(t)D_j^i(t)[H_j^i(t)\hat{x}(t) - y_j^i(t)] \quad \text{for a.e. } t \in [t_0, T],$$

(18)

$$\Delta\hat{p}(t)\mid_{t=t_i} = -(E + B_i^*)^{-1}B_i^*\hat{p}(t_i), \quad i = 1, \ldots, q, \quad \hat{p}(T) = 0, \tag{19}$$

$$\frac{d\hat{x}(t)}{dt} = A(t)\hat{x}(t) + B(t)(Q^{-1}(t)B^*(t)\hat{p}(t) + f_0(t)) \quad \text{for a.e. } t \in (t_0, T], \tag{20}$$

$$\Delta\hat{x}(t)\mid_{t=t_i} = B_i\hat{x}(t_i) + C_iQ_i^{-1}(C_i^*(E + B_i^*)^{-1}\hat{p}(t_i) + g_i),$$
$$i = 1, \ldots, q, \quad \hat{x}(t_0) = CQ_0^{-1}(C^*\hat{p}(t_0) + x_0^0), \tag{21}$$

*respectively. Problems* (14) – (17) *and* (18) – (21) *are uniquely solvable. Equations* (18) – (21) *are fulfilled with probability* 1.

The minimax estimation error $\sigma$ is determined by the formula

$$\sigma = [l(\hat{P})]^{1/2}, \tag{22}$$

*where*

$$\hat{P} = \Big(Q^{-1}(\cdot)(l_0(\cdot) + B^*(\cdot)\hat{z}(\cdot)), Q_1^{-1}(C_1^*(E + B_1^*)^{-1}\hat{z}(t_1) + a_1),$$
$$\ldots, Q_q^{-1}(C_q^*(E + B_q^*)^{-1}\hat{z}(t_q) + a_q), Q_0^{-1}(C^*\hat{z}(t_0) + x_0^0)\Big).$$

**Proof.** It is not difficult to verify, using the representation (1.21) from [2], that $I(u)$ is a weakly lower semicontinuous strictly convex functional on $H$. Therefore, since

$$I(u) \geq \sum_{i=1}^{q+1}\sum_{j=1}^{M_i}\int_{\Omega_j^i}((D_j^i)^{-1}(t)u_j^i(t), u_j^i(t))_l dt \geq c\|u\|_H^2 \quad \forall u \in H, \text{ c=const,}$$

by Theorems 13.2 and 13.4 (see [1]), there exists one and only one element $\hat{u} \in H$ such that $I(\hat{u}) = \inf_{u \in H} I(u)$. Hence, for any fixed $v \in H$ and $\tau \in \mathbb{R}$, the functions $s_1(\tau) := I(\hat{u} + \tau v)$ and $s_2(\tau) := I(\hat{u} + i\tau v)$ reach their minimums at a unique point $\tau = 0$ so that

$$\frac{1}{2}\frac{d}{d\tau}I(\hat{u} + \tau v)\Big|_{\tau=0} = 0 \quad \text{and} \quad \frac{1}{2}\frac{d}{d\tau}I(\hat{u} + i\tau v)\Big|_{\tau=0} = 0, \tag{23}$$

where $i = \sqrt{-1}$. Since $z(t; \hat{u} + \tau v) = z(t; \hat{u}) + \tau z(t; v)$ and $z(t; \hat{u} + i\tau v) = z(t; \hat{u}) + i\tau z(t; v)$, from (10) and (23), we obtain

$$0 = \int_{t_0}^T \Big(Q^{-1}(t)(B^*(t)z(t; \hat{u}) + l_0(t)), B^*(t)z(t; v)\Big)_r dt + (Q_0^{-1}(C^*z(t_0; \hat{u}) + a), C^*z(t_0; v))_m$$

$$+ \sum_{i=1}^q (Q_i^{-1}(C_i^*(E + B_i^*)^{-1}z(t_i; \hat{u}) + a_i), C_i^*(E + B_i^*)^{-1}z(t_i; v))_k$$

$$+ \sum_{i=1}^{q+1}\sum_{j=1}^{M_i}\int_{\Omega_j^i}((D_j^i)^{-1}(t)\hat{u}_j^i(t), v_j^i(t))_l dt. \tag{24}$$

Let $p(t)$ be a solution of the problem

$$\frac{dp(t)}{dt} = A(t)p(t) + B(t)Q^{-1}(t)(B^*z(t;\hat{u}) + l_0(t)) \quad \text{for a.e.} \quad t \in (t_0, T],$$

$$\Delta p(t)\,|_{t=t_i} = B_i p(t_i) + C_i Q_i^{-1}(C_i^*(E + B_i^*)^{-1}\hat{z}(t_i;\hat{u}) + a_i),$$
$$i = 1, \dots, q, \quad p(t_0) = CQ_0^{-1}(C^*\hat{z}(t_0) + a).$$

Taking this into account, transform the first summand in the right-hand side of (24). We have

$$\int_{t_0}^T \left(Q^{-1}(t)(B^*(t)z(t;\hat{u}) + l_0(t)), B^*(t)z(t;v)\right)_r dt = \sum_{i=1}^{q+1} \int_{t_{i-1}}^{t_i} \left(\frac{dp(t)}{dt} - A(t)p(t), z(t;v)\right)_n dt$$

$$= \sum_{i=1}^{q+1} \left((p(t_i), z(t_i;v))_n - (p(t_{i-1}^+), z(t_{i-1}^+;v))_n\right) - \sum_{i=1}^{q+1} \int_{t_{i-1}}^{t_i} \left(p(t), \frac{dz(t;v)}{dt} + A^*(t)z(t;v)\right)_n dt$$

$$= -\sum_{i=1}^{q}(Q_i^{-1}(C_i^*(E + B_i^*)^{-1}z(t_i;\hat{u}) + a_i), C_i^*(E + B_i^*)^{-1}z(t_i;v))_k,$$

$$-(Q_0^{-1}(C^*z(t_0;\hat{u}) + a), C^*z(t_0;v))_m - \int_{t_0}^T \left(p(t), \sum_{i=1}^{q+1}\sum_{j=1}^{M_i} \chi_{\Omega_j^i}(t)(H_j^i)^*(t)v_j^i(t)\right)_n dt. \quad (25)$$

From (24) and (25), we find

$$\sum_{i=1}^{q+1}\sum_{j=1}^{M_i} \int_{\Omega_j^i} ((D_j^i)^{-1}(t)\hat{u}_j^i(t), v_j^i(t))_l dt = \sum_{i=1}^{q+1}\sum_{j=1}^{M_i} \int_{\Omega_j^i} (p(t), (H_j^i)^*(t)v_j^i(t))_n dt$$

for any $v := (v_1^1(\cdot), \dots, v_{M_1}^1(\cdot), \dots, v_1^{q+1}(\cdot), \dots, v_{M_{q+1}}^{q+1}(\cdot)) \in H$, whence $\hat{u}_j^i(t)$, $i = 1, \dots, q+1$, $j = 1, \dots, M_i$, are defined by (12). Setting $u = \hat{u}$ in (11), (8) and (9) and denoting $\hat{z}(t) = z(t;\hat{u})$, we see that $\hat{z}(t)$ and $p(t)$ satisfy system (14) – (17); the unique solvability of this system follows from the fact that the functional $I(u)$ has one minimum point $\hat{u}$.

Now let us establish that $\sigma = [l(\hat{P})]^{1/2}$. Substituting expression (12) into (10), we obtain

$$\sigma^2 = \int_{t_0}^T (Q^{-1}(t)(B^*(t)\hat{z}(t) + l_0(t)), B^*(t)\hat{z}(t) + l_0(t))_r dt + (Q_0^{-1}(a + C^*\hat{z}(t_0)), a + C^*\hat{z}(t_0))_m$$

$$+ \sum_{i=1}^{q}(Q_i^{-1}(C_i^*(E + B_i^*)^{-1}\hat{z}(t_i) + a_i), C_i^*(E + B_i^*)^{-1}\hat{z}(t_i) + a_i)_k$$

$$+ \sum_{i=1}^{q+1}\sum_{j=1}^{M_i} \int_{\Omega_j^i} (H_j^i(t)p(t), D_j^i(t)H_j^i(t)p(t))_l dt. \quad (26)$$

However,

$$\int_{t_0}^T (Q^{-1}(t)(B^*(t)\hat{z}(t) + l_0(t)), B^*(t)\hat{z}(t))_r dt = \sum_{i=1}^{q+1} \int_{t_{i-1}}^{t_i} \left(\frac{dp(t)}{dt} - A(t)p(t), \hat{z}(t)\right)_n dt$$

$$= \sum_{i=1}^{q+1} \Big( (p(t_i), \hat{z}(t_i))_n - (p(t_{i-1}^+), \hat{z}(t_{i-1}^+))_n \Big) - \sum_{i=1}^{q+1} \int_{t_{i-1}}^{t_i} \Big( p(t), \frac{d\hat{z}(t)}{dt} + A^*(t)\hat{z}(t) \Big)_n dt$$

$$= - \sum_{i=1}^{q} Q_i^{-1} (C_i^*(E + B_i^*)^{-1}\hat{z}(t_i) + a_i), C_i^*(E + B_i^*)^{-1}\hat{z}(t_i))_k$$

$$-(Q_0^{-1}(C^* z(t_0; \hat{u}) + a), C^* z(t_0; v))_m - \sum_{i=1}^{q+1} \sum_{j=1}^{M_i} \int_{\Omega_j^i} (H_j^i(t)p(t), D_j^i(t)H_j^i(t)p(t))_l dt.$$

From here and from (26) it follows (22).

The representation $\widehat{\overline{l(F)}} = l(\hat{F})$ can be proved in much the same way as the representation

$$\widehat{\overline{l(F)}} = \sum_{i=1}^{q+1} \sum_{j=1}^{M_i} \int_{\Omega_j^i} (y_j^i(t), \hat{u}_j^i(t))_l dt + \hat{c}.$$

This completes the proof.

**Remark 4.1** In the representation $\widehat{\overline{l(F)}} = l(\hat{F})$ of the guaranteed mean square estimate of $l(F)$, where $F := (f, g_1, \ldots, g_q, x_0)$, $\hat{F} := (\hat{f}, \hat{g}_1, \ldots, \hat{g}_q, \hat{x}_0)$ with $\hat{f}(t) = f_0(t) + Q^{-1}(t)B^*(t)\hat{p}(t)$, $\hat{g}_i = g_i^0 + Q_i^{-1}C_i^*(E+B_i^*)^{-1}\hat{p}(t_i)$, $i = 1 \ldots, q$, $\hat{x}_0 = x_0^0 + Q_0^{-1}(t)C^*\hat{p}(t_0)$, the vector-function $\hat{f}(t)$ and vectors $\hat{g}_i$, and $\hat{x}_0$ do not depend on a specific form of the functional $l$.

## 5   Optimal Estimation Problem of Unknown Cauchy Data

Now consider the problem of finding the optimal estimate of the vector $g = LF$ among the estimates of the form

$$\hat{g} = \sum_{i=1}^{q+1} \sum_{j=1}^{M_i} U_j^i y_j^i(\cdot) + C; \tag{27}$$

here $y_j^i(\cdot)$ are observations (5), $L$ is a linear continuous operator acting from the space $\mathcal{H}$ into a separable complex Hilbert space $V$ with the inner product $(\cdot, \cdot)$ and the norm $\|\cdot\|$, $U_j^i$ are linear continuous operators acting from $(L^2(\Omega_j^i))^l$ to $V$, $C \in V$.

Let $\{e_1, e_2, \ldots\}$ be an orthonormal basis of $V$. Denote by $\sigma_1(U, C)$ and $\sigma_2(U, C)$ the quantities defined by

$$\sigma_1(U, C) = \sup_{G_1, G_2} \mathbb{E}\|g - \hat{g}\|^2$$

and

$$\sigma_2(U, C) = \sum_{k=1}^{\infty} \sup_{G_1, G_2} \mathbb{E}|(g - \hat{g}, e_k)|^2,$$

respectively, where $U := (U_1^1, \ldots, U_{M_1}^1, \ldots, U_1^{q+1}, \ldots, U_{M_{q+1}}^{q+1})$, $G_1$ and $G_2$ are defined on page 483.

**Definition 5.1** The estimates $\hat{\hat{g}}_1$ and $\hat{\hat{g}}_2$, which are determined from the condition

$$\hat{\hat{g}}_i \in \text{Argmin}_{\hat{g} \in \mathcal{L}} \sigma_i(U, C),$$

are called the guaranteed and optimal estimate of $g$, respectively, where by $\mathcal{L}$ we denote the set of all estimates of the form (27).

Parseval's formula implies that the following inequality holds:

$$\sigma_1(U, C) \le \sigma_2(U, C).$$

**Lemma 5.1** *Suppose that, for an arbitrary vector $e \in V$, there holds the equality*

$$\inf_{\overline{(g,e)}} \sup_{G_1, G_2} \mathbb{E}|(g, e) - \widehat{(g, e)}|^2 = \sup_{G_1, G_2} \mathbb{E}|(g, e) - \widehat{\overline{(g, e)}}|^2,$$

*where $\widehat{\overline{(g, e)}} = (\hat{g}, e)$, $\hat{g}$ does not depend on the vector $e$, and $\widehat{(g, e)}$ is a linear estimate of the inner product $(g, e)$. Then the vector $\hat{g}$ is the optimal estimate of the vector $g$.*

**Proof.** Notice that

$$\inf_{\hat{g} \in \mathcal{L}} \sigma_2(U, C) = \inf_{\hat{g} \in \mathcal{L}} \sum_{k=1}^{\infty} \sup_{G_1, G_2} \mathbb{E}|(g - \hat{g}, e_k)|^2 \ge \sum_{k=1}^{\infty} \inf_{\overline{(g, e_k)}} \sup_{G_1, G_2} \mathbb{E}|(g, e_k) - \widehat{(g, e_k)}|^2$$

$$= \sup_{G_1, G_2} \mathbb{E}|(g, e_k) - \widehat{\overline{(g, e_k)}}|^2 = \sum_{k=1}^{\infty} \sup_{G_1, G_2} \mathbb{E}|(g - \hat{\hat{g}}, e_k)|^2$$

and the lower bound is attained at $\hat{g} = \hat{\hat{g}}$. This completes the proof.

Next we obtain the optimal estimate of the element $g = LF$ using this lemma. Note first that for any $e \in V$, we have

$$(g, e) - (\hat{g}, e) = (LF, e) - \left(\sum_{i=1}^{q+1} \sum_{j=1}^{M_i} U_j^i y_j^i(\cdot) + C, e\right)$$

$$= (F, L^* e)_{\mathcal{H}} - \sum_{i=1}^{q+1} \sum_{j=1}^{M_i} \int_{\Omega_j^i} (y_j^i(t), (U_j^i)^* e(t))_n dt - (C, e)$$

$$= l(F) - \widehat{l(F)},$$

where $L^*$ and $(U_j^i)^*$ denote the adjoint operators of $L$ and $U_j^i$, respectively,

$$l(F) := (F, L^* e)_{\mathcal{H}} = \int_{t_0}^T (f(t), l_0(t))_r dt + \sum_{i=1}^{q} (g_i, a_i)_k + (x_0, a)_m,$$

with some $l_0 \in (L^2(t_0, T)^r$, $a_i \in \mathbb{C}^k$, and $a \in \mathbb{C}^m$,

$$\widehat{l(F)} := (\widehat{F, L^* e})_{\mathcal{H}} = \sum_{i=1}^{q+1} \sum_{j=1}^{M_i} \int_{\Omega_j^i} (y_j^i(t), u_j^i(t))_n dt + c,$$

where $u_j^i(t) = (U_j^i)^* e(t)$ are vector-functions belonging to $(L^2(\Omega_j^i))^l$, $c = (C, e) \in \mathbb{C}$.

By Theorem 4.1,

$$\inf_{\widehat{(F, L^* e)}_{\mathcal{H}}} \sup_{G_1, G_2} \mathbb{E}|(F, L^* e)_{\mathcal{H}} - \widehat{(F, L^* e)}_{\mathcal{H}}|^2 = \sup_{G_1, G_2} \mathbb{E}|(F, L^* e)_{\mathcal{H}} - \widehat{\overline{(F, L^* e)}}_{\mathcal{H}}|^2,$$

where $\widehat{\overline{(F, L^* e)}}_{\mathcal{H}} = (\hat{\hat{F}}, L^* e)_{\mathcal{H}}$ with $\hat{\hat{F}} := (\hat{f}, \hat{g}_1, \ldots, \hat{g}_q, \hat{x}_0)$ and $\hat{f}(\cdot), \hat{g}_1, \ldots, \hat{g}_q, \hat{x}_0$ being determined by (13). From the latter relationship and from the fact that $\hat{\hat{F}}$ does not depend on $L^* e$ (see Remark 1) it follows that the vector $\hat{g} = L\hat{F}$ satisfies the assumptions of Lemma 5.1. This proves the validity of the following assertion.

**Theorem 5.1** *The optimal estimates $\hat{\hat{F}}$ and $\hat{\hat{g}}$ of $F$ and $g = LF$ are determined by $\hat{\hat{F}} = (\hat{f}(\cdot), \hat{g}_1, \ldots, \hat{g}_q, , \hat{x}_0)$ and $L\hat{\hat{F}}$, respectively, where $\hat{f}(\cdot), \hat{g}_1, \ldots, \hat{g}_q, \hat{x}_0$ are defined by (13).*

**Remark 5.1** All the results of the paper remain valid if we assume that the components $\xi_j^i(\cdot)$ of the random elements $\xi := (\xi_1^1(\cdot), \ldots, \xi_{M_1}^1(\cdot), \ldots, \xi_1^{q+1}(\cdot), \ldots, \xi_{M_{q+1}}^{q+1}(\cdot))$ entering into the set $G_2$ are pairwise uncorrelated and satisfy the condition

$$\int_{\Omega_j^i} \mathrm{Tr}\,[D_j^i(t) R_j^i(t,t)] dt \leq 1, \quad i = 1, \ldots q+1, \quad j = 1, \ldots, M_i.$$

Let us present an example of applying the obtained results to the guaranteed estimation problem for the impulsive nonlinear differential equation.

In the population dynamics, for modeling of the processes of rapid change of the number of individuals of a population, the Gompers equation of the form

$$\frac{dx(t)}{dt} = \big(a(t) + b(t)\ln x(t)\big)x(t) \tag{28}$$

is applied. For the use of such models, it is required to know the parameters $a(t)$ and $b(t)$.

Let us show how to apply the above results, for example, for obtaining the guaranteed estimates for the function $a(t)$ by assuming that the function $b(t)$ is known and that $a(t)$ satisfies the following condition

$$\int_0^T \Big(\frac{da(t)}{dt}\Big)^2 dt \leq \gamma_T^2 \quad (\gamma_T = \mathrm{const}), \quad a(0) = 0.$$

Let the function

$$v(t) = \xi(t)x(t) \tag{29}$$

be observed on the set $(0, T) \backslash (\cup_{i=1}^q \{t_i\})$, where $\xi(t)$ is a realization of a stochastic process $\xi(t, \omega) > 0$, $x(t)$ satisfies equation (28) and the conditions

$$x(0) = 1, \quad \frac{x(t_k + 0)}{x(t_k - 0)} = c_k, \tag{30}$$

where $t_k$, $k = 1, \ldots, q$, are given impulse points such that $0 < t_1 < \cdots < t_q < T$, $c_k$ are prescribed numbers.

We will find the guaranteed estimate of the functional

$$L(a) = \int_0^T l(t)a(t)dt$$

in the class of estimates

$$\widehat{L(a)} = \int_0^T u(t)\ln v(t)dt,$$

where $l \in L^2(0, T)$ is a given function, $u \in L^2(0, T)$.

If we introduce the notation $\varphi_1(t) = \ln x(t)$, $\varphi_2(t) = a(t)$, $y(t) = \ln v(t)$, $\eta(t) = \ln \xi(t)$, then the guaranteed estimation problem of the functional $L(a)$ is reduced to the guaranteed estimation problem of the functional $L(\varphi_2)$ from the observations of the form

$$y(t) = \varphi_1(t) + \eta(t),$$

where $\varphi_1(t)$ and $\varphi_2(t)$ are found from solving the following system of linear impulsive differential equations:

$$\frac{d\varphi_1(t)}{dt} = \varphi_2(t) + b(t)\varphi_1(t) \quad \text{for a.e.} \quad t \in (0, T], \quad \varphi_1(0) = 0,$$

$$\frac{d\varphi_2(t)}{dt} = f(t) \quad \text{for a.e.} \quad t \in (0, T], \quad \varphi_2(0) = 0,$$

$$\varphi_1(t_k + 0) = \varphi_1(t_k - 0) + \ln c_k, \quad k = 1, \ldots, q,$$

$$\varphi_2(t_k + 0) = \varphi_2(t_k - 0), \quad k = 1, \ldots, q,$$

where $f(t) = \frac{da(t)}{dt}$.

Under certain restrictions on the correlation function of the process $\eta(t)$, we can apply the results of the present paper for obtaining the guaranteed estimates of the parameter $a(t)$.

## 6 Conclusion

The method proposed in the present paper enables one to obtain the optimal estimates of unknown data of Cauchy problems for first-order linear impulsive systems of ordinary differential equations from noisy observations of their solutions.

We deduce the boundary value problems for linear impulsive ordinary differential equations of the special kind that generate the optimal estimates.

The results presented above are aimed at elaborating mathematically justified estimation techniques for various forward and inverse problems with uncertainties describing evolution processes characterized by the combination of a continuous and abrupt change of their state.

## References

[1] I. B. Badriev and M. M. Karchevsky. *Duality Methods in Applied Problems.* Publ. of Kazan State University, Kazan, 1987.

[2] D. D. Bainov and P. S. Simeonov. *Impulsive Differential Equations. Asymptotic Properties of the Solutions.* World Scientifc, 1995.

[3] O. G. Nakonechny and Yu. K. Podlipenko. The minimax approach to the estimation of solutions to first order linear systems of ordinary differential periodic equations with inexact data. arXiv:1810.07228V1, 2018, P. 1-19.

[4] O. Nakonechnyi and Y. Podlipenko. Guaranteed Estimation of Solutions of First Order Linear Systems of Ordinary Differential Periodic Equations with Inexact Data from Their Indirect Noisy Observations. In: *Proceedings of 2018 IEEE First International Conference on System Analysis and Intelligent Computing (SAIC).*

[5] I. Rachunkova and J. Tomecek. *State-Dependent Impulses Boundary Value Problems on Compact Interval.* Atlantis Press, Amsterdam-Paris-Beijing, 2015.

[6] A. M. Samoilenko and N. A. Perestyuk. *Impulsive Differential Equations.* World Scientific, 1995.

# COVID-19 Outbreak Prediction in Indonesia Based on Machine Learning and SIRD-Based Hybrid Methods

E. R. M. Putri [1], M. Iqbal [1,*], M. L. Shahab [1], H. N. Fadhilah [1,2],
I. Mukhlash [1], D. K. Arif [1], E. Apriliani [1] and H. Susanto [3,4]

[1] *Department of Mathematics, Sepuluh Nopember of Institute Technology Kampus ITS Sukolilo-Surabaya 60111, Indonesia.*
[2] *Department of Data Science, Telkom Institute of Technology Surabaya, Jl. Ketintang No.156, Ketintang, Kec. Gayungan, Kota SBY, Jawa Timur 60231.*
[3] *Department of Mathematical Sciences, University of Essex, Wivenhoe Park, Colchester, United Kingdom, CO4 3SQ.*
[4] *Department of Mathematics, Khalifa University, Abu Dhabi Campus - PO Box 127788, Abu Dhabi, United Arab Emirates.*

**Abstract:** This paper aims to forecast and analyze the spread of COVID-19 outbreak in Indonesia by applying machine learning and hybrid approaches. We show the performance of each method, an ensemble-support vector regression (ensemble-SVR), a genetic algorithm and an SIRD model (GA-SIRD) and an extended Kalman filter, a genetic algorithm and an extended Kalman filter (EKF-GA-SIRD), in obtaining the prediction of the outbreak. The GA-SIRD model is built based on the data availability and is enhanced by employing an extended Kalman filter to better predict the spread of the outbreak. Without considering the epidemic model, the ensemble SVR can provide a higher accuracy compare to the two hybrid approaches in the case of short-term forecasting. Furthermore, the EKF-GA-SIRD can better adapt to the extreme change and shows a better performance than the GA-SIRD.

**Keywords:** *pandemic; SIRD model; Kalman filter; machine learning.*

**Mathematics Subject Classification (2010):** 70-08, 93A30.

---

\* Corresponding author: `mailto:iqbal@matematika.its.ac.id`

## 1 Introduction

The pandemic of the novel coronavirus or COVID-19 started in Wuhan, China, where the first case was reported on January 22nd, 2020, and the pandemic has spread worldwide in more than 200 countries. As China has passed through its first pandemic peak, some other countries such as the US, India, and Indonesia are still struggling to control the spread of the virus. The spread of COVID-19 in Indonesia was reported for the first time on March 2nd, 2020, in Jakarta, and currently, it reaches almost all provinces of Indonesia in less than two months. Statistical data of the outbreak in Indonesia is officially collected from `https://covid19.go.id/`.

The spread of the pandemic of novel coronavirus COVID-19 can be described mathematically in the so-called mathematics of epidemiology. There are some common models, a SIR model (Susceptible, Infected, Recovered) or a SIRD (Susceptible, Infected, Recovered, Dead), which are used by some researchers to describe the spread pattern of COVID-19. A modification of the SIR model, which includes the death variable of observation, is called a SIRD model. Some researchers have done studies about the spread of the pandemic of COVID-19 based on the SIRD model. Fanelli *et al.* [1] used the SIRD model to predict the spread of COVID-19 in China, Italy, and Iran. Parameters are estimated using stochastic differential evolution. However, inadequate accuracy is shown in the study [1] when the peak prediction is compared to the latest data. As an improvement, Susanto [2] suggested that a careful fitting of reported data to the SIR model should be done due to its sensitivity to the time-series information. Salgotra *et al.* [3] used a genetic-based algorithm for estimating the parameters. They have shown that the algorithm is highly reliable for predicting COVID-19 cases. Abdul Rahman [4] discussed machine learning to simulate the spread of COVID-19 based on the SIRD model. An error analysis and detail flow charts of the process are presented in his paper. The previous studies pointed out that the epidemic model is improved by machine learning in the parameters estimation process. Shortly, we may call the combination of the SIRD model and machine learning, a hybrid epidemic model.

In machine learning, regression models can offer promising forecasting by learning the given data set. Parbat *et al.* [5] applied *a support vector regression* to predict current and future COVID-19 cases in India without comparison to other regression models. Still with the cases in India, Sujath *et al.* [6] investigated *a linear regression* (LR), *a vector autoregression* (VA) and *a multilayer perceptron* (MLP) prediction. As to the results, the MLP showed better ones than the VA and LR. In addition, Tuli *et al.* [7] developed a real-time framework for the COVID-19 infected number prediction over the world by integrating cloud computing and machine learning. They adjusted iterative weighting on the generalized inverse Weibull distribution to have higher accuracy in the data-driven environment responding to the epidemic actively. Both the hybrid and the machine learning methods exhibit a relatively satisfying performance in predicting the spread of the COVID-19 outbreak. The use of the GA in estimating parameters of mathematical models give better performance than conventional methods [8].

Therefore, we attempt to propose new hybrid methods by integrating a genetic algorithm and a SIRD model (GA-SIRD), an extended Kalman filter (GA-EKF-SIRD) which provide a one-step updating process for predicting the spread of the outbreak in Indonesia. Furthermore, we proposed an ensemble-SVR method to forecast the COVID-19 cases without considering the SIRD model. The ensemble-SVR is a method that combines two different models under the SVR approach to tackle a limitation data on the decreasing

number of infected cases for the first time. In this study, we combine different COVID-19 case models of two countries that share similar distributions. More specifically, we focus on the COVID-19 cases in Indonesia by combining them with similar COVID-19 cases from another country, which has been through the first wave. Lastly, a comparison of the three methods is presented in this paper.

This paper is organized as follows. Section 2 and Section 3 discuss the hybrid of a genetic algorithm and a SIRD model, and accordingly, a genetic algorithm is incorporated into a hybrid of the extended Kalman filter and the SIRD model. We propose the use of the ensemble-SVR model in Section 4, respectively. Simulation and discussion are presented in Section 5 and conclusion is given in Section 6.

## 2   A Modified Extended Kalman Filter-SIRD Model

A SIRD model describes the evolution of an individual into classes: susceptible, infected, recovered, and dead. It is assumed that individuals in the same class have the same characteristics and the movement of individuals in the same class can be described. The infected individuals can recover without the possibility of being reinfected. A referenced total population is assumed to be constant, which means that the population's birth rate and death rate are the same.

A differential equation of the SIRD model, which describes the movement of individuals from one class to another class, is written as

$$
\begin{aligned}
\dot{S}(t) &= -rS(t)I(t), \\
\dot{I}(t) &= rS(t)I(t) - (a+d)I(t), \\
\dot{R}(t) &= aI(t), \\
\dot{D}(t) &= dI(t),
\end{aligned}
\tag{1}
$$

where $S(t)$ describes the individuals who are at a high risk of infection, $I(t)$ describes the number of infected individuals, $R(t)$ describes the recovered individuals after being infected, and $D(t)$ describes the number of dead individuals. Then $r, a, d$ are the rate of infection, recovery, and death, respectively. The SIRD model is used in this study due to data availability in the resource website such as `https://www.worldometers.info/coronavirus/#countries`. The dynamic of the SIRD model is estimated using an extended Kalman filter method in a discrete scheme.

An extended Kalman filter (EKF) method is a method for estimating a weakly non-linear stochastic dynamic system [9] such as the epidemic SIRD model. The EKF method has three main stages: an initialization of system and measurement model including the initialization of state variables values, time updates (prediction), and measurement updates (correction). In the non-linear system, the updates equations are intractable, so that an approximation to time update and measurement update equations are required to provide a computationally viable algorithm to apply to the filter.

The EKF method provides a one-step prediction based on the SIRD model, so that it is necessary to modify the method to get a longer prediction range based on limited measurement data. The modification is to generate new measurement data, expand the limited data, and add noise to get a longer prediction. This modification can be considered as our contribution. Briefly, the basic algorithm of a modified EKF can be seen in Algorithm 2.1.

---

**Algorithm 2.1** Modified Ensemble Kalman Filter

---

1: System model : $\dot{x} = f(x, u, t) + G(t)w$
2: Measurement model : $z_n = h[x(t_n), n] + v_n$, with $x(0) \sim (\bar{x}, P_0), w(t) \sim (0, Q), v_n \sim (0, R)$

---

3: Initialization : $x(0) = \bar{x}_0, \ \hat{P}(0) = P_0, \ z_n^- = z_k$

---

### Time Update

---

4: Estimate : $\dot{x} = f(x, u, t)$
5: Error covariance : $\dot{P} = A(\hat{x}, t)P + PA^T(\hat{x}, t) + GQG^T$
6: Jacobian : $A(x, t) = \frac{\partial f(x, u, t)}{\partial x}$

---

### Measurement Update

---

7: Kalman gain : $K_n = P^-(t_n)H^T(\hat{x}_n^-)\left[H(\hat{x}_n^-)P^-(t_n)H^T(\hat{x}_n^-) + R\right]^{-1}$
8: Error covariance : $P(t_n) = [I - K_n H(\hat{x}_n^-)]P^-(t_n)$
9: Generate measurement : $z_n = z_n^- + v_n$
10: Estimate : $\hat{x}_n = \hat{x}_n^- + K_n\left[z_n - h(\hat{x}_n^-, n)\right]$
11: Jacobian : $H(x) = \frac{\partial h(x, n)}{\partial x}$

---

The number of infected, recovered, and dead individuals are predicted using the modified EKF, which is applied to the SIRD model. The Jacobian matrix, which is considered as the value of the coefficient matrix of state variable $A$, and is based on the SIRD model, is obtained in (1) with the equilibrium point $(S, I, R, D) = (\frac{a+d}{r}, 0, 0, 0)$.

$$
A = \begin{bmatrix}
1 & 0 & 0 & 0 & 0 & 0 & 0 \\
0 & 1 & 0 & 0 & 0 & 0 & 0 \\
0 & 0 & 1 & 0 & 0 & 0 & 0 \\
0 & 0 & 0 & 0 & -(a+d) & 0 & 0 \\
0 & 0 & 0 & 0 & 1 & 0 & 0 \\
0 & 0 & 0 & 0 & a & 0 & 0 \\
0 & 0 & 0 & 0 & d & 0 & 0
\end{bmatrix}. \tag{2}
$$

A discretization of the non-linear model (1) results in the following:

$$
\begin{aligned}
S_k &= -rS_k^- I_k^- \, dt + S_k^-, \\
I_k &= \left[rS_k^- I_k^- - (a+d)I_k^-\right] dt + I_k^-, \\
R_k &= aI_k^- \, dt + R_k^-, \\
D_k &= dI_k^- \, dt + D_k^-.
\end{aligned} \tag{3}
$$

Suppose we have a system model $\dot{\hat{x}}$ and a measurement model $z_k$, the estimation result $\hat{x}_k$ can be obtained using the previous EKF algorithm in [9]. For the prediction stage using the modified EKF, we define $n = k + i$, where the time step is $i = 1, 2, \ldots$. Subsequently, the initial parameter values $r_0, a_0, d_0$, and $S_0$ are estimated using the genetic algorithm. The initial real data for $I_0, R_0, D_0$, are used to give the initial values in applying the modified EKF.

## 3   A Genetic Algorithm-SIRD

### 3.1   A genetic algorithm

A genetic algorithm (GA) is an algorithm that mimics a natural evolutionary model by using a genetic inheritance [10]. Chromosomes and fitness functions should be made before applying the algorithm. The chromosomes will be a solution to the problem addressed, and the fitness functions will be a tool to measure the value of a chromosome.

The genetic algorithm begins with creating an initial population containing several chromosomes as the solution to the problem. Usually, these allegations are chosen randomly from the points scattered within the search space. Then the genetic algorithm uses crossover and mutation operators to process the chromosomes in the population until it converges or finds the best results [11].

The crossover operator allows a merging of information from two or more chromosomes to form a new chromosome. The mutation operator is used to explore the search space even further in hopes of obtaining better chromosomes. A new population will be formed after the crossover and mutation have been applied to chromosomes in the initial population. Accordingly, a generation of the new population will increase by one level. The crossover and mutation processes continue until a certain number of iterations is exceeded or the termination criteria are met [11].

A genetic algorithm - SIRD (GA-SIRD) uses the SIRD model on daily data classified as the infected individual $I$, recovered individual $R$, and deceased individual $D$, which is solved by the genetic algorithm. In this study, we used the Indonesia daily data from March 2, 2020 until August 25, 2020 to obtain the initial values of $S_0, I_0, R_0$, and $D_0$, and the parameter values of $r, a$, and $d$.

Stages of the genetic algorithm - SIRD consist of:

1. Input
   The input used in the genetic algorithm is the daily data $I, R$, and $D$ from Indonesia, which starts from March 2, 2020 to August 25, 2020 (176 days). Next, the values will be called actual $I_k, R_k, D_k$ with $k = 1, 2, \ldots, n$ and $n = 176$. Finally, these values will be used in the process of calculating the fitness value of a chromosome.

2. Chromosome
   In this study, we used chromosomes in the form $x = (x_1, x_2, \ldots, x_7) \in \mathbb{R}^7$. Each element of $x$ represents one parameter of the SIRD model, which is $x_1 = S_0$, $x_2 = I_0$, $x_3 = R_0$, $x_4 = D_0$, $x_5 = r$, $x_6 = a$, and $x_7 = d$. In this genetic algorithm, we use an initial population with 100 chromosomes that are made randomly over a certain range.

3. Fitness Function
   The purpose of the genetic algorithm is to find a chromosome that minimizes the difference between the actual $I_k$, $R_k$, $D_k$ and predicted $I_k$, $R_k$, $D_k$. To obtain the predicted $I_k$, $R_k$, $D_k$, we use the discretization model (3) for $k = 1, \ldots, n-1$. For $k = 0$, we use $S_1 = S_0$, $I_1 = I_0$, $R_1 = R_0$, $D_1 = D_0$. In this case, because the data used is daily data, we use $\Delta t = 1$. Suppose $x = (x_1, x_2, \ldots, x_7)$ is the chromosome for which the fitness function is calculated. Using $S_0 = x_1$, $I_0 = x_2$, $R_0 = x_3$, $D_0 = x_4$, $r = x_5$, $a = x_6$, and $d = x_7$, we can calculate the predicted $S_k, I_k, R_k$, $D_k$ for $k = 1, 2, \ldots, n$. After we get the prediction of $I_k, R_k, D_k$ for $k = 1, 2, \ldots, n$,

we calculate the difference with the actual $I_k$, $R_k$, $D_k$ using the RMSE (Root Mean Square Error). Suppose that the predicted $I_k$, $R_k$, $D_k$ are symbolized by $\hat{I}_k$, $\hat{R}_k$, $\hat{D}_k$, then the fitness function of $x$ is

$$RMSE(x) = \sqrt{\frac{\sum_{k=1}^{n}(\hat{I}_k - I_k)^2 + (\hat{R}_k - R_k)^2 + (\hat{D}_k - D_k)^2}{3n}}.$$

The final solution of the genetic algorithm is a chromosome in the population that has the smallest RMSE (fitness function) value.

4. Crossover
The purpose of this kind of crossover is to take all the profits and get rid of all the losses. With this step, it can guarantee that the new chromosome is definitely better than or the same as the previous chromosome.

5. Mutation
A mutation is performed on chromosomes in the population with a pm chance. For example, $x = (x_1, x_2, \ldots, x_7) \in \mathbb{R}^7$ is the chromosome to be mutated. First, we calculate the fitness function of $x$. Then $x_1$ at $x$ is replaced with $x_1 + \epsilon$, where $-\frac{1}{2(u+1)} < \epsilon < \frac{1}{2(u+1)}$ and $u$ is the current generation of the genetic algorithm. Then the fitness function from the new $x$ is calculated. If the fitness function is better, then $x_1 + \epsilon$ is used to replace $x_1$. If the fitness function is worse, then $x_1 + \epsilon$ is replaced again with x1. Next, the same operation/step is performed on $x_2$, $x_3$, $\ldots$, $x_n$. This step can be guaranteed that the new chromosome is better than or the same as the previous chromosome.

### 3.2 SIRD optimal parameters based on the genetic algorithm

The genetic algorithm has several main parameters, for example, the number of chromosomes, the number of iterations, and the chance of mutations. These parameters can vary depending on the complexity of the problem. Selection of the interval in the determination of search space (domain) also dramatically affects the final results of the genetic algorithm. The wider the search space created, the more difficult the genetic algorithm for converging. Conversely, a too-small search space often results in genetic algorithms not converging to the optimum solution.

In this study, we initialize the number of chromosomes is 100, the number of iterations is 10000, and the minimum value of each element in a chromosome is 0. Moreover, the maximum value of each element can be seen in Table 1. Those intervals are obtained by

**Table 1**: The maximum value of each element in a chromosome.

| Parameter | Maximum Value |
|:---:|:---:|
| $x_1$ | 1000000 |
| $x_2$ | 1000 |
| $x_3$ | 100 |
| $x_4$ | 1000 |
| $x_5$ | $10^{-5}$ |
| $x_6$ | $10^{-1}$ |
| $x_7$ | $10^{-2}$ |

conducting several trials. In addition, we use $p_m = 1$ since there is a guarantee that the new chromosome obtained from the mutation is better than or the same as the previous chromosome.

Based on the steps explained before, we have found the best parameters for the SIRD model that fit actual data of the infected $I$, recovered $R$, and deceased $D$ individuals. The results obtained from the genetic algorithm are shown in Table 2. With those values, we will get a good enough SIRD model, where RMSE is equal to 836.0047.

**Table 2**: The parameters found by the genetic algorithm.

| Parameter | Value |
|-----------|-------|
| $S_0$ | 221269.8187 |
| $I_0$ | 305.9698464 |
| $R_0$ | 0 |
| $D_0$ | 433.6840396 |
| $r$ | 3.57028E-07 |
| $a$ | 0.033376181 |
| $d$ | 0.0024362 |

## 4   An Ensemble Model-SVR

Machine learning has three major learning problems such as: (1) supervised learning, (2) unsupervised learning and (3) reinforcement learning. In supervised learning, input data will be mapped to a particular output value. Supervised learning comprises two tasks: classification for categorical values and regression for continuous values based on the output domain. Following the nature of this application, we focus on regression. A bunch of regression models in machine learning has succeeded in solving many real-world problems, e.g., electricity consumption forecasting [12], electric load forecasting [13], a bus passenger forecasting [14], and high-frequency stock return forecasting [15].

In general, we may have difficulty stating the best regression model, which depends on the domain of applications. Hence, a study on model comparison is an essential step when dealing with a new problem. For instance, particular five regression models reviewed on electricity consumptions showing that a Linear Regression (LR) has better accuracy [12] and selected six supervised methods compared for a residential energy consumption prediction indicating the accurate one is a Gradient Boosting [16]. Moreover, one of the well-known regression models is a Support Vector Regression (SVR). The method was introduced by Harris Drucker *et al.* in 1996 [17]. The SVR is an extended version of a Support Vector Machine (SVMs)[1]. Hence, the procedure in SVR is similar to the SVM, with the main difference on the target function called the *regressor*.

Let $\mathsf{X} = \{\mathsf{x}_1, \ldots, \mathsf{x}_{|\mathsf{X}|}\}$ be an input set that consists of $\mathsf{x} = (i_n, r_n, d_n)$ and $1 \leq n \leq t$ and $\mathsf{Y} = \{\mathsf{y}_1, \ldots, \mathsf{y}_{|\mathsf{Y}|}\}$ be an output set that contains prediction results, $\mathsf{y} = (i_m, r_m, d_m), t + 1 \leq m \leq T$. In this study, $i_n$ and $i_m$ represent the number of infected cases, $r_n$ and $r_m$ represent the number of recovered cases, and $d_n$ and $d_m$ represent the number of death cases. We want to find three functions $f_i, f_r$ and $f_d$ for each COVID-19 case. For simplification, we will map each feature of $\mathsf{x}$ to a certain value of $\mathsf{y}$, $\mathbf{f} : \mathsf{X} \rightarrow \mathsf{Y}$. Considering on linear problems, we have $\mathbf{f} = w \cdot \mathsf{x} + b$ with $w$ and $b$ being the weight and

---

[1] A SVM is one of the classification models in machine learning.

bias parameters, respectively. In the SVR, we want to obtain support vectors which are close to $\mathbf{f}$. To do so, we create two margins that are close enough to $\mathbf{f}$ by minimizing the norm-value of $w \cdot w^T$. The problem can be formulated as a convex optimization below:

$$
\begin{aligned}
\text{minimize} \quad & \frac{1}{2} w \cdot w^T = \min \frac{1}{2} \|w\| \\
\text{subject to} \quad & \mathsf{y} - w \cdot \mathsf{x} - b \le \epsilon, \\
& w \cdot \mathsf{x} + b - \mathsf{y} \le \epsilon.
\end{aligned}
\tag{4}
$$

To deal with infeasible constraints, we add slack variables $\zeta$ and $\zeta'$ for each point called *the soft margin*. As a result, (4) can be written as a primal formula as follows:

$$
\begin{aligned}
\text{minimize} \quad & \mathcal{J}(w) = \frac{1}{2} w \cdot w^T + C \sum (\zeta + \zeta'); \\
\text{subject to} \quad & \mathsf{y} - w \cdot \mathsf{x} - b \le \epsilon + \zeta, \\
& w \cdot \mathsf{x} + b - \mathsf{y} \le \epsilon + \zeta', \\
& \zeta, \zeta' \ge 0,
\end{aligned}
\tag{5}
$$

where $C$ is a positive numeric value that assists in avoiding overfitting. Furthermore, we use the Lagrange dual formulation to save the computational time on solving the problem in (5). Let $\alpha$ and $\alpha'$ be non-negative multipliers. The dual formulation of (5) is described as follows:

$$
\begin{aligned}
\text{minimize} \quad & \mathcal{L}(\alpha) = \frac{1}{2} \sum_{i=1}^{N} \sum_{j=1}^{N} (\alpha_i - \alpha_i')(\alpha_j - \alpha_j') \mathsf{x}_i \mathsf{x}_j' + \epsilon \sum_{i=1}^{N} (\alpha_i + \alpha_i') + \sum_{i=1}^{N} \mathsf{y}_i (\alpha_i - \alpha_i'); \\
\text{subject to} \quad & \sum (\alpha - \alpha') = 0, \\
& 0 \le \alpha \le C, \\
& 0 \le \alpha' \le C.
\end{aligned}
\tag{6}
$$

However, this study problem is considered a nonlinear one. In this case, we replace the dot product of $\mathsf{x} \cdot \mathsf{x}'$ with a kernel function $K(\mathsf{x}, \mathsf{x}')$ that transforms $\mathsf{x}$ to high-dimensional space. There are several kernel functions: linear, Gaussian (or radial basis function), and polynomial.

This part shows the COVID-19 cases predictions using several regression methods. Based on the comparison results, we use the best method to predict COVID-19 cases in Indonesia for the long term by explaining the scenario, and the result will be shown in Section 4. The data set was collected starting from March 2, 2020, until August 25, 2020. Furthermore, the data set is split into a training set $\mathcal{D}$ from the first day until the $141^{th}$ day and testing set $T$ from the $142^{st}$ day to the $176^{th}$ day. In this study, we specified the parameters of the SVR $(C, \alpha, \epsilon) = (1, 0.1, 0.1)$. We use a radial basis function as the kernel parameter. Furthermore, the SVR will be compared with a Decision Tree (DT), a K-Nearest Neighbor (KNN), a Linear Regression (LR), a Gaussian Process Regression (GPR), and a Long Short Term Memory (LSTM) with ten-time steps as the mini-batch size. We utilized a mean absolute percentage error (MAPE) below for evaluating the performance

$$
MAPE = \frac{1}{|\mathsf{X}|} \sum_{k=1}^{|T|} \left| \frac{\mathsf{x}_k - y_k}{\mathsf{x}_k} \right|.
\tag{7}
$$
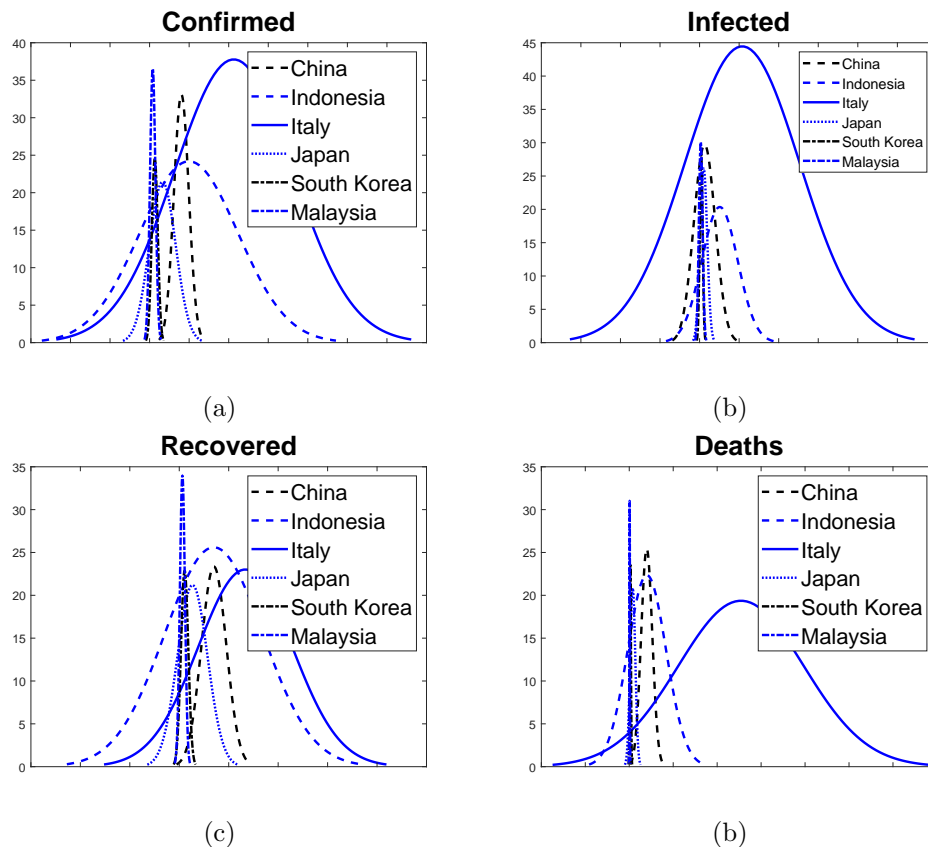
**Figure 1**: Data distribution of COVID-19 cases in several countries: (a) Confirmed cases, (b) Infected cases, (c) Recovered cases and (d) Death cases.

Overall, the GPR has better MAPE results than other models, as shown in Table 3. Both the DT and the LSTM did not display as the most accurate compared to the others. It is because the DT required a discretization step, leading to predicting the number of cases imprecisely, and the LSTM cannot update the learning parameters properly from insufficient information (only learn from small data). According to Table 3, a spatial factor is essential since some models showed different results on each country toward the cases. The GPR is dominant over others for South Korea. The SVR outperformed others for Indonesia and India. Therefore, this study further developed the SVR to forecast the spread of COVID-19 cases in Indonesia in Section 5.

In a naïve way, predicting long future data will take the output $y_{k+1}$ at each one step ahead as the one to be foreseen $y_{k+2}$. However, it might be hard to use the SVR to forecast the spread of COVID-19 in Indonesia. To the best of our knowledge, the infected case number in Indonesia is still not reduced up to August 25, 2020; thus, the SVR may provide either a sudden fall dramatically or a rise up continuously. To overcome the issue, we have drawn long-term data (after August 25, 2020) for each data class of COVID-19 in Indonesia based on some countries data distributions that have passed the peak of the

infected cases. More specifically, three countries, i.e., China, South Korea, and Malaysia, are examined. The data distribution for each data class is depicted in Figure 1.

From Figure 1(a), we can state that the number of the infected cases in Indonesia is close enough to that in South Korea and Malaysia. South Korea has no massive restrictions (or lockdowns), yet high awareness of both government and citizens plays an important role. As a result, South Korea has already passed the peak after a rapid spread (hit around 10.000 infected cases). Malaysia chose to apply a massive lockdown that has already made them pass the peak faster (less than 6000 infected cases). In addition, China is being considered in the ensemble model where the COVID-19 was first found. China was also the first country where the massive lockdown was applied to suppress the infected cases, and the country has already passed the peak of infected cases. As the population number in China is more extensive than in Indonesia, this study considers scaling on the population number when ensemble with the China COVID-19 model. The details are described in Section 5.

## 5  Simulation and Discussion

Simulation of the spread of the novel coronavirus COVID-19 in Indonesia is conducted based on official data released by the government of Indonesia and collected from `https://covid19.go.id/`. Data presented include the number of confirmed cases $N(t)$, number of infected cases $I(t)$, number of recovered cases $R(t)$, and number of death cases $D(t)$. The data is collected from March 2, 2020 until August 25, 2020. The simulation employs three methods. Firstly, an Ensemble-SVR method will be applied to the data to predict the growth of the outbreak. Secondly, a modified EKF-SIRD method and GA-SIRD method are used to describe the outbreak's dynamics.

Since the methods are applied based on the SIRD model, the number of infected cases $I(t)$ is obtained by $N(t) - R(t) - D(t)$. Infected cases data will be used as the input in variable infected $I(t)$. The initial values of the parameters $I(0)$, $R(0)$, $D(0)$ are taken from the first time step of data and, in particular, are used by the modified EKF-SIRD method. The initial value of $S(0)$, parameters $r$, $a$, and $d$ for the modified EKF-SIRD are estimated using the genetic algorithm. All parameters and the initial values are estimated using the genetic algorithm to put in the GA-SIRD method. For the Ensemble-SVR, the initial value is not required. The values are obtained directly from a random generator in the method.

The first results presented in Figure 2 are based on the Ensemble-SVR and show the prediction of COVID-19 spread for infected individuals ($I(t)$), recovered individuals ($R(t)$), and deceased individuals ($D(t)$). The simulation is conducted by, first, determining an ensemble model based on China, South Korea and Malaysia [2]. The three countries are chosen based on data characteristic analysis on the data distributions towards Indonesia data in Figure 1.

There are some differences of the simulation results based on the three countries, namely, China (see Figure 2(a)), South Korea (see Figure 2(b)), and Malaysia (see Figure 2(c)). The figures describe the possibilities of the dynamic of the outbreak as the data characteristics are similar to the Indonesia data.

The data reflects its conditions in China: many people at risk of infection and a total lockdown policy. Different policies are applied in South Korea. There is no lockdown policy but a high level of discipline in applying social distancing, mask-wearing, a vast

---

[2] Data is collected from `https://www.worldometers.info/coronavirus/#countries`.

Table 3: MAPE comparison of several regression models on COVID-19 cases prediction.

| COUNTRY | INFECTED | | | | | | DEATH | | | | | | RECOVERED | | | | | |
|---|---|---|---|---|---|---|---|---|---|---|---|---|---|---|---|---|---|---|
| | KNN | GPR | LSTM | DT | LR | SVR | KNN | GPR | LSTM | DT | LR | SVR | KNN | GPR | LSTM | DT | LR | SVR |
| CHINA | 0.1448 | **0.1368** | 0.2421 | 0.3515 | 25.8119 | 6.7098 | 0 | 0.0001 | 0.9985 | 0.00025 | 0.2083 | 0.0383 | 0.0113 | **0.00098** | 0.9736 | 0.002 | 0.0544 | 0.0544 |
| SOUTH KOREA | 0.1324 | **0.0172** | 0.8479 | 0.0949 | 1.562 | 0.2223 | 0.0358 | **0.0053** | 0.9885 | 0.0413 | 0.1233 | 0.0639 | 0.0419 | **0.0011** | 0.5792 | 0.0566 | 0.1384 | 0.0565 |
| ITALY | 0.1371 | 0.1256 | 0.9968 | 0.1592 | 1.0285 | **0.0846** | 0.0435 | **0.0031** | 0.9993 | 0.0544 | 0.0274 | 0.0551 | 0.1935 | **0.0054** | 0.9964 | 0.2408 | 0.1387 | 0.0215 |
| MALAYSIA | 0.1182 | **0.0798** | 0.9009 | 0.1174 | 0.3738 | 0.0946 | 0.0328 | **0.0034** | 0.9823 | 0.0403 | 0.1384 | 0.0481 | 0.1524 | 0.0536 | 0.0312 | 0.1658 | 0.0562 | **0.0481** |
| INDONESIA | 0.3106 | 0.0541 | 0.9938 | 0.3561 | 0.1146 | **0.0305** | 0.3062 | 0.0701 | 0.9877 | 0.3672 | 0.2746 | **0.0222** | 0.5379 | 0.7188 | 0.933 | 0.5945 | 0.1001 | **0.008** |
| SPANYOL | 0.0343 | **0.0084** | 0.9979 | 0.0305 | 0.3207 | 0.0091 | 0.0104 | **0.0072** | 0.9992 | 0.0186 | 0.0325 | 0.0471 | 0 | 0.0041 | 0.996 | 0.0227 | 0.2887 | 0.0144 |
| US | 0.113 | **0.018** | 0.9999 | 0.1358 | 0.1702 | 0.0407 | 0.1431 | **0.0236** | 0.9998 | 0.1906 | 0.3345 | 0.0308 | 0.3883 | 0.067 | 0.999 | 0.4117 | 0.0836 | **0.0372** |
| UK | 0.1491 | 0.1777 | 0.9995 | 0.1818 | **0.1442** | 0.1443 | 0.8012 | **0.4838** | 0.9061 | 1.0183 | 16.3876 | 1.2935 | 0.1145 | 0.1 | 0.9971 | 0.1316 | **0.0323** | 0.0324 |
| INDIA | 0.3127 | 0.0228 | 0.9993 | 0.3758 | 0.0888 | **0.0162** | 0.4081 | 0.3915 | 0.9887 | 0.4515 | 0.1268 | **0.0153** | 0.4027 | 0.6866 | 0.9994 | 0.4755 | 0.0107 | **0.0102** |
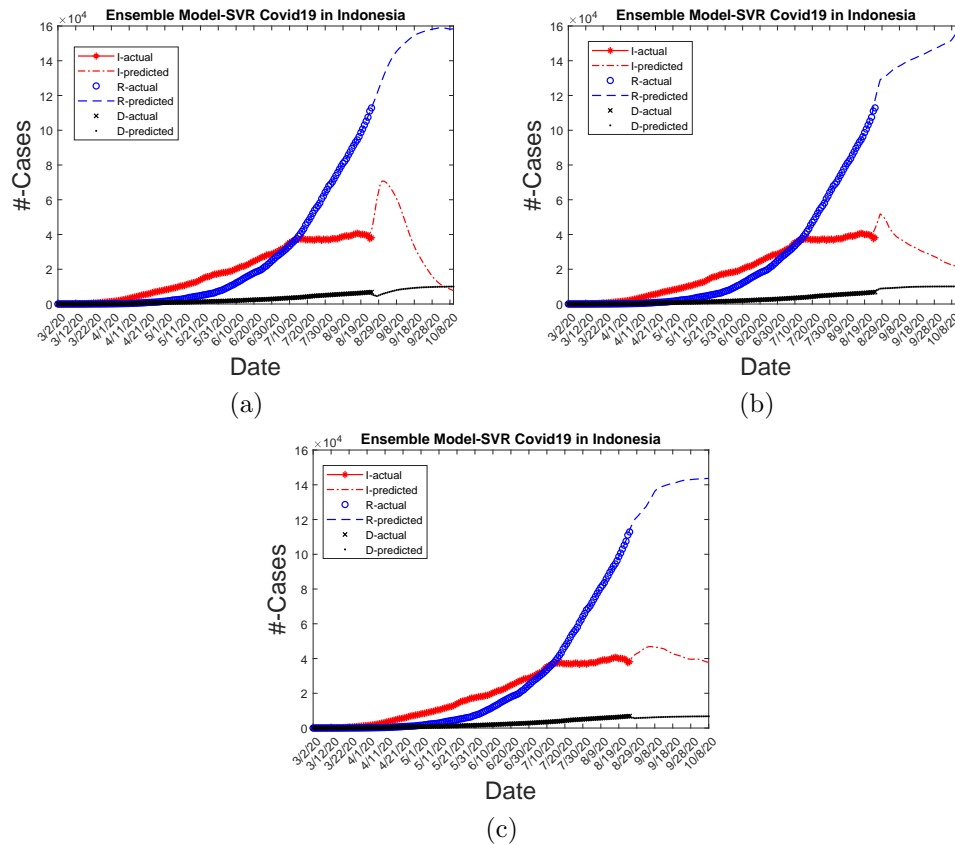
**Figure 2**: Ensemble Model-SVR prediction: (a) ensemble model with China, (b) ensemble model with South Korea and (c) ensemble model with Malaysia.

number of tests to its people, and readiness of its health system. As the nearest country to Indonesia, Malaysia has a total lockdown policy. The ensemble method tries to approximate the outbreak spread based on the data distribution of referenced countries. It implies that Indonesia is assumed to have similar conditions with the countries of reference. From Figure 2(a), Figure 2(b), and Figure 2(c), it can be seen that the accuracy of the method is satisfying with three possible models based on the countries of reference primarily for the next seven consecutive days.

Next, a simulation using a modified extended Kalman filter based on the SIRD model (shortly, modified EKF-SIRD) is conducted. It should be noted that the use of the modified EKF-SIRD method requires an estimation of the initial value $S_0$ and parameters $r$, $a$, and $d$, which are obtained using a genetic algorithm based on the Indonesia data. The fitting of the modified EKF-SIRD to the actual data in Figure 3 and the accuracy is relatively high for a short time prediction, approximately for the next seven consecutive days (August 26th - September 1st, 2020). If the prediction time range is longer, the accuracy will decrease as the data dynamic can not be captured well by the model. Therefore, for a longer prediction time, the parameters of the modified EKF-SIRD model should be updated to represent the dynamic of the data.
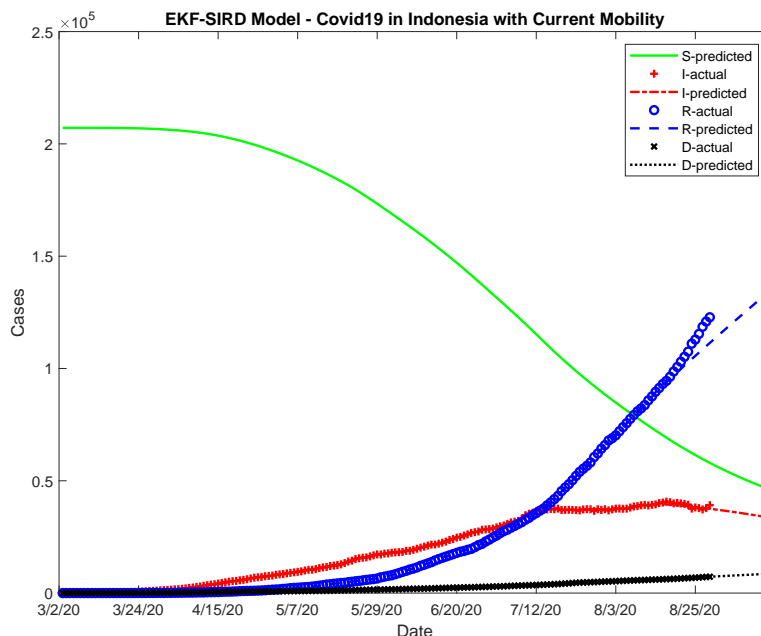
**Figure 3**: The dynamic of the number of infected, recovered, and deceased individual using a modified EKF-SIRD method in Indonesia.

The genetic algorithm is used not only for estimating the parameters of the modified EKF-SIRD model, but it is also used to modify the SIRD model itself. Then we name the model a GA-SIRD model. The dynamic of the SIRD model is trained by the GA algorithm based on the parameters found. However, in Figure 4, it seems that the GA-SIRD model is less capable of capturing the dynamic of COVID-19 data. The updated process of a GA-SIRD model based on the data can not perfectly follow the change of the actual data, mainly when there are extreme jumps in the actual data. This flaw results in lower accuracy in predicting the dynamics of the outbreak than the first method, the Ensemble-SVR.

This study also analyzed the three methods' performances based on the MAPE in (7), as shown in Table 4. We analyze the error trend for each class of compartments and each method as the MAPE shows different trends for those variations. In the infected compartment class, the modified EKF-SIRD and GA-SIRD methods show similar trends that the longer the time step for prediction, the higher the error. On the other hand, the MAPE of the Ensemble-SVR method does not have a trend, although the time step increases. For the recovered compartment class, both the modified EKF-SIRD and the GA-SIRD show trends that the longer the time step, the higher the errors. On the other hand, the Ensemble-SVR has a different trend than the other two. In the deceased compartment class, the modified EKF-SIRD has a more significant error when the number of time steps increases, but the GA-SIRD and the Ensemble-SVR do not show a trend of the errors.

In summary, the Ensemble-SVR method shows different behavior, as the prediction
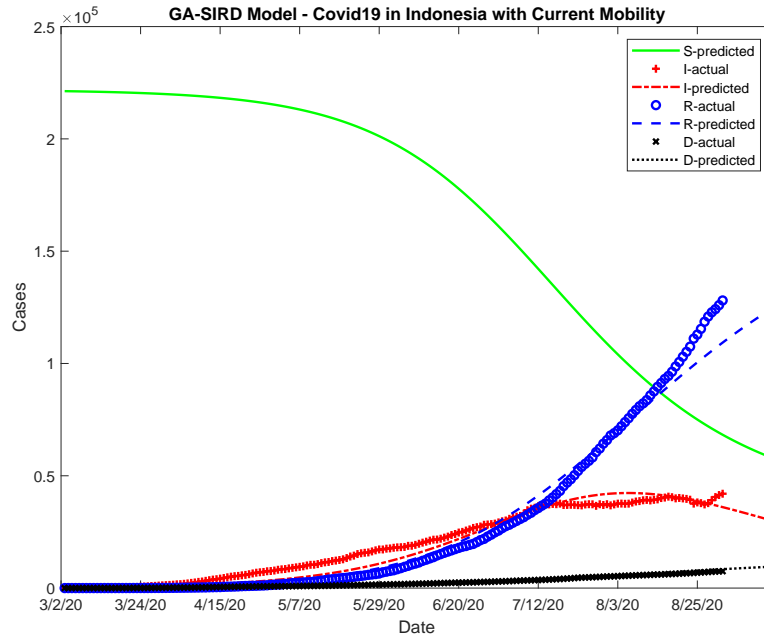
**Figure 4**: The dynamic of the number of infected, recovered, and deceased individual using a modified GA-SIRD method in Indonesia.

is made based on the data distribution and the results are long-term data randomly generated. Therefore, the method is not affected by the number of time steps. For the modified EKF-SIRD and GA-SIRD, predictions are likely to depend on the number of time steps as both methods have parameters used in the methods. The parameters do not change, although the number of time steps increases. The parameter changes only if the data set changes as the methods used herein are data-driven. Being considered time-dependent, the modified EKF-SIRD and GA-SIRD are less accurate if the number of time steps increases. That is, in general, the Ensemble-SVR outperforms the two other methods.

**Table 4**: MAPE comparison of the proposed models on forecasting the COVID-19 cases in Indonesia.

| Time steps | INFECTED | | | DEATH | | | RECOVERED | | |
|---|---|---|---|---|---|---|---|---|---|
| | EKF-SIRD | GA-SIRD | Ensemble SVR | EKF-SIRD | GA-SIRD | Ensemble SVR | EKF-SIRD | GA-SIRD | Ensemble SVR |
| $k = 1$ | 0.0029 | 0.0141 | 0.0143 | 0.0003 | 0.1325 | 0.0316 | 0.0118 | 0.1179 | 0.0203 |
| $k = 2$ | 0.0062 | 0.0198 | 0.0225 | 0.0057 | 0.1265 | 0.0320 | 0.0261 | 0.1307 | 0.0186 |
| $k = 3$ | 0.0144 | 0.0054 | 0.0222 | 0.0091 | 0.1229 | 0.0327 | 0.0328 | 0.1369 | 0.0190 |
| $k = 4$ | 0.0526 | 0.0486 | 0.0219 | 0.0107 | 0.1213 | 0.0335 | 0.0359 | 0.1400 | 0.0189 |
| $k = 5$ | 0.0901 | 0.0908 | 0.0210 | 0.0109 | 0.1211 | 0.0339 | 0.0349 | 0.1396 | 0.0190 |
| $k = 6$ | 0.1147 | 0.1201 | 0.0209 | 0.0101 | 0.1221 | 0.0339 | 0.0370 | 0.1420 | 0.0210 |
| $k = 7$ | 0.1322 | 0.1421 | 0.0231 | 0.0113 | 0.1207 | 0.0344 | 0.0415 | 0.1465 | 0.0200 |
| Average | 0.0590 | 0.0630 | 0.0196 | 0.0083 | 0.1240 | 0.0331 | 0.0314 | 0.1362 | 0.0195 |

## 6    Conclusion

This paper proposes three new hybrid methods named a modified EKF-SIRD, a GA-SIRD, and an Ensemble-SVR. We simulated the first two methods to present the dynamic of the COVID-19 outbreak for short-term predictions. As a result, these two methods exhibit their dependency on the number of time steps as the accuracy decreases when the prediction time window is wider. On the other hand, the Ensemble-SVR shows that prediction accuracy does not depend on the number of time steps. Therefore, the Ensemble-SVR is the best model amongst the other machine learning methods in terms of accuracy. The study results in the conclusion that the Ensemble-SVR method outperforms the modified EKF-SIRD and GA-SIRD.

As an extension, we will continue the study in predicting an effective reproduction number $R_t$ and dispersion number $K$. $R_t$ represents the growth rate of the infection from the infected individual to the healthy individual, and $K$ represents the ability of the infected individual to trigger new cases in a very short time. The two measures are essential for the policymaking process.

## References

[1] F. Duccio and P. Francesco. Analysis and forecast of COVID-19 spreading in China, Italy and France. *Chaos, Solitons & Fractals.* **134** (2020) 109761.

[2] H. Susanto, V. R. Tjahjono, A. Hasan, M. F. Kasim, N. Nuraini, E. R. M. Putri, R. Kusdiantara and H. Kurniawan. How Many Can You Infect? Simple (and Naive) Methods of Estimating the Reproduction Number. *Communication in Biomathematical Sciences* **3** (2020) 28–36.

[3] R. Salgotra, M. Gandomi and A.H. Gandomi. Time Series Analysis and Forecast of the COVID-19 Pandemic in India using Genetic Programming. *Chaos, Solitons & Fractals.* (2020) 109945.

[4] I. K. Abdulrahman. SimCOVID: An Open-Source Simulation Program for the COVID-19 Outbreak. *MedRxiv* (2020).

[5] D. Parbat and M. Chakraborty. A python based support vector regression model for prediction of COVID19 cases in India. *Chaos, Solitons & Fractals* **138** (2020) 109942.

[6] R. Sujath, J. M. Chatterjee and A. E. Hassanien. A machine learning forecasting model for COVID-19 pandemic in India. *Stochastic Environmental Research and Risk Assessment* **34** (2020) 959–972.

[7] T. Shreshth, T. Shikhar, T. Rakesh and S. S. Gill. Predicting the growth and trend of COVID-19 pandemic using machine learning and cloud computing. *Internet of Things* **11** (2020) 100222.

[8] N. Tutkun. Parameter estimation in mathematical models using the real coded genetic algorithms. *Expert Systems with Applications* **36** (2009) 3342–3345.

[9] F. Lewis, X. Lihua and P. Dan. *Optimal and Robust Estimation: With an Introduction to Stochastic Control Theory.* CRC press, 2017.

[10] H. Nazif and L. S. Lee. Optimised crossover genetic algorithm for capacitated vehicle routing problem. *Applied Mathematical Modelling* **36** (2012) 2110–2117.

[11] D. A. Coley. *An Introduction to Genetic Algorithms for Scientists and Engineers.* World Scientific Publishing Company, 1999.

[12] A. Gonzlez-Briones, G. Hernndez, J. M. Corchado, S. Omatu and M. S. Mohamad. Machine Learning Models for Electricity Consumption Forecasting: A Review. In: *2019 2nd International Conference on Computer Applications Information Security (ICCAIS),* 2019, 1–6.

[13] Z. Zhang, W. Hong and J. Li. Electric Load Forecasting by Hybrid Self-Recurrent Support Vector Regression Model with Variational Mode Decomposition and Improved Cuckoo Search Algorithm. *IEEE Access* **8** (2020) 14642–14658.

[14] C. Li, X. Wang, Z. Cheng and Y. Bai. Forecasting Bus Passenger Flows by Using a Clustering-Based Support Vector Regression Approach. *IEEE Access* **8** (2020) 19717–19725.

[15] S. Kavitha, S. Varuna and R. Ramya. A comparative analysis on linear regression and support vector regression. In: *2016 Online International Conference on Green Engineering and Technologies (IC-GET),* 2016, 1–6.

[16] A. Gonzlez-Briones, G. Hernndez, T. Pinto, Z. Vale, and J. M. Corchado. A Review of the Main Machine Learning Methods for Predicting Residential Energy Consumption.. In: *2019 16th International Conference on the European Energy Market (EEM),* 2019, 1–6.

[17] H. Drucker, C. J. C. Burges, L. Kaufman, A. Smola and V. Vapnik. Support Vector Regression Machines. In: *Proceedings of the 9th International Conference on Neural Information Processing Systems.* Denver, Colorado, 1996, 155–161.

# Progressive Type–II Censoring Power Function Distribution Under Binomial Removals

Mahmoud M. Smadi [1,*], Ahmad Zghoul [2] and Mahmoud H. Alrefaei [1]

[1] *Department of Mathematics and Statistics, Jordan University of Science and Technology, Jordan.*
[2] *Department of Mathematics, College of Science, The University of Jordan, Jordan.*

**Abstract:** Recently, progressive censoring received significant attention in many applications in engineering system reliability and survival analysis. Different lifetime models are used in the literature for progressive censoring, such as the Pareto, exponential, generalized exponential, Gompertz, Burr Type−XII, Rayleigh, generalized logistic, and exponentiated gamma distributions. A power function model is characterized by its simple mathematical structure and is easily implemented to determine failure rates and reliability values. The model is found to be useful in modeling electrical components. This work considers the estimation problem for a power function model based on progressive Type−II censoring using binomial removals. A simulation study was performed to investigate the behavior of the estimators using different sample sizes, parameter values and censored proportions. As an illustration, an application to failure time data set is presented.

---

* Corresponding author: `smadi@just.edu.jo`

## 1  Introduction

The theory of reliability systems plays an important role in industry, manufacturing, safety engineering and quality. The lifetime of equipment or apparatus is a random time from the beginning of the operation until the appearance of a complete failure. Reliability is the ability of a system to perform its stated purpose adequately for a specified period of time under specified operational conditions. The system defined here could be an electronic or mechanical hardware product, a software product, a manufacturing process. For example, in the case of a mechanical system, a failure is a breakdown of some of its parts or an increase in vibration above the permitted level. The reliability characteristics are usually expressed in terms of the lifetime. Modeling and analyzing lifetime data are important issues for engineering reliability, industry, quality control, and clinical trials, etc. Different lifetime data can be modeled by different continuous probability distributions such as exponential, Lindley, Weibull, lognormal, and Frechet as well as their generalizations [1, 2].

In reliability and survival analysis, it is difficult to collect lifetime data for all components under consideration due to time and cost constraints. Various types of censoring schemes can be used for such purpose based on the model and available information using both parametric and nonparametric methods. Recently, progressive censoring sampling is of special importance in reliability and survival analysis. Progressive censoring was first introduced by Cohen [3]. Extensive studies are available in the literature related to the progressive censoring [4–6]. Different parametric survival models have been considered in progressive censoring using binomial removals, they are the Type-II generalized logistic distribution [7], the exponential distribution [8], the generalized exponential distribution [9], the exponentiated gamma distribution [10], the Pareto distribution [11–13], the Rayleigh distribution [14], the Burr Type-XII distribution [15], and the Gompertz distribution [16]. For more details about Type-I and Type-II censored samples, one can refer to Salah [17], Lin *et al.* [18], Balakrishnan [19], Balakrishnan *et al.* [20], and Salah [21, 22].

Type-II progressively censored life test is conducted as follows. For $n$ identical units in a test, at the time of the first failure, $R_1$ units from the remaining $n-1$ survival items are removed. At the time of the second failure, $R_2$ units from the remaining $n-R_1-1$ items are removed, and so forth. Finally, at the time of $m-$th failure, the reaming survival units, would be $R_m$ can be removed. In this case, censoring takes place progressively in $m$ stages. Clearly, this scheme includes, as special cases, the complete sample situation (when $m = n$ and $R_1 = ... = R_m = 0$) and the conventional Type$-$II right censoring situation (when $R_1 = ... = R_{m-1} = 0$ and $R_m = n-m$). The corresponding scheme *($r_1$, $r_2$, . . . , $r_m$)* is known as the progressive Type-II right censoring scheme.

Different versions of the power function distributions are reported in the literature [23]. These power function distributions can be easily implemented to determine the failure rates and reliability values compared to other distributions such as lognormal, Weibull, logistic and others. The particular parameterization of the power distribution function to be considered in this work has the following cumulative distribution function (CDF) form:

$$F(x) = 1 - \left(\frac{\theta - x}{\theta - \alpha}\right)^{\beta}, \; \alpha < x < \theta, \; \beta > 0, \tag{1}$$

where $\theta$ and $\alpha$ are the scale parameters and $\beta$ is the shape parameter.

The probability density function (PDF) is given by

$$f(x) = \frac{\beta}{\theta - \alpha} \left( \frac{\theta - x}{\theta - \alpha} \right)^{\beta - 1}, \ \alpha < x < \theta, \ \beta > 0. \tag{2}$$

The power function distribution is a member of the Beta family of distributions. Sarhan and Pandey [24] obtained the best linear unbiased estimates of the parameters of the above power distribution function in terms of $k-th$ upper record values. The power function distribution has applications in industrial and mechanical engineering [24]. Meniconi and Barry [25] explored the performance of the power function distribution on certain electrical components and showed that it is the most suitable distribution function as compared to the lognormal, Weibull and exponential models. Statistical properties of the power function distribution were reported by Johnson *et al.* [26].

This work considers progressive Type-II censoring for a power function distribution with binomial removals. The maximum likelihood estimators (MLEs) of the model parameters are determined. A simulation study is performed to determine the behavior of the MLEs via bias and the root mean square error (RMSE) using different sample sizes, parameter values and censored proportions. An example related to lifetime data of electronic devices will be presented to illustrate the approach developed in this work.

## 2   Model

Assume the lifetime random variable follows the power function distribution given in equation (1), it is a realistic assumption to assume the location parameter (lower bound) $\alpha = 0$, the cumulative distribution function (CDF) reduces to

$$F(x) = 1 - \left( \frac{\theta - x}{\theta} \right)^{\beta}, \ 0 < x < \theta, \ \beta > 0, \tag{3}$$

where $\theta$ is the scale parameter and $\beta$ is the shape parameter.

The probability density function (PDF) reduces to

$$f(x) = \frac{\beta}{\theta} \left( \frac{\theta - x}{\theta} \right)^{\beta - 1}, \ 0 < x < \theta, \ \beta > 0. \tag{4}$$

The reliability function is given by

$$r(x) = P(T > x) = \left( \frac{\theta - x}{\theta} \right)^{\beta}, 0 < x < \theta, \beta > 0.$$

The hazard rate function is given by

$$h(x) = \frac{f(x)}{R(x)} = \frac{\beta}{\theta - x}, 0 < x < \theta, \beta > 0.$$

Figure 1 shows a graphical representation of the probability density function (PDF) for the values of the shape parameter $\beta$ of 0.2, 0.7, 1.5, 3, 4 and $\theta = 1$. The probability density function exhibits various behaviors depending on the values of the shape parameter $\beta$. Figure 2 shows the graphical representation of the hazard function using selected shape parameter values. According to Figure 2, it is seen that the power function distribution is characterized by increasing J-shaped hazard rates.
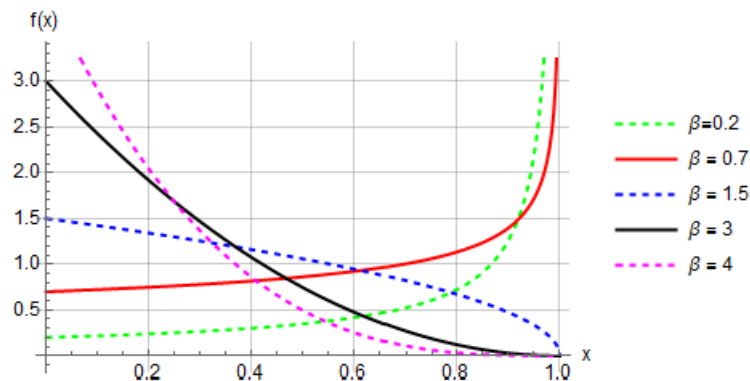
**Figure 1**: PDF plot of power function distribution.
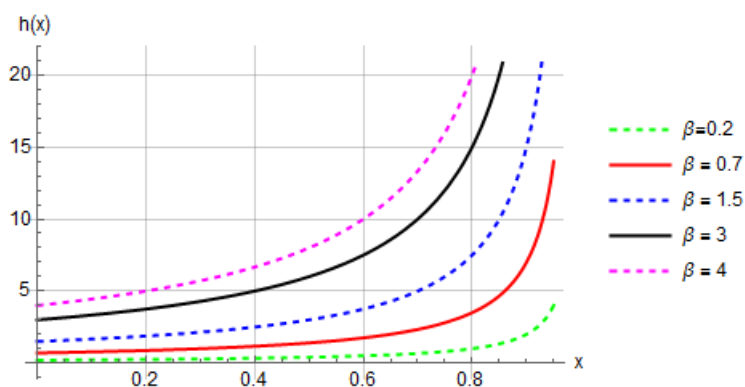


**Figure 2**: Hazard rate curves of power function distribution.

## 3   Maximum Likelihood Estimation

We first consider estimating the parameters based on the complete observed sample $x_1, ..., x_n$. Let $x_{(1)}, ..., x_{(n)}$ be the corresponding order statistics. Given the sample, the likelihood function of the density in (4) is

$$L(\beta, \theta) \equiv L(\beta, \theta | x_1, ..., x_n) = \left( \frac{\beta}{\theta} \right)^n \prod_{j=1}^{n} \left( 1 - \frac{x_j}{\theta} \right)^{\beta - 1} I_{(x_{(n)}, \infty)^{(\theta)}}, \beta > 0,$$

where $I_A(x)$ is the zero−one indicator function. We notice that the support of the density depends on the scale parameter and therefore the MLE may not be calculated directly as a solution to the likelihood equations.

For fixed $\beta = \beta_0$, the limits of the likelihood function when approaching its boundaries

are given by

$$\lim_{\theta \downarrow x_{(n)}} L(\beta_0, \theta) = \begin{cases} \infty, & 0 < \beta_0 < 1, \\ 0, & \beta_0 > 1, \\ \left(x_{(n)}\right)^{-n}, & \beta_0 = 1, \end{cases}$$

and

$$\lim_{\theta \uparrow \infty} L(\beta_0, \theta) = 0, \forall \beta_0 > 0.$$

For $0 < \beta_0 \leq 1$, $L(\beta_0, \theta)$ is maximized at $\theta = x_{(n)}$. However, for $\beta_0 > 1$, $L(\beta_0, \theta)$ attains its maximum at some $\theta > x_{(n)}$ and not at $x_{(n)}$. To illustrate this, the graphs of $L(\beta_0, \theta)$ based on a sample of size 10 from the power function distribution with $\theta = 2$ and $\beta_0 = 1.2$, 2, and 4, respectively, are displayed in Figures 3, 4 and 5. The values of $x_{(n)}$ are approximately 1.99, 1.79 and 0.56, respectively. Notice that for $\beta_0 = 1.2$, the maximum of $L(\theta)$ is approximately 1.75, which is very close to $x_{(n)}=1.71$, for $\beta_0 = 2$, we have $x_{(n)}=1.22$ and $L(\theta)$ is approximately maximized at $\theta = 1.49$, and for $\beta_0 = 4$, $x_{(n)} = 0.75$ and $L(\theta)$ attains its maximum at $\theta = 1.83$, approximately. We observe that the maximizer of $L(\theta)$ deviates from $x_{(n)}$ with increasing $\beta$.
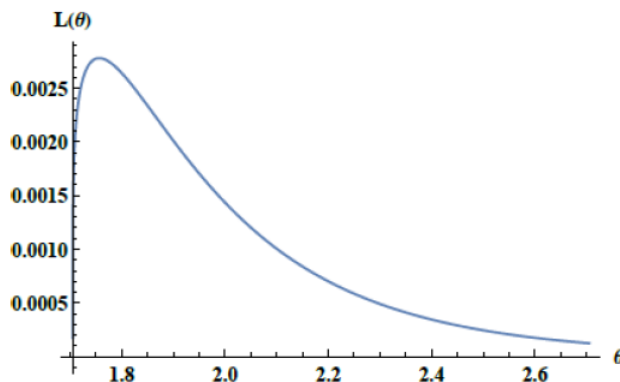


**Figure 3**: Likelihood function based on a sample of size 10 generated from the power function distribution with $\beta = 1.2$ and $= 2$.

Now we investigate the MLE of the parameter vector $\boldsymbol{\theta} = (\beta, \theta)$. Necessary conditions for the existence and uniqueness of the MLE of a parameter vector $\boldsymbol{\theta} = (\theta_1, ..., \theta_k)$ are in [27]:

1. $L(\boldsymbol{\theta})$ is a twice continuously differentiable likelihood function varying in a connected open subset $\boldsymbol{\Theta} \subset R^k$.

2. $L(\boldsymbol{\theta})$ satisfies the following two conditions:

   (i) $\lim_{\boldsymbol{\theta} \to \partial \boldsymbol{\Theta}} L(\boldsymbol{\theta}) = 0,$
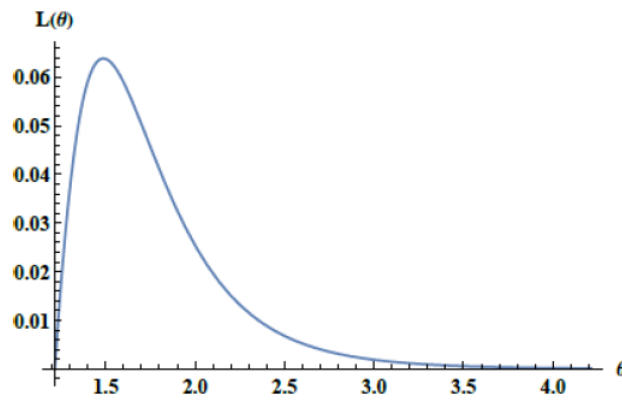
**Figure 4**: Likelihood function based on a sample of size 10 generated from the power function distribution with $\beta = 2$ and $= 2$.
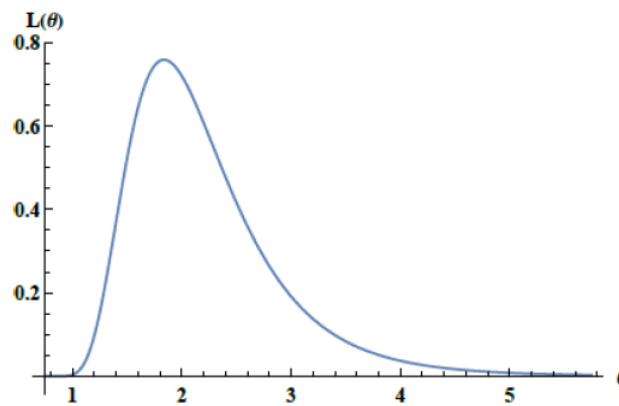


**Figure 5**: Likelihood function based on a sample of size 10 generated from the power function distribution with $\beta = 4$ and $= 2$.

(ii) The Hessian matrix of second partial derivatives

$$
H = \begin{pmatrix} \frac{\partial^2 L}{\partial \theta^2} & \frac{\partial^2 L}{\partial \theta \partial \beta} \\ \frac{\partial^2 L}{\partial \beta \partial \theta} & \frac{\partial^2 L}{\partial \beta^2} \end{pmatrix}
$$

is negative definite at every point $\boldsymbol{\theta} \in \boldsymbol{\Theta}$ for which the vector $\nabla L = (\partial L / \partial \theta_i) = 0$.

These conditions also apply to the log−likelihood function with $\lim_{\boldsymbol{\theta}\to\partial\boldsymbol{\Theta}} l(\boldsymbol{\theta}) = 0$ being replaced by $\lim_{\boldsymbol{\theta}\to\partial\boldsymbol{\Theta}} L(\boldsymbol{\theta}) = -\infty$.

The domain of the likelihood function of the power function distribution based on a sample of size n is the rectangle $(0, \infty) \times (x_{(n)}, \infty)$ which is an open connected set in $R^2$. The boundaries of $\boldsymbol{\Theta}$ are the lines $\theta = x_{(n)}, \beta \in (0, \infty)$ and $\beta = 0, \theta \in (x_{(n)}, \infty)$. It is clear that $\lim_{\boldsymbol{\theta}\to\partial\boldsymbol{\Theta}} L(\boldsymbol{\theta}) = 0$ when   approaching each of these two lines. So, to prove the existence and uniqueness of the MLE, it remains to show that the Hessian matrix $\mathbf{H}$ is nonnegative definite at the zeros of the first partial derivatives of $L(\boldsymbol{\theta})$ or, equivalently, of $l(\boldsymbol{\theta})$.

Given the observed sample $x_1, ..., x_n$, the log-likelihood function is

$$l(\beta, \theta) \equiv \log L(\beta, \theta) = n \log \beta - n \log \theta + (\beta - 1) \sum_{j=1}^{n} \log \left( 1 - \frac{x_{(j)}}{\theta} \right). \qquad (5)$$

For $\beta > 0$, we have

$$\frac{\partial l(\beta, \theta)}{\partial \beta} = \frac{n}{\beta} + \sum_{j=1}^{n} \log \left( 1 - \frac{x_{(j)}}{\theta} \right) = 0, \qquad (6)$$

and for $\theta > x_{(n)}$, we have

$$\frac{\partial l(\beta, \theta)}{\partial \theta} = -\frac{n}{\theta} + (\beta - 1) \sum_{j=1}^{n} \frac{x_{(j)}}{\theta \left( \theta - x_{(j)} \right)} = 0. \qquad (7)$$

Solving (6) for $\beta$, we obtain

$$\beta \equiv \beta(\theta) = -\frac{n}{\sum_{j=1}^{n} \log \left( 1 - \frac{x_{(j)}}{\theta} \right)} \qquad (8)$$

and solving (7) for $\beta$, we have

$$\beta - 1 = \frac{n}{\sum_{j=1}^{n} x_j \left( \theta - x_j \right)^{-1}}. \qquad (9)$$

Since

$$\frac{\partial^2 l(\beta, \theta)}{\partial \beta^2} = -\frac{n}{\beta^2} < 0,$$

it follows for fixed $\theta$, $l(\beta, \theta)$ is maximized at

$$\beta(\theta) = -\frac{n}{\sum_{j=1}^{n} \log \left( 1 - \frac{x_{(j)}}{\theta} \right)},$$

provided that the maximum exists. Replacing $\beta$ by $\beta(\theta)$, the log-likelihood (5) can be written as

$$\begin{aligned} l(\theta) \equiv \sup_{\beta} l(\beta, \theta) &= n \log\beta(\theta) - n \log\theta + (\beta(\theta) - 1) \sum_{j=1}^{n} \log \left( 1 - \frac{x_{(j)}}{\theta} \right) \\ &= n \log\beta(\theta) - n \log\theta + (\beta(\theta) - 1) \frac{-n}{\beta(\theta)} \\ &= n \log\frac{\beta(\theta)}{\theta} + \frac{n}{\beta(\theta)} - n. \end{aligned}$$

The second partial derivatives of $l(\beta, \theta)$ are

$$\frac{\partial^2 l(\beta, \theta)}{\partial \beta^2} = -\frac{n}{\beta^2}, \tag{10}$$

$$\frac{\partial^2 l(\beta, \theta)}{\partial \theta^2} = \frac{n}{\theta^2} - (\beta - 1) \sum_{j=1}^{n} \frac{x_{(j)}(2\theta - x_{(j)})}{\theta^2(\theta - x_{(j)})^2}, \tag{11}$$

$$\frac{\partial^2 l(\beta, \theta)}{\partial \theta \partial \beta} = \frac{\partial^2 l(\beta, \theta)}{\partial \beta \partial \theta} = \sum_{j=1}^{n} \frac{x_{(j)}}{\theta(\theta - x_{(j)})}. \tag{12}$$

From (9) and (12), we have $\frac{\partial^2 l(\beta, \theta)}{\partial \theta \partial \beta} = \frac{1}{\theta} \sum_{j=1}^{n} \frac{x_{(j)}}{(\theta - x_{(j)})} = \frac{1}{\theta} \frac{n}{\beta - 1}$. Thus, **H** can be written as

$$H = \begin{pmatrix} -\frac{n}{\beta^2} & \frac{n}{\theta(\beta-1)} \\ \frac{n}{\theta(\beta-1)} & \frac{n}{\theta^2} - (\beta - 1) \sum_{j=1}^{n} \frac{x_j(2\theta - x_j)}{\theta^2(\theta - x_j)^2} \end{pmatrix}.$$

The determinant of **H** is

$$D = -\frac{n}{\beta^2} \left[ \frac{n}{\theta^2} - (\beta - 1) \sum_{j=1}^{n} \frac{x_j(2\theta - x_j)}{\theta^2(\theta - x_j)^2} \right] - \left( \frac{n}{\theta(\beta - 1)} \right)^2. \tag{13}$$

Completing the square of the numerator of the term inside the sum on the right-hand side of (13), we get

$$D = -\frac{n}{\beta^2} \left[ \frac{n}{\theta^2} + (\beta - 1) \sum_{j=1}^{n} \frac{\{(\theta - x_j)^2 - \theta^2\}}{\theta^2(\theta - x_j)^2} \right] - \left( \frac{n}{\theta(\beta - 1)} \right)^2$$

$$= -\frac{n}{\beta^2} \left[ \frac{n\beta}{\theta^2} - (\beta - 1) \sum_{j=1}^{n} \frac{1}{(\theta - x_j)^2} \right] - \left( \frac{n}{\theta(\beta - 1)} \right)^2$$

$$= -\frac{n}{\beta^2} \left[ \frac{n\beta}{\theta^2} + \frac{n\beta^2}{\theta^2(\beta - 1)^2} - (\beta - 1) \sum_{j=1}^{n} \frac{1}{(\theta - x_j)^2} \right].$$

For $D$ to be negative definite, we need to show that the term between the square brackets is positive. That is,

$$\frac{n\beta}{\theta^2} \left( 1 + \frac{\beta}{(\beta - 1)^2} \right) - (\beta - 1) \sum_{j=1}^{n} \frac{1}{(\theta - x_j)^2} > 0, \text{ or}$$

$$\frac{n\beta}{\theta^2} \left( 1 + \frac{\beta}{(\beta - 1)^2} \right) > (\beta - 1) \sum_{j=1}^{n} \frac{1}{(\theta - x_j)^2}.$$

Then for each $j = 1, \ldots, n$, we have $\theta - x_j < \theta$, which implies that

$$\sum_{j=1}^{n} \frac{1}{(\theta - x_j)^2} > \sum_{j=1}^{n} \frac{1}{\theta^2} = \frac{n}{\theta^2}.$$

So, the above inequality reduces to

$$\frac{n\beta}{\theta^2(\beta-1)}\left(1+\frac{\beta}{(\beta-1)^2}\right) > \frac{n}{\theta^2}.$$

Multiplying both sides of the above inequality by $\theta^2/n$, after some algebra, we get

$$\frac{\beta^3 - \beta^2 + 1 - (\beta-1)^3}{(\beta-1)^3} > 0.$$

We have noticed earlier that for $0 < \beta \le 1$, the MLE is $X_{(n)}$, so we only examine here the case $\beta > 1$. After expanding the numerator and noticing that the denominator is positive, the last inequality reduces to $2\beta^2 - 3\beta + 2 = 2(\beta-1)^2 + \beta > 0$, which is true for all $\beta$ and hence for $\beta > 1$. Thus,

$$\frac{n\beta}{\theta^2} + \frac{n\beta^2}{\theta^2(\beta-1)^2} - (\beta-1)\sum_{j=1}^{n}\frac{1}{(\theta-x_j)^2} > 0, \forall\beta > 1, \text{and}$$

$$-\frac{n}{\beta^2}\left[\frac{n\beta}{\theta^2} + \frac{n\beta^2}{\theta^2(\beta-1)^2} - (\beta-1)\sum_{j=1}^{n}\frac{1}{(\theta-x_j)^2}\right] < 0, \forall\beta > 1.$$

We have shown that the Hessian matrix $\mathbf{H}$ is negative definite at the zeros of the first partial derivatives of the log-likelihood function. Thus, all necessary conditions for the existence and uniqueness of the MLE are met.

Let $(X_1, R_1), (X_2, R_2), \ldots, (X_m, R_m)$ be a progressively censored sample, where $X_1 < X_2 < \ldots < X_m$. With a predetermined number of removals, such as $R_1 = r_1, R_2 = r_2, \ldots, R_m = r_m$, the conditional likelihood function can be written as [3]

$$L(\theta,\beta; x|R = r) = A\prod_{i=1}^{m} f(x_i)\left(1 - F(x_i)\right)^{r_i}, \tag{14}$$

where $A = n(n - r - 1)...(n - \sum_{i=1}^{m-1} r_i + 1)$.

After substituting (3) and (4) into equation (14), the likelihood function becomes

$$L(\theta,\beta; x|R = r) = A\prod_{i=1}^{m}\frac{\beta}{\theta}\left(\frac{\theta-x_i}{\theta}\right)^{\beta-1}\left(\left(\frac{\theta-x_i}{\theta}\right)^{\beta}\right)^{r_i}. \tag{15}$$

Suppose that an individual unit being removed from the test at the $i^{th}$ failure, $i = 1, 2, \ldots, m - i$, is independent of the others but with the same probability $p$. Therefore, $R_i, i = 1, 2, .., m - 1$, follows a binomial distribution with parameters $n - m - \sum_{k=1}^{m-1} r_k$ and $p$. Thus,

$$P(R_1 = r_1) = \binom{n-m}{r_1} p^{r_1}(1-p)^{n-m-r_1}, \tag{16}$$

$$P\left(R_i = r_i|R_{i-1} = r_{i-1}, \ldots, R_1 - r_1\right)$$
$$= \binom{n-m-\sum_{k=1}^{m-1}r_k}{r_i} p^{r_i}(1-p)^{n-m-\sum_{k=1}^{i}r_k}, i = 1, 2, ..., m-1, \tag{17}$$

where $0 \le r_i \le n - m - \sum_{j=1}^{i-1} r_j$.

The full likelihood function takes the following form:

$$L(\theta, \beta, p; x, r) = L(\theta, \beta; x|R) = r(P(R = r|p)), \tag{18}$$

where $P(R = r|p))$ is the joint conditional distribution and is given by

$$P(R = r|p) =$$

$$P(R_1 = r_1)P(R_2 = r_2|R_1 = r_1)...P(R_{m-1} = r_{m-1}|R_{m-2} = r_{m-2}, ...., R_1 = r_1) \tag{19}$$

$$= \frac{\text{(n-m)!p}^{\sum_{i=1}^{m-1} r_i}(1-p)^{(m-1)(n-m)\sum_{i=1}^{m-1}(m-i)r_i}}{\left(n - m - \sum_{i=1}^{m-1} r_i\right) \ ! \ \prod_{i=1}^{m-1} r_i!}.$$

Using equations (15), (18) and (19), we can write the full likelihood function as

$$L(\theta, \beta, p; x, r) = AL_1(\theta, \beta) L_2(p),$$

where

$$L_1(\theta, \beta) = \prod_{i=1}^{m} \frac{\beta}{\theta} \left(\frac{\theta - x_i}{\theta}\right)^{\beta-1} \left(\left(\frac{\theta - x_i}{\theta}\right)^{\beta}\right)^{r_i}$$

$$= \left(\frac{\beta}{\theta}\right)^{m} \prod_{i=1}^{m} \left(\frac{\theta - x_i}{\theta}\right)^{\beta(1+r_i)-1},$$

$$L_2(p) = p^{\sum_{i=1}^{m-1} r_i}(1-p)^{(m-1)(n-m)\sum_{i=1}^{m-1}(m-i)r_i}$$

and

$$A = \frac{c(n - m)!}{\left(n - m - \sum_{i=1}^{m-1} r_i\right) \ ! \ \prod_{i=1}^{m-1} r_i!}.$$

It is clear that $A$ is parameter free and $L_2(p)$ is independent of $\theta$ and $\beta$.

The MLE of $\beta$ can be obtained by maximizing

$$L_1(\beta, \theta) = \prod_{i=1}^{m} \frac{\beta}{\theta} \left(\frac{\theta - x_i}{\theta}\right)^{\beta(r_i+1)-1}$$

or, equivalently, the log-likelihood function

$$l_1(\beta, \theta) = m \log(\beta) - m \log(\theta) + \sum_{i=1}^{m} [\beta(r_i + 1) - 1] \log\left(\frac{\theta - x_i}{\theta}\right). \tag{20}$$

The corresponding likelihood equations are

$$\frac{\partial l_1}{\partial \beta} = \frac{m}{\beta} + \sum_{i=1}^{m} (r_i + 1) \log\left(\frac{\theta - x_i}{\theta}\right) = 0, \tag{21}$$

$$\frac{\partial l_1}{\partial \theta} = -\frac{m}{\theta} + \sum_{i=1}^{m} [\beta(r_i + 1) - 1] \log\frac{x_i}{\theta(\theta - x_i)} = 0. \tag{22}$$

Solving (21) for $\beta$, we obtain

$$\beta \equiv \beta(\theta) = -\frac{m}{\sum_{i=1}^{m}(r_i+1)\log\left(\frac{\theta-x_i}{\theta}\right)}. \tag{23}$$

Substitute (23) into (22) to obtain

$$\sum_{i=1}^{m}[\beta(\theta)(r_i+1)-1]\log\frac{x_i}{\theta\,(\theta-x_i)} = \frac{m}{\theta}. \tag{24}$$

As clarified before, the MLE of $\theta$ is $X_{(m)}$ if $0 < \beta(r_i+1) \leq 1$, in this case the MLE of $\beta$ is

$$\hat{\beta} = -\frac{m}{\sum_{i=1}^{m}(r_i+1)\log\left(\frac{x_{(m)}-x_i}{x_{(m)}}\right)}.$$

For $\beta(r_i+1) > 1$, we use numerical methods to solve (24) for $\theta$ and then apply (23) to solve for $\beta$. The MLE of $p$ is easily derived by maximizing $\log L_2(p)$:

$$\hat{p} = \frac{\sum_{i=1}^{m-1} r_i}{\sum_{i=1}^{m-1} r_i + (m-1)(n-m) - \sum_{i=1}^{m-1}(m-i)r_i}.$$

## 4    Numerical Results

### 4.1    Simulation study

A simulation study was performed to deduce the behavior of the maximum likelihood estimators. Different sample sizes, namely, n = 25, 50 and 100 were used. Different combinations of the parameter values of $\theta$ and $\beta$ were considered. The values of the parameter $p$ used in the simulation study are 0.25, 0.5 and 0.75. The simulation results were based on 1000 replicates. The means and root mean square errors (RMSE) of the maximum likelihood estimators for the three parameters $p$, $\theta$ and $\beta$ are displayed in Tables 1, 2 and 3.

The following concluding remarks can be drawn based on the results shown in Tables 1, 2, and 3:

1. For a fixed value of m, as n increases, the bias and RMSE show a decreasing trend.

2. For a fixed value of n, as m increases, the bias and RMSE decrease for the maximum likelihood estimators for $\theta$ and $\beta$; on the other hand, the RMSE increases for the maximum likelihood estimator for $p$.

3. As the shape parameter $\beta$ increases, the bias and RMSE increase.

4. As the value of the probability parameter $p$ increases, the bias and RMSE for the estimators of $p$ and $\beta$ increase.

### 4.2    Study on real data

A real-life data set is considered which represents the failure times (in minutes) for a sample of 15 electronic components in an accelerated life test [5]. The data set is 1.4, 5.1, 6.3, 10.8, 12.1, 18.5, 19.7, 22.2, 23.0, 30.6, 37.3, 46.3, 53.9, 59.8, 66.2.

**Table 1**: Mean and RMSE of the MLEs and for p = 0.25 and different choices n, m, $\theta$ and $\beta$.

| $n$ | $m$ | $\hat{\theta}$ | $\hat{\beta}$ | $\hat{p}$ | | $\hat{\theta}$ | | $\hat{\beta}$ | |
|---|---|---|---|---|---|---|---|---|---|
| | | | | Mean | RMSE | Mean | RMSE | Mean | RMSE |
| 25 | 15 | 1 | 0.5 | 0.26926 | 0.07899 | 0.99366 | 0.01187 | 0.51518 | 0.14276 |
| | | 1.5 | 1 | 0.26926 | 0.07910 | 1.41241 | 0.08126 | 0.91826 | 0.26551 |
| | | 2 | 1.5 | 0.26926 | 0.07900 | 1.72610 | 0.17629 | 1.20655 | 0.37488 |
| | 20 | 1 | 0.5 | 0.29167 | 0.12260 | 0.99592 | 0.00899 | 0.57428 | 0.13269 |
| | | 1.5 | 1 | 0.29166 | 0.12261 | 1.43108 | 0.06667 | 1.03523 | 0.24506 |
| | | 2 | 1.5 | 0.29166 | 0.12261 | 1.76733 | 0.15360 | 1.37200 | 0.35504 |
| 50 | 30 | 1 | 0.5 | 0.25922 | 0.05237 | 0.99796 | 0.00422 | 0.52328 | 0.10064 |
| | | 1.5 | 1 | 0.25922 | 0.05237 | 1.45143 | 0.04723 | 0.96558 | 0.18577 |
| | | 2 | 1.5 | 0.25922 | 0.05237 | 1.81607 | 0.12262 | 1.30226 | 0.26939 |
| | 40 | 1 | 0.5 | 0.27079 | 0.07868 | 0.99892 | 0.00234 | 0.54803 | 0.08874 |
| | | 1.5 | 1 | 0.27079 | 0.07868 | 1.46462 | 0.03431 | 1.02557 | 0.16921 |
| | | 2 | 1.5 | 0.27079 | 0.07868 | 1.85091 | 0.09830 | 1.39968 | 0.25315 |
| 100 | 80 | 1 | 0.5 | 0.25909 | 0.05182 | 0.99969 | 0.00068 | 0.52754 | 0.05999 |
| | | 1.5 | 1 | 0.25909 | 0.05182 | 1.48124 | 0.01857 | 1.01082 | 0.11601 |
| | | 2 | 1.5 | 0.25909 | 0.05182 | 1.90260 | 0.06567 | 1.41151 | 0.17877 |
| | 90 | 1 | 0.5 | 0.27079 | 0.07868 | 0.99977 | 0.00045 | 0.52939 | 0.05726 |
| | | 1.5 | 1 | 0.27079 | 0.07868 | 1.48350 | 0.01589 | 1.01832 | 0.11180 |
| | | 2 | 1.5 | 0.27079 | 0.07868 | 1.91029 | 0.05957 | 1.42767 | 0.17258 |

The failure times were analyzed in order to validate the proposed progressive Type-II censoring scheme using the power function distribution model. The validity of the power distribution function was checked based on the maximum likelihood estimated parameters $\theta$ and $\beta$ of 66.2 and 1.1573, respectively. The Kolmogorov-Smirnov (K−S) test was used for this data set. It is noted that the K−S distance between the fitted and the empirical distribution functions equals to 0.21, and the corresponding critical value at $\alpha$ =0.05 equals to 0.33. Thus, the power function distribution fits the above data set reasonably well.

Five progressively censored samples were generated from the above data for the values of $m$ = 14, 13, 12, 11, 10. Uniform random removal of subjects was used to generate $(r_1, r_2, ..., r_m)$.

Progressive censoring with $m$ =14 (1 observation removed): (1.4, 0), (5.1,1), (6.3,0), (10.8,0), (12.1,0), (18.5,0), (19.7,0), (22.2,0), (23.0,0), (30.6,0), (37.3,0), (53.9,0), (59.8,0), (66.2).

Progressive censoring with $m$ =13 (2 observations removed): (1.4,1), (5.1,0), (6.3,0), (10.8,0), (12.1,0), (18.5,0), (22.2,0), (23.0,0), (30.6,0), (37.3,1), (53.9,0), (59.8,0), (66.2,0).

Progressive censoring with $m$ =12 (3 observations removed): (1.4,1), (6.3,0), (10.8,0), (12.1,0), (18.5,1), (19.7,0), (22.2,0), (23.0,0), (30.6,0), (37.3,1), (59.8,0), (66.2,0).

Progressive censoring with $m$ =11 (4 observations removed): (1.4,1), (5.1,0), (10.8,0), (12.1,1), (18.5,0), (19.7,1), (22.2,0), (23.0,0), (30.6,0), (37.3,1), (53.9,0).

Progressive censoring with $m$ =10 (5 observations removed): (1.4,1), (5.1,0), (6.3,1), (10.8,1), (12.1,0), (18.5,0), (19.7,1), (22.2,0), (37.3,0), (46.3,1).

The maximum likelihood estimates for the model parameters $\beta$ and $\theta$ using the five

**Table 2**: Mean and RMSE of the MLEs $\hat{p}, \hat{\theta}$, and $\hat{\beta}$ for $p = 0.5$ and different choices of $n, m, \theta$ and $\beta$.

| $n$ | $m$ | $\hat{\theta}$ | $\hat{\beta}$ | $\hat{p}$ | | $\hat{\theta}$ | | $\hat{\beta}$ | |
|---|---|---|---|---|---|---|---|---|---|
| | | | | Mean | RMSE | Mean | RMSE | Mean | RMSE |
| 25 | 15 | 1 | 0.5 | 0.52050 | 0.11961 | 0.99366 | 0.01187 | 0.57897 | 0.15603 |
| | | 1.5 | 1 | 0.52050 | 0.11961 | 1.41241 | 0.08126 | 1.03978 | 0.28820 |
| | | 2 | 1.5 | 0.52050 | 0.11961 | 1.72610 | 0.17649 | 1.35124 | 0.40669 |
| | 20 | 1 | 0.5 | 0.55036 | 0.17118 | 0.99592 | 0.00899 | 0.59603 | 0.13753 |
| | | 1.5 | 1 | 0.55036 | 0.17118 | 1.43108 | 0.06666 | 1.07318 | 0.25358 |
| | | 2 | 1.5 | 0.55036 | 0.17118 | 1.76733 | 0.15360 | 1.42118 | 0.36723 |
| 50 | 30 | 1 | 0.5 | 0.51021 | 0.08361 | 0.99796 | 0.00422 | 0.55312 | 0.10559 |
| | | 1.5 | 1 | 0.51021 | 0.08361 | 1.45143 | 0.04723 | 1.01860 | 0.19525 |
| | | 2 | 1.5 | 0.51021 | 0.08361 | 1.81607 | 0.12262 | 1.37170 | 0.28424 |
| | 40 | 1 | 0.5 | 0.52049 | 0.11961 | 0.92545 | 0.04940 | 1.41970 | 0.25714 |
| | | 1.5 | 1 | 0.52049 | 0.11961 | 1.46462 | 0.03431 | 1.04072 | 0.17182 |
| | | 2 | 1.5 | 0.52049 | 0.11961 | 1.85091 | 0.09880 | 1.41970 | 0.25719 |
| 100 | 80 | 1 | 0.5 | 0.51021 | 0.08361 | 0.99969 | 0.00068 | 0.52127 | 0.06048 |
| | | 1.5 | 1 | 0.51021 | 0.08361 | 1.48124 | 0.01857 | 1.01775 | 0.11693 |
| | | 2 | 1.5 | 0.51021 | 0.08361 | 1.90260 | 0.06567 | 1.42089 | 0.18018 |
| | 90 | 1 | 0.5 | 0.52050 | 0.11961 | 0.99877 | 0.00045 | 0.53083 | 0.05737 |
| | | 1.5 | 1 | 0.52050 | 0.11961 | 1.48347 | 0.01589 | 1.02103 | 0.11204 |
| | | 2 | 1.5 | 0.52050 | 0.11961 | 1.91029 | 0.05957 | 1.43137 | 0.17302 |

progressive censoring schemes with m=14, 13, 12, 11 and 10 are (1.1880, 66.2), (1.1348, 66.2), (1.1882, 66.2), (1.0772, 53.9) and (0.7553, 46.3), respectively.

## 5   Conclusion

We develop some results on the power function distribution when progressive Type-II censoring is used with binomial removals. The maximum likelihood estimators for the model parameters were derived. The simulation results showed that as the sample size increases, the performance of the estimators improves in terms of the bias and the RMSE. The biases and the RMSEs for $p$ and $\beta$ decrease as $m$ increases. The bias and RMSE increase with the increase in the shape parameter $\beta$. The bias and RMSE for the estimators of $p$ and $\beta$ increase with the increase in parameter $p$. An application of real lifetime data was conducted, it illustrates the proposed censoring scheme.

**Table 3**: Mean and RMSE of the MLEs and for $p = 0.75$ and different choices of $n, m, \theta$ and $\beta$.

| $n$ | $m$ | $\hat{\theta}$ | $\hat{\beta}$ | $\hat{p}$ | | $\hat{\theta}$ | | $\hat{\beta}$ | |
|-----|-----|-----|-----|------|------|------|------|------|------|
| | | | | Mean | RMSE | Mean | RMSE | Mean | RMSE |
| 25 | 15 | 1 | 0.5 | 0.76234 | 0.12057 | 0.97366 | 0.01187 | 0.60158 | 0.16142 |
| | | 1.5 | 1 | 0.76234 | 0.12057 | 1.41241 | 0.08126 | 1.06821 | 0.29896 |
| | | 2 | 1.5 | 0.76234 | 0.12057 | 1.72261 | 0.17649 | 1.40003 | 0.42009 |
| | 20 | 1 | 0.5 | 0.77827 | 0.16000 | 0.99592 | 0.00899 | 0.60243 | 0.13902 |
| | | 1.5 | 1 | 0.77827 | 0.16000 | 1.43108 | 0.06666 | 1.00416 | 0.25630 |
| | | 2 | 1.5 | 0.77827 | 0.16000 | 1.76733 | 0.15360 | 1.43519 | 0.37113 |
| 50 | 30 | 1 | 0.5 | 0.75463 | 0.08281 | 0.99796 | 0.00422 | 0.56249 | 0.10805 |
| | | 1.5 | 1 | 0.75463 | 0.08281 | 1.45143 | 0.04723 | 1.03510 | 0.19815 |
| | | 2 | 1.5 | 0.75463 | 0.08281 | 1.81607 | 0.12262 | 1.39312 | 0.28874 |
| | 40 | 1 | 0.5 | 0.76234 | 0.12057 | 0.99892 | 0.00234 | 0.55915 | 0.09050 |
| | | 1.5 | 1 | 0.76234 | 0.12057 | 1.46462 | 0.03431 | 1.04560 | 0.17262 |
| | | 2 | 1.5 | 0.76234 | 0.12057 | 1.85091 | 0.09830 | 1.42612 | 0.25041 |
| 100 | 80 | 1 | 0.5 | 0.75463 | 0.08281 | 0.99969 | 0.00068 | 0.53249 | 0.06060 |
| | | 1.5 | 1 | 0.75463 | 0.08281 | 1.48124 | 0.01857 | 1.01997 | 0.11713 |
| | | 2 | 1.5 | 0.75463 | 0.08281 | 1.90260 | 0.06567 | 1.42390 | 0.19050 |
| | 90 | 1 | 0.5 | 0.76234 | 0.12057 | 0.99977 | 0.00045 | 0.53132 | 0.05744 |
| | | 1.5 | 1 | 0.76234 | 0.12057 | 1.48347 | 0.01589 | 1.02195 | 0.11218 |
| | | 2 | 1.5 | 0.76234 | 0.12057 | 1.91029 | 0.05957 | 1.43261 | 0.17326 |

## References

[1] L. M. Leemis. *Reliability, Probabilistic Models and Statistical Methods*. Prentice Hall, New Jersey, 1995.

[2] M. M. Smadi and A. A. Jaradat. System Reliability of Ailamujia Model and additive failure rate models. *Nonlinear Dynamics and System Theory* **21** (2) (2021) 193–201.

[3] A. C. Cohen. Progressively censored samples in life testing. *Technometrics* **5** (1963) 327–329.

[4] Balakrishnan and R. Aggarwala. *Progressive Censoring: Theory, Methods and Applications*. Birkhauser, Boston, 2000.

[5] J. F. Lawless. *Statistical Models and Methods for Lifetime Data*. John Wiley and Sons, 2003.

[6] N. R. Mann, R. E. Schafer and N. D. Singpurwalla. *Methods for Statistical Analysis of Reliability and Life Data*. John Wiley and Sons, 1974.

[7] N. Balakrishnan and A. Hossain. Inference for the Type II generalized logistic distribution under progressive Type II censoring. *Journal of Statistical Computation and Simulation* **77** (12) (2007) 1013–1031.

[8] M. M. Sarhan and A. Abuammoh. Statistical Inference Using Progressively Type−II Censored Data with Random Scheme. *International Mathematical Forum* **3** (35) (2008) 1713-1725.

[9] B. Pradhan and D. B. Kundu. On progressively censored generalized exponential distribution. *Test* **18** (3) (2009) 497–515.

[10] S. K. Singh, U. Singh and D. Kumar. Bayesian estimation of the exponentiated gamma parameter and reliability function under asymmetric loss function. *Revstat – Statistical Journal* **9** (3) (2011) 247–260.

[11] S. Parsi , M. Ganjali and N. F. Sanjari. Simultaneous Confidence Intervals for the Parameters of Pareto Distribution under Progressive Censoring. *Communications in Statistics - Theory and Methods* **39** (1) (2009) 94–106.

[12] S. J. Wu. Estimation for the two-parameter Pareto distribution. under progressive censoring with uniform removals. *Journal of Statistical Computation and Simulation* **73** (2) (2003) 125-134.

[13] S. J. Wu and C. T. Chang. Inference in the Pareto distribution based on progressive Type II censoring with random removals. *Journal of Applied Statistics* **30** (2) (2003) 163–172.

[14] A. Azimi and F. Yaghmaei. Bayesian Estimation Based on Rayleigh Progressive Type II Censored Data with Binomial Removals. *Journal of Quality and Reliability Engineering* (2013) 1–6.

[15] G. Prakash. Progressive Censored Burr Type-XII Distribution Under Random Removal Scheme: Some Inferences. *Afrika Statistika* **12** (2) (2017) 1275–1286.

[16] M. Chacko and R. Mohan. Statistical Inference for Gompertz Distribution based on Progressive Type-II Censored Data with Binomial Removals. *Sstatistica* **78** (3) (2018) 251–272.

[17] M. Salah. Moments from progressive type-II censored data of Marshall-Olkin exponential. *International Journal of Applied Mathematical Research* **1**(4) (2012) 771–786.

[18] C.-T. Lin, S. J. S. Wu and N. Balakrishnan. Inference for loggamma distribution based on progressively type-II censored data. *Communications in Statistics Theory and Methods* **35** (7) (2006) 1271-1292.

[19] N. Balakrishnan. Progressive censoring methodology: an appraisal. *Test* **16** (2) (2007) 211–259.

[20] N. Balakrishnan, E. Cramer, U. Kamps and N. Schenk. Progressive type II censored order statistics from exponential distributions. *Statistics* **35** (4) (2001) 537–556.

[21] M. Salah. Moments of upper record values from Marshall-Oklin exponential distribution. *Journal of Statistics Applications and Probability* **5** (2) (2016) 1–7.

[22] M. Salah. Bayesian estimation of the scale parameter of the Marshall-Olkin exponential distribution under progressively type-II censored samples. *Journal of Statistical Theory and Applications* **17** (1) (2018) 1–14.

[23] M. H. Tahir, M. Alizadeh, M. Mansoor and G. M. Cordeiro. The Weibull-power function distribution with applications. Hacettepe *Journal of Mathematics and Statistics* **45** (1) (2014) 245–265.

[24] J. Sarhan and A. Pandey. Estimation of parameters of a power function distribution and its characterization by k-th record values. *Statistica*, anno LXIV **3** (2004) 523–536.

[25] M. Meniconi and D. M. Barry. The Power Function Distribution: A Useful and Simple Distribution to Assess Electrical Component Reliability. *Journal Microelectron Reliability* **36** (9) (1996) 1207–1212.

[26] N. L. Johnson, S. Kutz and N. Balakrishnan. *Continuous Univariate Distributions*. Vol. 1-2. *John Wiley & Sons*, 1994.

[27] T. Makelainen, K. Schmidt and G. P. H. Styan. On the existence and uniqueness of the maximum likelihood estimate of a vector-valued parameter in fixed-size samples. *The Annals of Statistics* **9** (4) (1981) 758–767.

# On Self-Organization Structure for Fluid Dynamical Systems via Solitary Waves

H.M. Tenkam [1*], E.F. Doungmo Goufo [2] and S. Kumar [3]

[1] *Department of Mathematics and Applied Mathematics, North-west University, Private Bag X6001 Potchefstroom, 2520 South Africa.*
[2] *Department of Mathematical Sciences, University of South Africa,Florida Campus, 0003 South Africa.*
[3] *Department of Mathematics, National Institute of Technology, Jamshedpur, 831014 India.*

**Abstract:** The process of self-organization occurs and is used in many aspects of life with applications found in domains of biological, physical and machining systems. Finding ways to create this kind of processes has attracted the interest of many scientists around the world. We combine in this paper some mathematical concepts to model and generate the self-organization process happening in wave motion. We make use of the Harry Dym system together with the fractal and fractional operators. The resulting model is solved numerically and its stability results are provided. Numerical simulations show the combined system involved in a self-organization dynamic with the replication of the initial objects and the formation of subsequent fractal patterns which vary with the fractional operator. The results prove that we are in the presence of a system capable of artificially structuring fractals using mathematical concepts, numerical techniques, codes and simulations.

**Keywords:** *mathematical models; self-organization process; numerical simulation; fractal-fractional structures.*

**Mathematics Subject Classification (2010):** 70K75, 28A80, 26A33, 33F05, 93-00.

---

* Corresponding author: mailto:michel.djouosseutenkam@nwu.ac.za

## 1　Introduction

The self-organization process is found in many natural structures and represents the main concept of the Systems Science field. It sometimes refers to the formation of various patterns in some physical and biological systems. For instance, we can see it in the rippled dune formation in a sand desert or in the cells combination that creates highly structured and ordered tissues. In most of these systems, the order and structure are acquired thanks to the proximate means characterizing them. It is then possible to view the pattern formation at the global level of the structure due to interactions between components of lower levels. The whole process is specifically governed by natural selection characterizing physical and biological systems. However, some other systems (found in nature) can become organized due to external commands, for instance, human interventions (protocols, algorithms, simulations) that lead to the building of sophisticated societies, structures or machines. We are exploring the later case with the specific domain of wave-motion where the model of Harry Dym is considered [1–8].

It is important to recall that the self-organization process is closely related to the dynamical system theory. A number of dynamical systems have been investigated several times in the course of science history, but the concept remains fascinating for scientists. One of the reasons is the unpredictable trajectories that characterize the vast amount of applications found in engineering, physics, biology, (applied) mathematics, and medical sciences [4, 9–12, 14]. A simple example includes the study of chaotic systems with complicated bifurcations that exist there. The literature comprises diverse types of dynamical systems [10, 11, 13–15], namely, the classical dynamical system and also the open dynamical system. The later can be seen in Fig.1, where different orbits and trajectories can be observed. It starts with the initial trajectories (Fig.1 (upper right)) of an agent dynamical system in isolation in its suitable space $\mathcal{S}_\pi$. The process goes on with a decoupled agent dynamical system, see Fig.1 (upper left), well defined on its suitable total space $\mathfrak{S}_\tau$ and which joints together to form the total system shown in Fig.4 (lower left). The system is completed by the projection or paths, see Fig.1 (lower right), showing how an agent behaves in a particular environment ($\mathcal{S}_\pi$). The behavior of the system in this last space ($\mathcal{S}_\pi$) is the major symbolism at the core of the so-called open dynamical system as it contrasts with the agent in isolation (Fig.1 (upper right)). Particularly, the orbits in the open phase portrait for the embedded agent dynamical system (Fig.1 (lower right)) overlap, which is not the case for those of the agent in isolation (Fig.1 (upper right)). This is what makes open dynamical systems generally hard to study. This statement is supported by the types of dynamics observed in complex systems like fractals. Some of these dynamics are depicted in Fig.2 and Fig.3. These representations show different sorts of waves involved in fractal-type motifs. The fractal patterns are artificially (numerically) formed due to mathematical simulations issued from modeling the type of movements observed in nature around us. The fractal motif include sound-type fractal waves, heat-type fractal waves, particle fractal waves, ocean chaotic fractal waves, spiral wave fractal swirls, fluffy cloud chaotic fractal wave spirals, chaotic fractal light waves and so on.

### 1.1　Approximation results for the classical Harry Dym model

Let $\Omega = (a, b)$, $\mathbb{R} \ni T > 0$ $\mathbb{R} \ni b > a \in \mathbb{R}$ and $g \in C^0\left[[0, T] \times \Omega\right]$. Let $\alpha \in [0; 1], \beta \in (0, +\infty)$, then consider the non-linear Dym equation in its classical form. Existence and uniqueness of the exact solution are shown for the model under investigation that reads
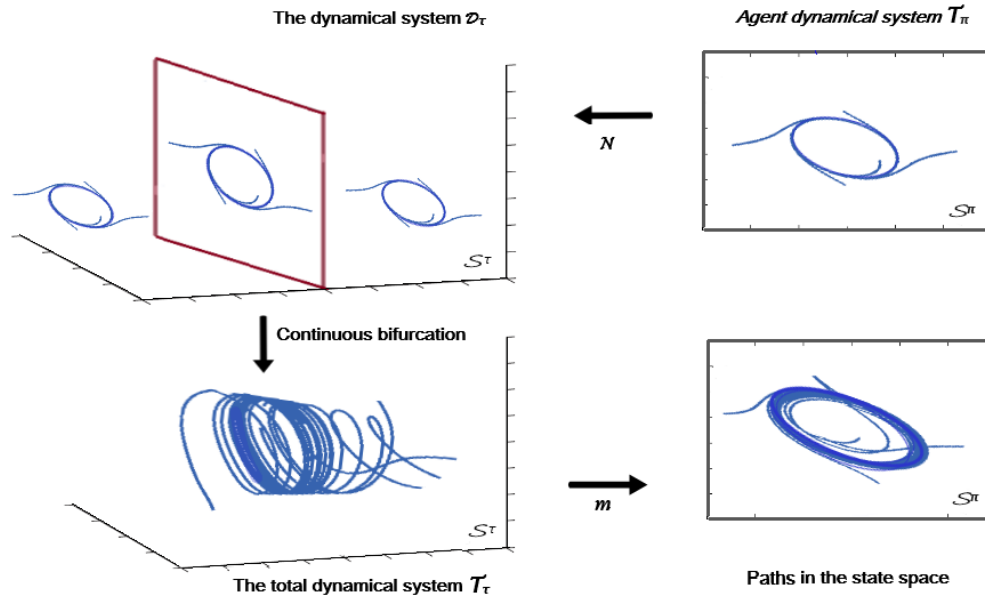
**Figure 1**: Basic principle of the open dynamical system. We can see the initial trajectories (upper right) of an agent dynamical system in isolation in its suitable space $\mathcal{S}_\pi$. The process goes on with a decoupled agent dynamical system (upper left), well defined on its suitable total space $\mathfrak{S}_\tau$ and which joints together to form the total system shown (lower left). The system is completed by the projection or paths (lower right) showing how an agent behaves in a particular environment ($\mathcal{S}_\pi$). The behavior of the system in this last space ($\mathcal{S}_\pi$) is the major symbolism at the core of the so-called open dynamical system as it contrasts with the agent in isolation (upper right). Particularly, the orbits in the open phase portrait for the embedded agent dynamical system (lower right) overlap, which is not the case for those of the agent in isolation (upper right).
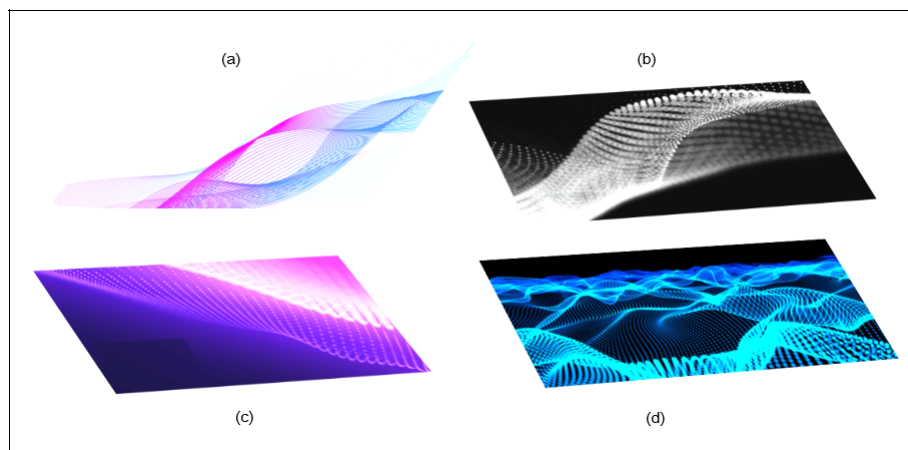


**Figure 2**: Simulation showing different sorts of waves involved in fractal-type motifs. The fractal patterns here are artificially (numerically) formed due to mathematical simulations issued from modeling the type of movements observed in nature. In (a) we have sound fractal waves, in (b) heat fractal waves, in (c) particle fractal wave and (d) ocean chaotic fractal wave.
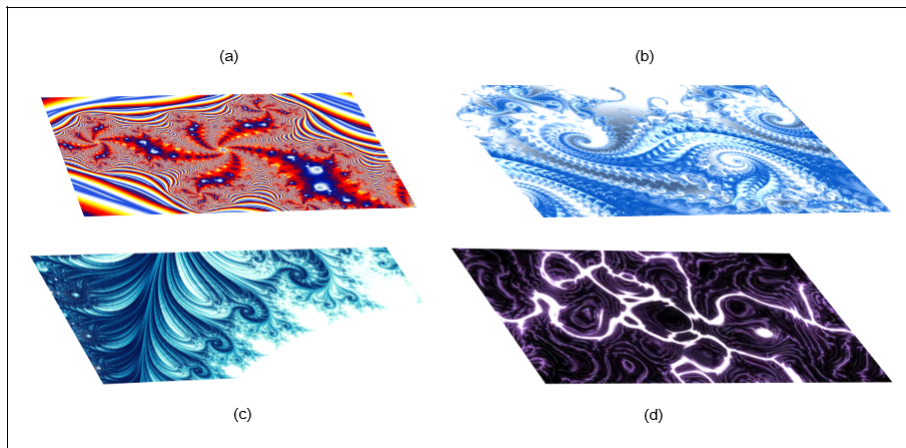
**Figure 3**: Simulation showing different sorts of waves involved in fractal-type patterns. The fractal motifs here are artificially (numerically) formed due to mathematical simulations issued from modeling the type of movements observed in nature. In (a) fractal wave multi color motion glowing lines, in (b) spiral wave fractal swirl, (c) fluffy cloud chaotic fractal wave spirals, in (d) chaotic fractal light waves.

as

$$\frac{\partial}{\partial t}g(t,x) = g^3 g_{xxx}(t,x), \tag{1}$$

subject to the initial condition

$$g(0,x) = g_0(x) \tag{2}$$

with $g: \ \Omega \longmapsto \mathbb{R}_+$.

The function $g$ can be approximated in the form

$$g(t,x) = \sum_{j=0}^{\infty} e_j \mathbf{H}_j(x), \tag{3}$$

here the coefficients $e_j$ are given by

$$e_j = 2^k \int_0^1 g(t,x)\mathbf{H}_j(x)dx, \tag{4}$$

where $j = 2^k + l, \ k \geq 0$ and $0 \leq l < 2^k$. Moreover, the $x$-dependant function $\mathbf{H}_j(x)$ is the Haar wavelet function [1, 9, 16–18]

$$\mathbf{H}_j(x) = \begin{cases} 1, & \text{if } \frac{l}{p} \leq x < \frac{l+1/2}{p}; \\ -1, & \text{if } \frac{l+1/2}{p} \leq x < \frac{l+1}{p}; \\ 0, & \text{elsewhere} \end{cases} \tag{5}$$

with $p = 2^k, \ k = 1, 2, \cdots, L$, where $L$ denotes the chosen resolution's level and $l$ represents the translation parameter which can take the values $0, 1, \cdots, p-1$. Because the

series of function $g(t, x)$ comprises an infinite number of terms, it can be obtained using the following definite sum:

$$g(t, x) = \sum_{j=0}^{p-1} e_j \mathbf{H}_j(x), \tag{6}$$

which takes the form

$$g(t, x) = {}^t \mathbf{e_p} \mathbf{H_p}(x)$$

with ${}^t \mathbf{e_p}$ being the transpose of

$$\mathbf{e_p} = \begin{pmatrix} e_0 \\ e_1 \\ \vdots \\ e_{p-1} \end{pmatrix} \quad \text{and} \quad \mathbf{H_p} = \begin{pmatrix} \mathbf{H}_0 \\ \mathbf{H}_1 \\ \vdots \\ \mathbf{H}_{p-1} \end{pmatrix}.$$

Now, using the Haar wavelet technique to solve the model (1) and (2), we can assume that the $t$-partial derivative $\frac{\partial g_{xxx}}{\partial t}(t, x)$ is expandable as follows:

$$\frac{\partial g_{xxx}}{\partial t}(t, x) = \sum_{j=0}^{2P} e_j \mathbf{H}_j(x), \quad t_r < t \le t_{r+1}, \tag{7}$$

where $2P$ is the number of collocation points calculated as

$$x_i = \frac{i - 1/2}{2P}, \quad \text{with } i = 1, 2, \cdots, 2P. \tag{8}$$

Integration of (7) respectively with respect to variables $t$ and $x$ leads to

$$g_{xxx}(t, x) = g_{xxx}(t_r, x) + (t - t_r) \sum_{j=1}^{2P} e_j \mathbf{H}_j(x),$$

$$g_{xx}(t, x) = g_{xx}(t, 0) - g_{xx}(t_r, 0) + g_{xx}(t_r, x) + (t - t_r) \sum_{j=1}^{2P} e_j \mathbf{M}_1^j(x)$$

and

$$g_x(t, x) = g_x(t, 0) - g_x(t_r, 0) + g_x(t_r, x) + x[g_{xx}(t, 0)] - g_{xx}(t_r, 0) + (t - t_r) \sum_{j=1}^{2P} e_j \mathbf{M}_2^j(x),$$

which finally leads to

$$g(t, x) = g(t, 0) + g(t_r, x) - g(t_r, 0) + x[g_x(t, 0) - g_x(t_r, 0)]$$

$$+ \frac{x^2}{2}[g_x(t, 1) - g_x(t, 0) + g_x(t_r, 0) - g_x(t_r, 1)] \tag{9}$$

$$(t - t_r) \sum_{j=1}^{2P} e_j \left( -\frac{x^2}{2} \mathbf{M}_2^j(1) + \mathbf{M}_3^j(x) \right),$$

where we have considered at the point $x = 1$ the operational matrix $\mathbf{M}$ defined in its general expression for the indexes $j = l + p + 1$ by

$$\mathbf{M}_s^j(x) = \begin{cases} \frac{1}{s!}(x - l/p)^s, & \text{if } \frac{l}{p} \leq x < \frac{l+1/2}{p}; \\ \frac{1}{s!}\left[(x - l/p)^s - 2(x - \frac{l+1/2}{p})^s\right], & \text{if } \frac{l+1/2}{p} \leq x < \frac{l+1}{p}; \\ \frac{1}{s!}\left[(x - l/p)^s - 2(x - \frac{l+1/2}{p})^s + (x - \frac{l+1}{p})^s\right], & \text{if } \frac{l+1/2}{p} \leq x < \frac{l+1}{p}; \\ 0, & \text{elsewhere.} \end{cases} \quad (10)$$

The differentiation of (9) with respect to variable $t$ is followed by the discretization at the point $(t_r, x_i)$

$$g(t_{r+1}, x_i) = g(t_{r+1}, 0) + g(t_r, x_i) - g(t_r, 0) + x_i[g_x(t_{r+1}, 0) - g_x(t_r, 0)]$$

$$+ \frac{x_i^2}{2}[g_x(t_{r+1}, 1) - g_x(t_{r+1}, 0) + g_x(t_r, 0) - g_x(t_r, 1)]$$

$$(t_{r+1} - t_r) \sum_{j=1}^{2P} e_j \left(-\frac{x_i^2}{2}\mathbf{M}_2^j(1) + \mathbf{M}_3^j(x_i)\right),$$

$$\frac{\partial g}{\partial t}(t_{r+1}, x_i) = \frac{\partial g}{\partial t}(t_{r+1}, 0) + x_i \frac{\partial g_x}{\partial t}(t_{r+1}, 0) + \frac{x_i^2}{2}[\frac{\partial g_x}{\partial t}(t_{r+1}, 1) - \frac{\partial g_x}{\partial t}(t_{r+1}, 0)] \quad (11)$$

$$\sum_{j=1}^{2P} e_j \left(-\frac{x_i^2}{2}\mathbf{M}_2^j(1) + \mathbf{M}_3^j(x_i)\right).$$

Still, using the discretization at the point $(t_r, x_i)$ and the substitution into (1) leads to

$$\sum_{j=1}^{2P} e_j \left(\frac{x_i^2}{2}\mathbf{M}_2^j(1) - \mathbf{M}_3^j(x_i) + g^3(t_r, x_i)(t_{r+1} - t_r)\mathbf{H}_j(x_i)\right)$$

$$= \frac{\partial g}{\partial t}(t_{r+1}, 0) - g^3(t_r, x_i)g_{xxx}(t_r, x_i) + x_i \frac{\partial g_x}{\partial t}(t_{r+1}, 0) + \frac{x_i^2}{2}[\frac{\partial g_x}{\partial t}(t_{r+1}, 1) + \frac{\partial g_x}{\partial t}(t_{r+1}, 0)], \quad (12)$$

equivalently,

$$\sum_{j=1}^{2P} e_j \left(\frac{x_i^2}{2}\mathbf{M}_2^j(1) - \mathbf{M}_3^j(x_i) + g^3(t_r, x_i)(t_{r+1} - t_r)\mathbf{H}_j(x_i)\right)$$

$$+ g^3(t_r, x_i)g_{xxx}(t_r, x_i) - \frac{1}{t_{r+1} - t_r}[g(t_{r+1}, 0) - g(t_r, 0)] - x_i \left[\frac{\partial g}{\partial t}(t_{r+1}, 0) - \frac{\partial g}{\partial t}(t_r, 0)\right]$$

$$- \frac{x_i^2}{2(t_{r+1} - t_r)}\left[\left(\frac{\partial g}{\partial t}(t_{r+1}, 1) - \frac{\partial g}{\partial t}(t_r, 1)\right) - \left(\frac{\partial g}{\partial t}(t_{r+1}, 0) - \frac{\partial g}{\partial t}(t_r, 0)\right)\right] = 0, \quad (13)$$

where we have used the scheme

$$\frac{\partial g}{\partial t}(t_{r+1}, 0) = \frac{1}{t_{r+1} - t_r}[g(t_{r+1}, 0) - g(t_r, 0)]$$

and

$$\frac{\partial g}{\partial t}(t_{r+1}, 1) = \frac{1}{t_{r+1} - t_r}[g(t_{r+1}, 1) - g(t_r, 1)].$$
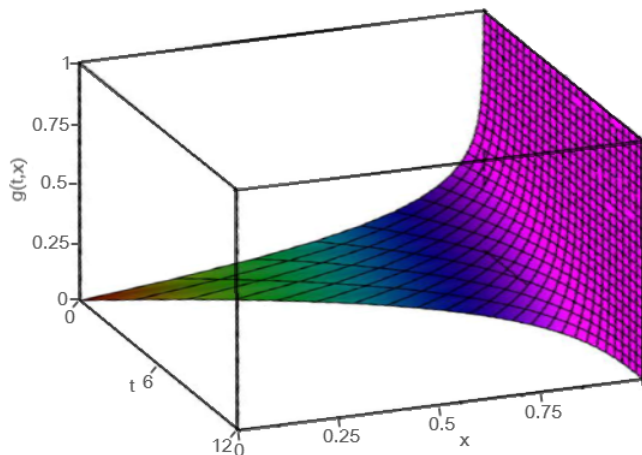
**Figure 4**: Three-dimensional representation of the solution $g(t,x)$ to model (1) and (2) when $g_0(x) = x^2$.

Hence, equation (13) allows the calculation of the Haar wavelet coefficients, which are used to establish the numerical solution (9). The related numerical simulations are depicted in Fig.1 to Fig.5 relating the usual wave dynamics with different given initial conditions.

## 1.2 Recent progress in self-organization operators

To help with the advancement of sciences and try to understand and describe many unsolved problems that were too complex to model, fractional derivatives were proposed. Those operators have since shown their infinite importance in applied sciences modelling. Today some authors classify them into two types: local and non-local [19–22]. Since the moment when Riemann and Liouville proposed their integral, from which derivatives of fractional were constructed, there has been a huge development in the domain with various and variant definitions proposed by a number of authors. In fact, the latest related literature comprises (but is not limited to) the following definitions.

**Formerly:**

- The Riemann–Liouville derivative $^{RL}D_t^\gamma$ with fractional order $\gamma$ reads as

$$^{RL}D_t^\gamma g(t,x) = \frac{1}{\Gamma(n-\gamma)} \left(\frac{d}{dt}\right)^n \int_0^t (t-\upsilon)^{n-\gamma-1} g(\upsilon,x)\, d\upsilon, \qquad (14)$$

$n-1 < \gamma \leq n$.

- The Caputo derivative $^CD_t^\gamma$ with fractional order $\gamma$ reads as

$$^CD_t^\gamma g(t,x) = \frac{1}{\Gamma(n-\gamma)} \int_0^t (t-\upsilon)^{n-\gamma-1} \left(\frac{d}{d\upsilon}\right)^n g(\upsilon,x)\, d\upsilon, \qquad (15)$$

$n-1 < \gamma \leq n$.
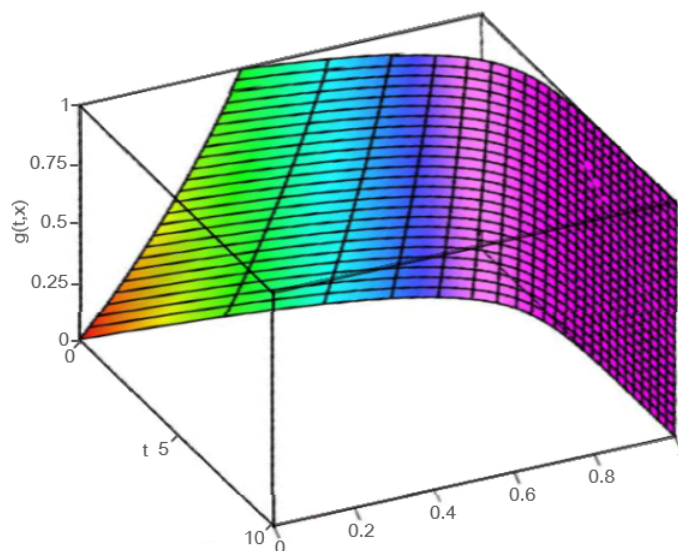
**Figure 5**: Three-dimensional representation of the solution $g(t, x)$ to model (1) and (2) when $g_0(x) = e^x - 1$.
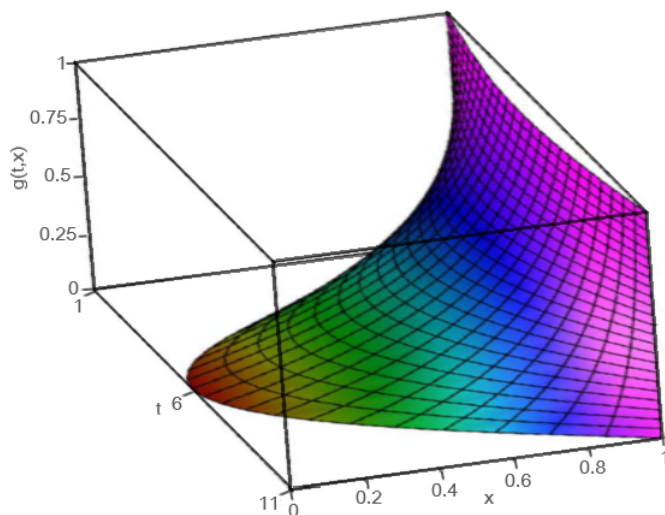


**Figure 6**: Three-dimensional representation of the solution $g(t, x)$ to model (1) and (2) when $g_0(x) = xe^x$.

**More recently [14, 20, 23, 24]:**

- The Caputo-Fabrizio derivative $^{CF}D_t^\gamma$ with fractional order $\gamma$ reads as

$$^{CF}D_t^\gamma g(t,x) = \frac{\mathbf{n}(\gamma)}{(1-\gamma)} \int_0^t \frac{\partial g}{\partial v}(v,x) \exp\left(-\gamma(t-v)(1-\gamma)^{-1}\right) dv, \qquad (16)$$

where $\mathbf{n}(\gamma)$ satisfies

$$\mathbf{n}(0) = \mathbf{n}(1) = 1. \qquad (17)$$

- The new-Riemann–Liouville derivative $^{nRL}D_t^\gamma$ with fractional order $\gamma$ is given by

$$^{nRL}D_t^\gamma g(t,x) = \frac{(2-\gamma)\mathbf{n}(\gamma)}{2(1-\gamma)} \frac{d}{dt} \int_0^t g(v,x) \exp\left(-\gamma(t-v)(1-\gamma)^{-1}\right) dv. \qquad (18)$$

- The Atangana-Baleanu-Caputo derivative $^{ABC}D_t^\gamma$ with fractional order $\gamma$ reads as

$$^{ABC}D_t^\gamma g(t,x) = \frac{\mathbf{n}(\gamma)}{(1-\gamma)} \int_0^t \frac{\partial g}{\partial v}(v,x) E_\gamma\left[-\gamma(t-v)^\gamma(1-\gamma)^{-1}\right] dv. \qquad (19)$$

In the definitions here above, the function $g$ is assumed to belong to the Sobolev space

$$S^1(\alpha,\beta) = \{g : g, \frac{\partial}{\partial t}g \in L^2(\alpha,\beta)\}. \qquad (20)$$

- The Caputo-sense two-parameter derivative $^{CG}D_t^{\gamma,\theta}$ with fractional order $\gamma$, when knowing the parameter $\theta \in \mathbb{R}$, reads as

$$^{CG}D_t^{\gamma,\theta} g(t,x) = \frac{\theta\tilde{\mathbf{n}}(\gamma,\theta)}{(\theta-\gamma)} \int_0^t \frac{\partial g}{\partial v}(v,x) (t-v)^{\theta-1} E_{\gamma,\theta}\left[-\gamma\theta(t-v)^\gamma(\theta-\gamma)^{-1}\right] dv, \qquad (21)$$

where $\theta \in \mathbb{R}$ and $\tilde{\mathbf{n}}(\gamma,\theta)$ verifies $\tilde{\mathbf{n}}(0,1) = \tilde{\mathbf{n}}(1,1) = 1$.

**Introduction to fractal-fractional derivative**

Initially defined to be the convolution operation between a fractal differential operator and the usual law functions found in fractional calculus, the fractal-fractional derivative [25] was introduced in order to attract and describe a huge number of non-local problems in real life while respecting the fractal structure that characterizes them. In the recent literature, one can find a number of versions for the definitions of fractal-fractional operation and this mainly depends on the kind of law function we choose to use. Some are given as follows.

**Definition 1.1** We consider $\Omega \in \mathbb{R}^3$, $\quad T \in \mathbb{R}$, and assume that $g(t,x)$ defined on $(0,T) \times \Omega$ is $t$–fractal differentiable with the order $\gamma$ on the interval $(0,T)$, then:

1. The fractal-fractional derivative of $g$ of order $\gamma$ in the sense of Riemann-Liouville with the power law reads as

$$^{FRp}D_t^\gamma g(t,x) = \frac{1}{\Gamma(1-\gamma)} \frac{\partial}{\partial t^\gamma} \int_0^t g(\vartheta,x)(t-\vartheta)^{-\gamma} d\vartheta, \qquad (22)$$

where $\frac{\partial}{\partial t^\gamma}g$ is defined as

$$\frac{\partial}{\partial t^\gamma}g(t,x_0) = \lim_{t \to t_0} \frac{g(t,x) - g(t,x_0)}{t^\gamma - t_0^\gamma}.$$

The generalized version of (22) is defined by

$$^{FRp}D_t^{\gamma,\varsigma}g(t,x) = \frac{1}{\Gamma(1-\gamma)}\frac{\partial^\varsigma}{\partial t^\gamma}\int_0^t g(\vartheta,x)(t-\vartheta)^{-\gamma}d\vartheta, \tag{23}$$

with $\varsigma > 0$ and $\frac{\partial^\varsigma}{\partial t^\gamma}g$ given by

$$\frac{\partial^\varsigma}{\partial t^\gamma}g(t,x_0) = \lim_{t\to t_0}\frac{g^\varsigma(t,x) - g^\varsigma(t,x_0)}{t^\gamma - t_0^\gamma}.$$

Similarly, the Caputo version of this definition can be given.

2. The fractal-fractional derivative of $g$ of order $\gamma$ in the sense of Caputo with the power law reads as

$$^{FCp}D_t^\gamma g(t,x) = \frac{1}{\Gamma(1-\gamma)}\int_0^t \frac{\partial}{\partial\vartheta^\gamma}g(\vartheta,x)(t-\vartheta)^{-\gamma}d\vartheta, \tag{24}$$

the generalized version is

$$^{FCp}D_t^{\gamma,\varsigma}g(t,x) = \frac{1}{\Gamma(1-\gamma)}\int_0^t \frac{\partial^\varsigma}{\partial\vartheta^\gamma}g(\vartheta,x)(t-\vartheta)^{-\gamma}d\vartheta. \tag{25}$$

The following definitions are related to the exponential law.

3. The fractal-fractional derivative of $g$ of order $\gamma$ in the sense of Riemann-Liouville with the exponential law reads as

$$^{FRe}D_t^\gamma g(t,x) = \frac{\mathbf{n}(\gamma)}{(1-\gamma)}\frac{\partial}{\partial t^\gamma}\int_0^t g(\vartheta,x)\exp\left(\frac{-\gamma(t-\vartheta)}{1-\gamma}\right)d\vartheta, \tag{26}$$

where $\mathbf{n}(0) = \mathbf{n}(1) = 1$, with

the generalized version

$$^{FRe}D_t^{\gamma,\varsigma}g(t,x) = \frac{\mathbf{n}(\gamma)}{(1-\gamma)}\frac{\partial^\varsigma}{\partial t^\gamma}\int_0^t g(\vartheta,x)\exp\left(\frac{-\gamma(t-\vartheta)}{1-\gamma}\right)d\vartheta. \tag{27}$$

4. The fractal-fractional derivative of $g$ of order $\gamma$ in the sense of Caputo with the exponential law reads as

$$^{FCe}D_t^\gamma g(t,x) = \frac{\mathbf{n}(\gamma)}{(1-\gamma)}\int_0^t \frac{\partial}{\partial\vartheta^\gamma}g(\vartheta,x)\exp\left(\frac{-\gamma(t-\vartheta)}{1-\gamma}\right)d\vartheta, \tag{28}$$

with the generalized version

$$^{FCe}D_t^{\gamma,\varsigma}g(t,x) = \frac{\mathbf{n}(\gamma)}{(1-\gamma)}\int_0^t \frac{\partial^\varsigma}{\partial\vartheta^\gamma}g(\vartheta,x)\exp\left(\frac{-\gamma(t-\vartheta)}{1-\gamma}\right)d\vartheta. \tag{29}$$

The following definitions are related to the Mittag-Leffler law.

5. The fractal-fractional derivative of $g$ of order $\gamma$ in the sense of Riemann-Liouville with the Mittag-Leffler law reads as

$$^{FRm}D_t^\gamma g(t,x) = \frac{\mathbf{n}(\gamma)}{(1-\gamma)} \frac{\partial}{\partial t^\gamma} \int_0^t g(\vartheta,x) E_\gamma \left( \frac{-\gamma(t-\vartheta)^\gamma}{1-\gamma} \right) d\vartheta, \qquad (30)$$

where $\mathbf{n}(\gamma)$ is a regularization function. Here the generalized version is

$$^{FRm}D_t^{\gamma,\varsigma} g(t,x) = \frac{\mathbf{n}(\gamma)}{(1-\gamma)} \frac{\partial^\varsigma}{\partial t^\gamma} \int_0^t g(\vartheta,x) E_\gamma \left( \frac{-\gamma(t-\vartheta)^\gamma}{1-\gamma} \right) d\vartheta. \qquad (31)$$

6. Then the fractal-fractional derivative of $g$ of order $\gamma$ in the sense of Caputo with the Mittag-Leffler law reads as

$$^{FCm}D_t^\gamma g(t,x) = \frac{\mathbf{n}(\gamma)}{(1-\gamma)} \int_0^t \frac{\partial}{\partial \vartheta^\gamma} g(\vartheta,x) E_\gamma \left( \frac{-\gamma(t-\vartheta)^\gamma}{1-\gamma} \right) d\vartheta, \qquad (32)$$

where $\mathbf{n}(\gamma)$ is a regularization real function related to the definition and with

the more general version given as

$$^{FCm}D_t^{\gamma,\varsigma} g(t,x) = \frac{\mathbf{n}(\gamma)}{(1-\gamma)} \int_0^t \frac{\partial^\varsigma}{\partial \vartheta^\gamma} g(\vartheta,x) E_\gamma \left( \frac{-\gamma(t-\vartheta)^\gamma}{1-\gamma} \right) d\vartheta. \qquad (33)$$

**Remark 1.1** In this analysis, we make use of the operator given by (26). To proceed, we have to associate to it another great concept, its associated fractal-fractional operator. Whence, we define the fractal-fractional integral of order $\gamma$, associated to (26), as follows:

$$^{FRe}\mathbf{I}_t^\gamma g(t,x) = \frac{\gamma(1-\gamma)t^{\gamma-1}g(t,x)}{\mathbf{n}(\gamma)} + \frac{\gamma^2}{\mathbf{n}(\gamma)} \int_0^t \upsilon^{\gamma-1} g(\upsilon) d\upsilon, \quad t > 0. \qquad (34)$$

## 2  Self-Organization Process for Harry Dym Model

### 2.1  Stability of the fractal Dym model

In this section we consider the following system:

$$^{FRe}D_t^\gamma g(t,x) = g^3 g_{xxx}(t,x), \qquad (35)$$

subject to the initial condition

$$g(0,x) = g_0(x), \qquad (36)$$

where we have combined the Dym model with the fractal-fractional derivative [25, 26], recalled to be defined in (26) as

$$^{FRe}D_t^\gamma g(t,x) = \frac{\mathbf{n}(\gamma)}{(1-\gamma)} \frac{\partial}{\partial t^\gamma} \int_0^t g(\vartheta,x) \exp\left( \frac{-\gamma(t-\vartheta)}{1-\gamma} \right) d\vartheta, \qquad (37)$$

where $\mathbf{n}(0) = \mathbf{n}(1) = 1$. To proceed further in the analysis, the fractal-fractional operator (37) should be associated with its anti-derivative called the fractal-fractional integral of order $\gamma$, and given by

$$^{FF}\mathbf{I}_t^\gamma g(t,x) = \frac{\gamma}{\Gamma(\gamma)} \int_0^t \varpi^{-\gamma} g(\mathbf{x},\varpi)(t-\varpi)^{\gamma-1} d\varpi, \quad t > 0. \qquad (38)$$

We have solved the classical model in Subsection 1.1 using the Haar wavelet method, which has provided a comprehensive analysis of the system and a global picture of the dynamic in the absence of the fractal influence. We are now using the Legendre wavelets method ( [27, 28]) to solve the fractal-fractional system (35)–(36). Hence, we can transform it into a compact form with the application of the associated fractional integral on both sides of the model to have

$$^{FF}D_t^\gamma g(t, x) = {}^T M_m \Psi_m(t), \tag{39}$$

where the matrix $\Psi_m(t)$ is given with the elements defining the Legendre wavelets which are expressed by

$$\psi_{nm}(t) = \begin{cases} 2^{l/2}\sqrt{2m+1}L_m^*(2^l t - n)), & \text{if } t \in [\frac{n}{2^l}, \frac{n+1}{2^l}]; \\ 0, & \text{elsewhere.} \end{cases} \tag{40}$$

Recall that the shifted Legendre polynomial, given by $L_m^*$, is defined on $[0, 1]$ by $L_m^*(t) = L_m(2t - 1)$, with $(L_m(2t - 1))_m$ representing the family

$$L_0 = 1, \ L_1 = x, \ L_{m+1}(x) = \frac{1 + 2m}{m + 1}xL_m(x) - \frac{m}{1 + m}L_{m-1}(x), \quad m = 1, 2, \cdots, N - 1. \tag{41}$$

Recall also that we have considered $\mathbb{N} \ni J$ points $x = x_1, x_2, \cdots, x_J$ and $N$ is a positive integer number, $n = 1, 2, \cdots, 2^l - 1$ and $l = 0, 1, 2, \cdots$. $M_m = {}^T [\mathbf{m}_m^1, \mathbf{m}_m^2, \cdots, \mathbf{m}_m^m]$ are coefficients to be found with $^T M_m$ being the transpose of the matrices $M_m$, respectively. Associating the initial conditions yields

$$g(t, x_j) \approx {}^T M_m Q_{m \times m}^\gamma \Psi_m(t) + g_0(x_j), \tag{42}$$

where $Q_{m \times m}^\gamma$ is the Legendre operational matrix of integration and the subscript $m$ denotes its dimension. We know that [27,28] that the Legendre wavelets can be expanded into an $m$-term form as

$$\Psi_m(t) = \Upsilon_{m \times m} A_m(t), \tag{43}$$

where $A_m(t) = {}^T [a_1(t), a_2(t), \cdots, a_m(t)]$ are the block pulse functions so that

$$a_l(t) = \begin{cases} 1, & \text{if } t \in [\frac{l-1}{m}, \frac{l}{m}]; \\ 0, & \text{elsewhere} \end{cases} \tag{44}$$

for each $l = 1, 2, \cdots m$, and $\Upsilon$ is the Legendre wavelet matrix

$$\Upsilon_{m \times m} = \left[ \Psi_m \left( \frac{1}{2m} \right) \Psi_m \left( \frac{3}{2m} \right) \cdots \Psi_m \left( \frac{2m - 1}{2m} \right) \right].$$

Now the substitution of (43) into system (42) leads to

$$g(t, x_j) \approx {}^T M_m^1 Q_{m \times m}^\gamma \Upsilon_{m \times m} A_m(t) + [[g_0(x_j)]_i]A_m(t), \tag{45}$$

where

$$[[g_0(x_j)]_i] = [[g_0(x_j)]_1, g_0(x_j)]_2, \cdots, g_0(x_j)]_m].$$

Now let

$$^{T}M_{m}^{i}Q_{m\times m}^{\gamma}\Upsilon_{m\times m} = \mathcal{M}_{1\times m}^{\gamma,i} = [\mathbf{m}_{1}^{\gamma,i}, \mathbf{m}_{2}^{\gamma,i}, \cdots, \mathbf{m}_{m}^{\gamma,i}]. \tag{46}$$

Now the use of the collocations points $t_i = \frac{2i-1}{2^{l+1}N}$, $i = 1, 2, 3, \cdots, m$, $N \in \mathbb{N}$, to disperse $t$ and the substitution of (45) and (46) into the system (35) lead to

$$
\begin{aligned}
^{T}M_{m}^{1}\Upsilon_{m\times m} &= \tfrac{x_{i}^{2}}{2}\mathcal{M}_{1\times m}^{\gamma,i}(1) - \mathcal{M}_{1\times m}^{\gamma,i}(x_{i}) + g^{3}(t_{r}, x_{i})(t_{r+1} - t_{r})\Upsilon_{1\times m}(x_{i}) \\
&\quad + \left[\mathbf{m}_{1}^{\gamma,2}, \mathbf{m}_{2}^{\gamma,2}, \cdots, \mathbf{m}_{m}^{\gamma,2}\right]^{T}\left[\mathbf{m}_{1}^{\gamma,j}, \mathbf{m}_{2}^{\gamma,j}, \cdots, \mathbf{m}_{m}^{\gamma,j}\right] \\
&\quad + [[g_{0}(x_{j})]_{1}, [g_{0}(x_{j})]_{2}, \cdots, [g_{0}(x_{j})]_{m}].
\end{aligned}
\tag{47}
$$

Hence, we obtain this non-linear system of equations with $3m$ unknown coefficients $\mathbf{m}_{l}^{\gamma,i}$, $1 \le i \le 3$, $1 \le l \le m$, which are easily found using the Newton iteration method. Then exploiting the model (42) leads to the expected numerical solution $(g(t, x))$.

## 2.2 Error analysis

Consider $\mathbb{N} \ni J$ points $x = x_1, x_2, \cdots, x_J$. We assume here that the solution $g = g(t, x_i)$ is a function whose second order derivative with respect to $t$ is bounded as

$$\left|\frac{\partial^2 g}{\partial t^2}\right| \le \alpha_0^1.$$

Making use of the Legendre wavelet schemes described here above to approximate the solution $g(t, x_i)$ means it can be expanded as a uniformly convergent series that reads as

$$g(t, x_i) = \sum_{n=0}^{\infty}\sum_{m=0}^{\infty} \mathbf{m}_{nm}^{\gamma,1}\psi_{nm}(t)$$

with

$$\mathbf{m}_{nm}^{\gamma,1} = \langle g(t, x_i), \psi_{nm}(t)\rangle. \tag{48}$$

We have the following convergence results.

**Proposition 2.1** *Let* $i = 1, 2, \cdots, J \in \mathbb{N}$ *and* $\alpha_0^1 > 0$. *Assume that the solution* $g(t, x_i)$ *is a continuous function on* $[0, T]$ *whose second order derivative with respect to* $t$ *is bounded as*

$$\left|\frac{\partial^2 g}{\partial t^2}\right| \le \alpha_0^1,$$

*then the coefficients* $\boldsymbol{m}_{nm}^{\gamma,1}$ *satisfy*

$$|\boldsymbol{m}_{nm}^{\gamma,1}| < \frac{(12)^{1/2}\alpha_0^1}{(2m-3)^2\left(\sqrt{2n}\right)^5}.$$

***Proof.*** For $i \in \mathbb{N}$, let us consider the function $g = g(t, x_i)$ and using the definition of the Legendre wavelet coefficients given in (48) and taking into account (40), we have

$$
\begin{aligned}
\mathbf{m}_{nm}^{\gamma,1} &= \int_0^1 g(t, x_i)\psi_{nm}(t)dt \\
&= \int_{\frac{n}{2^l}}^{\frac{n+1}{2^l}} g(t, x_i)2^{l/2}\sqrt{2m+1}L_m^*(2^l t - n)dt \\
&= \sqrt{\frac{1+2m}{2^l}} \int_0^1 g\left(\frac{n+\xi}{2^l}, x_i\right) L_m^*(\xi)d\xi
\end{aligned}
$$

(where we have changed the variable as $t = \dfrac{n+\xi}{2^l}$)

$$
\begin{aligned}
&= \sqrt{\frac{1}{(2m+1)2^{3l+2}}} \int_0^1 \frac{\partial g}{\partial t}\left(\frac{n+\xi}{2^l}, x_i\right)\left(L_{m+1}^*(\xi) - L_{m-1}^*(\xi)\right)d\xi \\
&= \sqrt{\frac{1}{(2m+1)2^{5l+2}}} \int_0^1 \frac{\partial^2 g}{\partial t^2}\left(\frac{n+\xi}{2^l}, x_i\right)\left(\frac{L_{m+2}^*(\xi) - L_m^*(\xi)}{6+4m} - \frac{L_m^*(\xi) - L_{m-2}^*(\xi)}{-2+4m}\right)d\xi,
\end{aligned}
$$

where we have used the derivative properties of the shifted Legendre polynomials [27,28]. Hence

$$
\begin{aligned}
|\mathbf{m}_{nm}^{\gamma,1}| &\leq \left|\sqrt{\frac{1}{(2m+1)2^{5l+2}}}\right| \\
&\quad \int_0^1 \left|\frac{\partial^2 g}{d\partial t^2}\left(\frac{n+\xi}{2^l}, x_i\right)\right|\left|\left(\frac{L_{m+2}^*(\xi) - L_m^*(\xi)}{6+4m} - \frac{L_m^*(\xi) - L_{m-2}^*(\xi)}{-2+4m}\right)\right|d\xi.
\end{aligned} \tag{49}
$$

Developing the right-hand side of the inequality and making use of the constraint property $|x''(t)| \leq \alpha_0^1$ and the orthogonality property of the shifted Legendre polynomials finally lead to

$$
|\mathbf{m}_{nm}^{\gamma,1}| \leq \sqrt{\frac{1}{\sqrt{2m+1}}} \cdot \frac{1}{2^{(5/2)l+1}} \cdot \alpha_0^1 \cdot \sqrt{\frac{\sqrt{3}}{(2m-3)}} \cdot \frac{1}{2m-1} < \frac{(12)^{1/2}\alpha_0^1}{(2m-3)^2\left(\sqrt{2n}\right)^5},
$$

and the proposition is concluded. This result leads to the following error estimate.

**Corollary 2.1** *Let $i = 1, 2, \cdots, J \in \mathbb{N}$ and $\alpha_0^1 > 0$. Assume that the solution $g(t, x_i)$ is a continuous function on $[0,1]$ whose second order derivative with respect to $t$ is bounded as*

$$
\left|\frac{\partial^2 g}{\partial t^2}\right| \leq \alpha_0^1,
$$

*then the error made when $g_{kN} = \sum_{n=0}^{2^l-1}\sum_{m=0}^{N-1}\mathbf{m}_{nm}^{\gamma,1}\psi_{nm}(t)$ approximates $g(t, x_i)$ satisfies*

$$
\Delta_{kN}^1 < (12)^{1/2}\alpha_0^1\sqrt{\sum_{n=2^l}^{\infty}\sum_{m=N}^{\infty}\frac{1}{32n^5(2m-3)^4}}.
$$
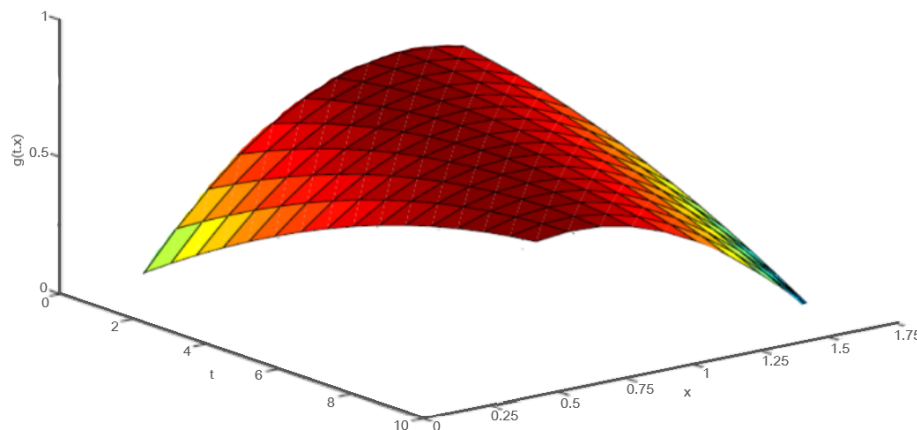
**Figure 7**: Three-dimensional representation of the solution $g(t,x)$ to model (35)–(36) when $g_0(x) = \frac{6}{10}\mathrm{e}^x$ and $\gamma = 1$.

## 2.3  Numerical applications

Now, having solved the model and shown its stability results, we perform in this section some numerical simulations showing the behavior of the fractal-fractional system (35)–(36). The graphs in Fig.7 to Fig.12 show such behavior in three-dimensional and two-dimensional space. In Fig.7, we can see the three-dimensional representation of the solution $g(t,x)$ when $\gamma = 1$ with $g_0(x) = \frac{6}{10}\mathrm{e}^x$. The two-dimensional representation is depicted in Fig.8. For $\gamma = 0.85$, the behavior of the solution $g(t,x)$ changes as depicted in Fig.9 – Fig.10 in three and two dimensions, respectively. The dynamic becomes involved in a self-organization process. This process consists of structuring itself in such a manner that the initial object is replicated approximately exactly to itself or to a part of itself. The process continues with the self-organization process which expands and multiplies in a similar way, for $\gamma = 0.65$, as shown in Fig.11 – Fig.12. Briefly, the system is shown to create diverse pattern formation processes, in this case, very important in the wave-motion domain. Thus, the system is capable of artificially structuring the fractals using mathematical concepts, numerical techniques, codes and simulations.

## 3  Concluding Remarks

We have combined some mathematical concepts and been able to model, solve and simulate a self-organization process related to the dynamics of wave motion. The resulting model, that includes the Harry Dym system, the fractal and fractional operators, has been solved numerically and its stability results have been given. Numerical simulations have proven a dynamic involved in a self-organization process where initial objects are replicated and various fractal patterns are formed. Numerical simulations have also proven that the fractal patterns vary with the fractional order derivative. Hence, this paper improves the preceding works in the domain as it reveals a system capable of artificially structuring the fractal patterns using mathematical concepts.
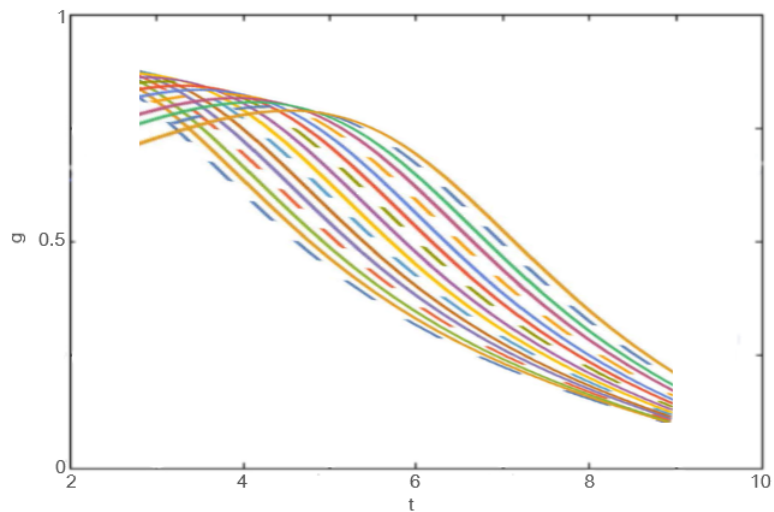
**Figure 8**: Two-dimensional representation of the solution $g(t, x)$ to model (35)–(36) when $g_0(x) = \frac{6}{10}\mathrm{e}^x$ and $\gamma = 1$.
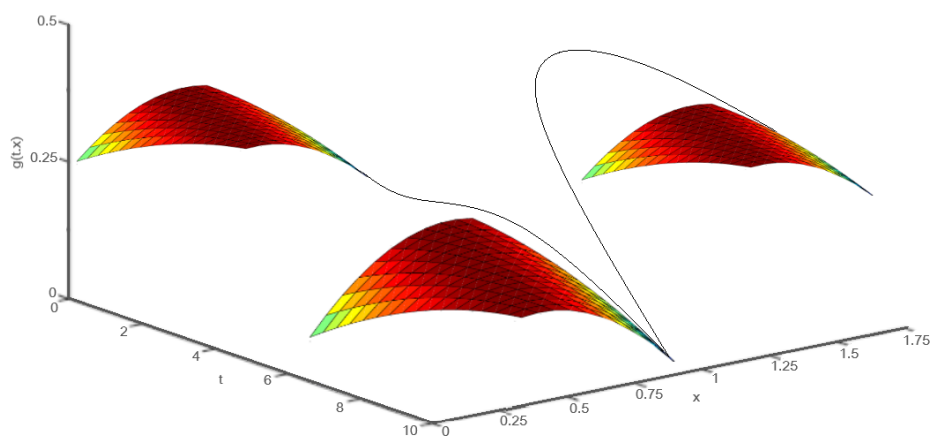


**Figure 9**: Three-dimensional representation of the solution $g(t, x)$ to model (35)–(36) when $g_0(x) = \frac{6}{10}\mathrm{e}^x$ and $\gamma = 0.85$. Here, the dynamic is involved in a self-organization process, which consists of getting a structure in which the initial object is replicated approximately exactly to itself or to a part of itself.
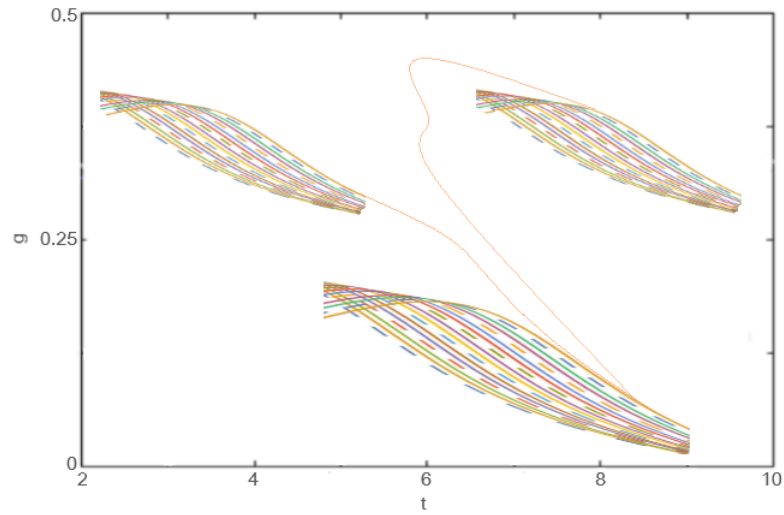
**Figure 10**: Two-dimensional representation of the solution $g(t, x)$ to model (35)–(36) when $g_0(x) = \frac{6}{10}e^x$ and $\gamma = 0.85$. Here, we can see the projection on the plan $(t, g)$ of the self-organization dynamic.
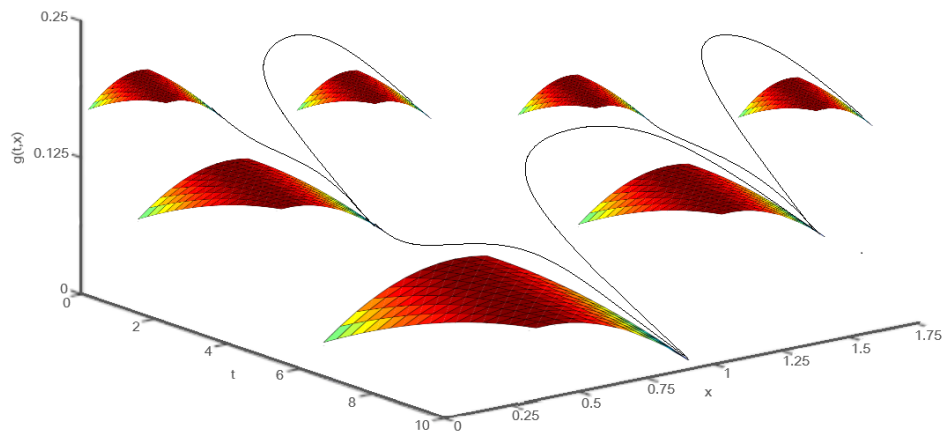


**Figure 11**: Three-dimensional representation of the solution $g(t, x)$ to model (35)–(36) when $g_0(x) = \frac{6}{10}e^x$ and $\gamma = 0.65$. Here, the self-organization dynamic is maintained and continues further, as it expands and multiplies in a similar way.
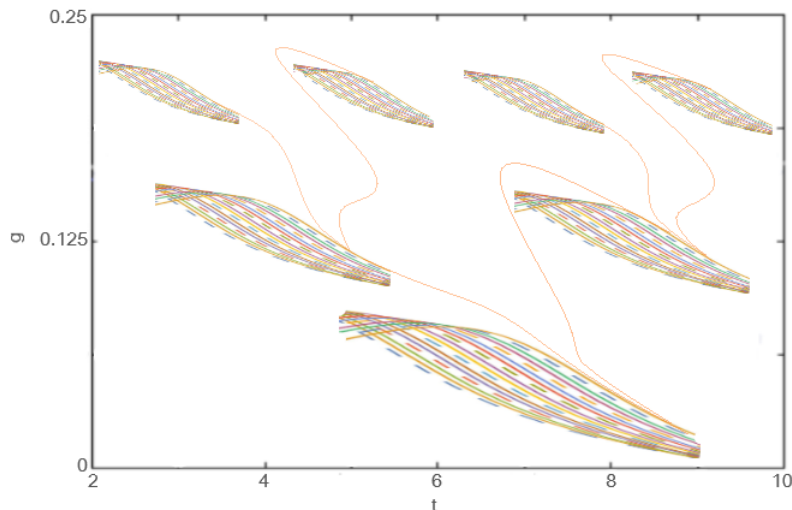
**Figure 12**: Two-dimensional representation of the solution $g(t, x)$ to model (35)–(36) when $g_0(x) = \frac{6}{10}e^x$ and $\gamma = 0.65$. Here, we can see the projection on the plan $(t, g)$ of the self-organization dynamic that is maintained and continues further, as it expands and multiplies.

## References

[1] E. F. Doungmo Goufo. Application of the Caputo-Fabrizio fractional derivative without singular kernel to Korteweg-de Vries-Burgers equation. *Mathematical Modelling and Analysis* **21** (2) (2016) 188–198.

[2] C. Rogers. The Harry Dym equation in 2+1 dimensions: A reciprocal link with the Kadomtsev-Petviashvili equation. *Physics Letters A* **120** (1) (1987) 15–18.

[3] E. Goufo, P. Tchepmo, Z. Ali and A. Kubeka. A comparative analysis of the Harry Dym model with and without singular kernel. *Journal Of Computational Analysis And Applications* **25** (2018) 228–240.

[4] D. Goufo, E. Franc and S. Kumar. Shallow water wave models with and without singular kernel: existence, uniqueness, and similarities. *Mathematical Problems in Engineering* **2017** (2017) 1–9.

[5] A. Yokuş and S. Gülbahar. Numerical solutions with linearization techniques of the fractional Harry Dym equation. *Applied Mathematics and Nonlinear Sciences* **4** (1) (2019) 35–42.

[6] F. Jarad, T. Abdeljawad and Z. Hammouch. On a class of ordinary differential equations in the frame of Atangana-Baleanu fractional derivative. *Chaos, Solitons & Fractals* **117** (2018) 16–20.

[7] J. Singh, D. Kumar and S. Kumar. An efficient computational method for local fractional transport equation occurring in fractal porous media. *Computational & Applied Mathematics* **39** (3) (2020).

[8] E. F. Doungmo Goufo. The Proto-Lorenz system in its chaotic fractional and fractal structure. *International Journal of Bifurcation and Chaos* **30** (12) (2020) P. 2050180.

[9] E. F. Doungmo Goufo. Solvability of chaotic fractional systems with 3D four-scroll attractors. *Chaos, Solitons & Fractals* **104** (2017) 443–451.

[10] P. Melby, N. Weber and A. Hübler. Dynamics of self-adjusting systems with noise. *Chaos: An Interdisciplinary Journal of Nonlinear Science* **15**(3) (2005) P. 033902.

[11] S. Hotton and J. Yoshimi. Extending dynamical systems theory to model embodied cognition. *Cognitive Science* **35** (3) (2011) 444–479.

[12] A. Kumar, S. Kumar and S.-P. Yan. Residual power series method for fractional diffusion equations. *Fundamenta Informaticae* **151** (1-4) (2017) 213–230.

[13] E. F. Doungmo Goufo. On chaotic models with hidden attractors in fractional calculus above power law. *Chaos, Solitons & Fractals* **127** (2019) 24–30.

[14] E. F. Doungmo Goufo and J. J. Nieto. Attractors for fractional differential problems of transition to turbulent flows. *Journal of Computational and Applied Mathematics* **339** (2018) 329–342.

[15] E. F. Doungmo Goufo, S. Kumar and S. Mugisha. Similarities in a fifth-order evolution equation with and with no singular kernel. *Chaos, Solitons & Fractals* **130** (2020) P. 109467.

[16] E. Babolian and A. Shahsavaran. Numerical solution of nonlinear fredholm integral equations of the second kind using Haar wavelets. *Journal of Computational and Applied Mathematics* **225**(1) (2009) 87–95.

[17] Ü. Lepik and H. Hein. *Haar Wavelets: With Applications* (Springer Science & Business Media, 2014).

[18] E. F. Doungmo Goufo. Mathematical analysis of peculiar behavior by chaotic, fractional and strange multiwing attractors. *International Journal of Bifurcation and Chaos* **28** (10) (2018) P. 1850125.

[19] M. Caputo. Linear models of dissipation whose Q is almost frequency independent–II. *Geophysical Journal International* **13** (5) (1967) 529–539; Reprinted in: Fract. Calc. Appl. Anal. **11** (1) (2008) 3–14.

[20] E. F. Doungmo Goufo. Application of the Caputo-Fabrizio fractional derivative without singular kernel to Korteweg-de Vries-Bergers equation. *Mathematical Modelling and Analysis* **21** (2) (2016) 188–198.

[21] S. Das. Convergence of Riemann-Liouvelli and Caputo derivative definitions for practical solution of fractional order differential equation. *International Journal of Applied Mathematics and Statistics* **23** (D11) (2011) 64–74.

[22] A. A. A. Kilbas, H. M. Srivastava and J. J. Trujillo. *Theory and Applications of Fractional Differential Equations*. Elsevier Science Limited, 2006.

[23] M. Caputo and M. Fabrizio. A new definition of fractional derivative without singular kernel. *Progr. Fract. Differ. Appl.* **1** (2) (2015) 1–13.

[24] EF. Doungmo Goufo and Y. Khan. A new auto-replication in systems of attractors with two and three merged basins of attraction via control. *Communications in Nonlinear Science and Numerical Simulation* **96** (2021).

[25] A. Atangana. Fractal-fractional differentiation and integration: Connecting fractal calculus and fractional calculus to predict complex system. *Chaos, Solitons & Fractals* **102** (2017) 396–406.

[26] E. F. Doungmo Goufo. Fractal and fractional dynamics for a 3D autonomous and two-wing smooth chaotic system. *Alexandria Engineering Journal* (2020).

[27] M. Razzaghi and S. Yousefi. The Legendre wavelet operational matrix of integration. *International Journal of Systems Science* **32** (4) (2001) 495–502.

[28] Y. Chen, X. Ke and Y. Wei. Numerical algorithm to solve system of nonlinear fractional differential equations based on wavelets method and the error analysis. *Applied Mathematics and Computation* **251** (2015) 475–488.

# A Modified Harmonic Balance Method for Solving Strongly Generalized Nonlinear Damped Forced Vibration Systems

M. Wali Ullah [1,2], M. Alhaz Uddin [1,*] and M. Saifur Rahman [3]

[1] *Department of Mathematics, Khulna University of Engineering & Technology, Khulna-9203, Bangladesh.*
[2] *Department of Computer Science & Engineering, Northern University of Business and Technology Khulna, Bangladesh.*
[3] *Department of Mathematics, Rajshahi University of Engineering & Technology Rajshahi-6205, Bangladesh.*

**Abstract:** A modified harmonic balance method is proposed for solving damped forced generalized nonlinear oscillators with strong nonlinearity. In the classical harmonic balance method, a set nonlinear algebraic equation of the unknown coefficients is solved by the numerical method to determine the unknown coefficients. However, in the present method, only one nonlinear equation and a set of linear algebraic equations are required for solution, thereby reducing the computational effort. Comparison between the results obtain by the proposed method and the numerical method is presented in figures which show a good agreement with the numerical results. The proposed method can play an important role for handling such nonlinear dynamical systems.

---

* Corresponding author: mailto:alhazuddin@math.kuet.ac.bd

## 1  Introduction

Nonlinear oscillators are very important in many areas of applied mathematics, physics, and engineering. Most of the physical problems are governed by the nonlinear differential equations. The exact solutions of these nonlinear equations are rarely obtained. Therefore, many researchers focused on analytical approximation methods. Among them, the perturbation method [1,2], homotopy analysis method [3,4], homotopy perturbation method [5–7], variational iteration technique [8,9], harmonic balance method (HBM)[10–13] are well known. The perturbation methods [14–20] are widely used techniques for dealing with the nonlinear differential systems and they were originally developed for weakly nonlinear dynamical systems. Jones [20] modified the perturbation method to extend the accuracy of the solution when the parameter was not small. Further, a modification of the Lindstedt-Poincare technique was presented by Cheung et al. [21] based on the Jones technique [20. The modified Lindstedt-Poincare method has been generalized by Alam, et al.[22] and it is applicable for a wide variety of nonlinear oscillators. The harmonic balance method (HBM) is another powerful technique to obtain the periodic solution of the nonlinear oscillators. According to this method, the solution is chosen as a truncated Fourier series. Usually, a set of strongly nonlinear algebraic equations appears among the unknown coefficients of several harmonic terms and these equations are solved by the numerical method. Further, this method has been modified by several researchers [23–28]. Rahman et al. [23] used a modified HBM to study the Van der Pol equation. Rahman and Lee [26] developed a modified residue HBM to handle nonlinear vibrating problems of beam. Wu [27] developed the harmonic balance method for the Yao-Cheng oscillator. Wagner and Lentz [28] developed a HBM to handle the Duffing oscillator with a forcing term with cubic nonlinearity. Younesian et al. [29] applied He's frequency-amplitude formulation and He's energy balance method to handle strongly nonlinear the generalized Duffing oscillators without forcing term. Uddin et al.[30] presented an analytical approximation technique for handling the generalized nonlinear Duffing equation with strong nonlinearity without external forcing term. Rafieipour et al. [31] developed an analytical approximate solution for the generalized nonlinear vibration of a micro electro mechanical system by using He's frequency amplitude formulation. Karahan and Pakdemirli [32] studied free and forced vibration response of the strongly nonlinear cubic-quintic Duffing oscillators by using the multiple time scale method. Ullah et al. [33] developed a modified harmonic balance method to handle nonlinear oscillators with cubic nonlinearity in the presence of external forcing term. Rahman et al. [34] presented a modified harmonic balance method to solve the nonlinear vibration problem of a beam resting on nonlinear foundation. Recently, Yeasmin et al. [35] have presented an analytical technique for handing the quadratic nonlinear oscillator based on the harmonic balance method for free vibration nonlinear problems. Cheib et al. [36] presented an analysis of the dynamics of a two-degree-of-freedom nonlinear mechanical system under harmonic excitation. It is noticed that the approximate analytical techniques for solving the damped forced generalized nonlinear oscillators with strong nonlinearity are almost untouched. To fill this gap, a modified harmonic balance method has been presented for handling strongly generalized nonlinear damped forced oscillators. The convenience of this method is that only one nonlinear algebraic equation and a set of linear algebraic equations are required to solve by the numerical method, which reduces the heavy computational effort that is required in classical harmonic balance methods. The obtained results are compared with the corresponding numerical results in graphs and it shows a

good agreement with these numerical results.

## 2   Method

Let us assume a strongly generalized nonlinear damped forced oscillator [29–33] of the form

$$\ddot{x} + \mu\dot{x} + \omega_0^2 x + \epsilon(\alpha_3 f_3(x) + \alpha_5 f_5(x) + ..... + \alpha_n f_n(x)) = E\cos(\omega t), \qquad (1)$$

where over-dots denote differentiation with respect to time $t$, $\omega_0$ is the natural frequency, $\mu$ is the linear damping coefficient, $f_i(x)$ are given general nonlinear functions of $x$, $\alpha_i$ $(i = 1, 3, 5, ...n)$ are constants, $\epsilon$ is a positive parameter which is not necessarily small, $E$ is the amplitude of the excitation force and $\omega$ is the forcing frequency. All of the parameters are positive. We assume that $\mu = 0$ in our idealized systems. But damped motion is important for most of the physical and engineering vibration problems. In this paper, we are going to assume that $\mu \neq 0$. This is a non-autonomous system since time $t$ explicitly appears in the right-hand side of the given equation. In particular, periodically forced harmonic oscillators depended explicitly on time $t$ and exhibited quite interesting behavior. When a damped Duffing-type oscillator is driven with a periodic forcing function, the result may be a periodic response at the same frequency as the forcing function. Since the unforced oscillation is the dissipated energy due to the damping, we are not surprised to find that it is absent from the steady state forced behavior. According to the proposed method, the approximate solution of Eq.(1) is assumed [33] in the following form:

$$x = a\cos(\omega t) + b\sin(\omega t) + a_3\cos(3\omega t) + b_3\sin(3\omega t) + ...., \qquad (2)$$

where $a$, $b$, $a_3, b_3...$ are the unknown coefficients. Now, differentiating Eq.(2) twice with respect to $t$ and then putting into Eq.(1) and expanding $f_i(x)$ as a truncated Fourier series expansion and taking the coefficients of equal harmonics from both sides, we obtain the following set of algebraic equations:

$$a(-\omega^2 + \omega_0^2) + b\mu\omega + \epsilon C_1(a, b, a_3, b_3, ...) = E, \qquad (3a)$$

$$a(-\omega^2 + \omega_0^2) - a\mu\omega + \epsilon S_1(a, b, a_3, b_3, ...) = 0, \qquad (3b)$$

$$a_3(-9\omega^2 + \omega_0^2) + 3b_3\mu\omega + \epsilon C_3(a, b, a_3, b_3, ...) = 0, \qquad (3c)$$

$$b_3(-9\omega^2 + \omega_0^2) - 3a_3\mu\omega + \epsilon S_3(a, b, a_3, b_3, ...) = 0. \qquad (3d)$$

Eliminating $\omega^2$ from the Eqs.(3b)-(3d) with the help of Eq.(3a), we get

$$\omega^2 = \omega_0^2 + b\mu\omega/a + \epsilon C_1(a, b, a_3, b_3, ...) - E/a, \qquad (4a)$$

$$-b^2\mu\omega/a - a\mu\omega - \epsilon bC_1(a, b, a_3, b_3, ...) + \epsilon S_1(a, b, a_3, b_3, ...) + bE/a = 0, \qquad (4b)$$

$$-8\omega_0^2 a_3 + 3b_3\mu\omega - 9a_3 b\mu\omega/a - 9\epsilon a_3 C_1(a, b, a_3, b_3, ...) + \epsilon C_3(a, b, a_3, b_3, ...) + 9a_3 E/a = 0, \qquad (4c)$$

$$-8\omega_0^2 b_3 - 3a_3\mu\omega - 9b_3 b\mu\omega/a - 9\epsilon b_3 C_1(a, b, a_3, b_3, ...) + \epsilon S_3(a, b, a_3, b_3, ...) + 9b_3 E/a = 0. \qquad (4d)$$

Now, using Eq.(4b), eliminating $\omega$ from the Eqs.(4c)-(4d) and taking only the linear terms of $a_3$, $b_3$ and neglecting the terms of insignificant effects, we obtain two linear equations for $a_3$ and $b_3$. From these equations $a_3$ and $b_3$ are determined. After putting

$a_3$ and $b_3$ into Eq.(4b), $b$ is expressed as a power series of small parameter $\lambda(\mu, \omega, E)$ in the following form:

$$b = m_0 + m_1\lambda + m_2\lambda^2 + m_3\lambda^3 + ..., \qquad (5)$$

where $m_0$, $m_1$, $m_2$ are the functions of $a$. Finally, after putting $a_3$, $b_3$ and $b$ into Eq.(4a) and then solving this equation, the values of $a$ are determined. Consequently, the desired values of $b$, $a_3$ and $b_3$ are calculated.

## 3   Example

Consider a generalized nonlinear (cubic-quintic) damped forced oscillator [29-33] of the following form:

$$\ddot{x} + \mu\dot{x} + x + \epsilon(\alpha_3 x^3 + \alpha_5 x^5) = E\cos(\omega t), \qquad (6)$$

where $\omega_0^2 = 1$. According to the truncated Fourier series, the solution of Eq.(6) is assumed as [33]

$$x = a\cos(\omega t) + b\sin(\omega t) + a_3\cos(3\omega t) + b_3\sin(3\omega t) + .... \qquad (7)$$

Putting Eq.(7) with its derivatives into Eq.(6) and then equating the coefficients of equal harmonics on both sides, we obtain

$$
\begin{aligned}
&16(a + b\mu\omega - a\omega^2) + 12\epsilon((a^2 - b^2)a_3 + 2aa_3^2 + a(a^2 + b^2 + 2bb_3 + 2b_3^2) \\
&+ 5\epsilon(6(a^2 - b^2)a_3^3 + 6aa_3^4 + 12aa_3^2(a^2 + b^2 + bb_3 + b_3^2) + a_3(5a^4 - 6a^2b^2 - 3b^4 \\
&+ 6(a^2 - b^2)b_3^2) + 2a((a^2 + b^2)^2 + 2(3a^2b + b^3)b_3 + 6(a^2 + b^2)b_3^2 + 6bb_3^3 \\
&+ 3b_3^4))\alpha_5 = 16E,
\end{aligned} \qquad (8a)
$$

$$
\begin{aligned}
&-16(a\mu\omega + b(-1 + \omega^2)) + 12\epsilon(b(a^2 + b^2) - 2aba_3 + 2ba_3^2 + (a^2 - b^2)b_3 + 2bb_3^2)\alpha_3 \\
&+ 5\epsilon(2b(a^2 + b^2)^2 - 12aba_3^3 + 6ba_3^4 + (3a^4 + 6a^2b^2 - 5b^4)b_3 + 12b(a^2 + b^2)b_3^2 \\
&+ 6(a^2 - b^2)b_3^3 + 6bb_3^4 - 4aba_3(a^2 + 3b^2 + 3b_3^2) + 6a_3^2(2b(a^2 + b^2) \\
&+ (a^2 - b^2)b_3 + 2bb_3^2))\alpha_5 = 0,
\end{aligned} \qquad (8b)
$$

$$
\begin{aligned}
&48\mu\omega b_3 + \epsilon(30a(a^2 - 3b^2)a_3^2\alpha_5 + 10a_3^5\alpha_5 + 10a(a^2 - 3b^2)b_3^2\alpha_5 + a(a^2 - 3b^2)(4\alpha_3 + \\
&5(a^2 + b^2)\alpha_5) + 4a_3^3((3\alpha_3 + 5(3(a^2 + b^2) + b_3^2)\alpha_5)) + 2a_3(8 - 72\omega^2 + 6\epsilon(2(a^2 + b^2) \\
&+ b_3^2)\alpha_3) + 5\epsilon(3(a^2 + b^2)^2 + (6a^2b - 2b^3)b_3 + 6(a^2 + b^2)b_3^4)\alpha_5) = 0,
\end{aligned} \qquad (8c)
$$

$$
\begin{aligned}
&10\epsilon a_3^4 b_3\alpha_5 + \epsilon(-30b(-3a^2 + b^2)b_3^2\alpha_5 + 10b_3^5\alpha_5 + 12b_3^3(\alpha_3 + 5(a^2 + b^2)\alpha_5)) \\
&- b(-3a^2 + b^2)(4\alpha_3 + 5(a^2 + b^2)\alpha_5)) + 2b_3(8 - 72\omega^2 + 12\epsilon(a^2 + b^2)\alpha_3 \\
&+ 15\epsilon(a^2 + b^2)^2\alpha_5) - 4a_3(12\mu\omega - 5\epsilon a(a^2 - 3b^2)b_3\alpha_5) + 2\epsilon a_3^2(-5b(-3a^2 + b^2)\alpha_5 \\
&+ 10b_3^3\alpha_5 + 6b_3(\alpha_3 + 5(a^2 + b^2)\alpha_5)) = 0.
\end{aligned} \qquad (8d)
$$

Eliminating $\omega^2$ from the Eqs.(8b)-(8d) with the help of Eq.(8a), and ignoring the terms whose responses are negligible, we obtain the following equations:

$$
\begin{aligned}
&-16(-bE + a^2\mu\omega + b^2\mu\omega) - 3\epsilon(ba_3(3a^2 - b^2)(4\alpha_3 + 5(a^2 + b^2)\alpha_5) \\
&- ab_3(a^2 - 3b^2)(4\alpha_3 + 5(a^2 + b^2)\alpha_5)) = 0,
\end{aligned} \qquad (9a)
$$

$$
\begin{aligned}
&- 4a_3(4(8a - 9E + 9b\mu\omega) + \epsilon a(21(a^2 + b^2)\alpha_3 + 15(a^2 + b^2)^2\alpha_5)) \\
&+ a(48\mu\omega b_3 + \epsilon a(a^2 - 3b^2)(4\alpha_3 + 5(a^2 + b^2)\alpha_5)) = 0,
\end{aligned}
\tag{9b}
$$

$$
\begin{aligned}
&- 48a\mu\omega a_3 + \epsilon ab(3a^2 + b^2)(4\alpha_3 + 5(a^2 + b^2)\alpha_5) - 4b_3(4(8a - 9E + 9b\mu\omega) \\
&+ \epsilon a((21(a^2 + b^2)\alpha_3 + 15(a^2 + b^2)\alpha_5)) = 0.
\end{aligned}
\tag{9c}
$$

Now, using Eq.(9b), eliminating $\omega$ from the Eqs.(9c) and (9d) and taking only the linear terms of $a_3$, $b_3$ and omitting the terms whose response is negligible, we obtain

$$
\begin{aligned}
&\epsilon a(a^4 - 2a^2b^2 - 3b^4)(4\alpha_3 + 5(a^2 + b^2)\alpha_5) - 4a_3(4(8a^2 + 8b^2 - 9aE) \\
&+ \epsilon(21(a^2 + b^2)^2\alpha_3 + 15(a^2 + b^2)^3\alpha_5)) = 0,
\end{aligned}
\tag{10a}
$$

$$
\begin{aligned}
&- \epsilon b(3a^4 + 2a^2b^2 - b^4)(4\alpha_3 + 5(a^2 + b^2)\alpha_5) + 4b_3(4(8a^2 + 8b^2 - 9aE) \\
&+ \epsilon(21(a^2 + b^2)^2\alpha_3 + 15(a^2 + b^2)^3\alpha_5)) = 0.
\end{aligned}
\tag{10b}
$$

After solving Eqs.(10a) and (10b), $a_3$ and $b_3$ are determined as follows:

$$
\begin{aligned}
a_3 &= \epsilon a(a^4 - 2a^2b^2 - 3b^4)(4\alpha_3 + 5(a^2 + b^2)\alpha_5) \\
&/4(4(8a^2 + 8b^2 - 9bE) + \epsilon(21(a^2 + b^2)^2)\alpha_3 + 15(a^2 + b^2)^3\alpha_5),
\end{aligned}
\tag{11a}
$$

$$
\begin{aligned}
b_3 &= \epsilon b(3a^4 + 2a^2b^2 - b^4)(4\alpha_3 + 5(a^2 + b^2)\alpha_5) \\
&/4(4(8a^2 + 8b^2 - 9bE) + \epsilon(21(a^2 + b^2)^2)\alpha_3 + 15(a^2 + b^2)^3\alpha_5).
\end{aligned}
\tag{11b}
$$

Inserting the values of $a_3$ and $b_3$ into Eq.(9a), we then expand $b$ in a power series of the small parameter $\lambda$ as follows:

$$
b = l_0 + l_1\lambda + l_2\lambda^2 + l_3\lambda^3 + ...,
\tag{12}
$$

where $\lambda = 2\mu\omega/E$, $l_0 = a^2\mu\omega/E$, $l_1 = a^4\mu^2\omega^2/E^2$, $l_2 = 2a^6\mu^3\omega^3/E^3$, .... Finally, upon inserting $a_3$, $b_3$ and $b$ into Eq.(8a) and solving, the values of $a$ are obtained. Consequently, the values $b$, $a_3$ and $b_3$ are determined.

## 4  Results and Discussion

The solutions determined by the present technique are compared with the corresponding numerical solution to justify the validity and the accuracy of the proposed technique. Comparisons between the solution curves obtained by the proposed method and a numerical method are shown graphically in Figures 1-4 in the presence of various damping and different values of the system parameters for strongly generalized nonlinear forced vibration problems.

From the figures, it is seen that the approximate results agree nicely with those solutions obtained by the numerical procedure.

## 5  Conclusion

In this study, a modified harmonic balance method is presented for handling strongly generalized nonlinear damped forced vibration problems. Some limitations of the classical HBM are overcome by the proposed method. The advantage of the present technique is that only one nonlinear algebraic equation is needed for solution. As a result, the computational effort is reduced and less effort is required than in the existing classical
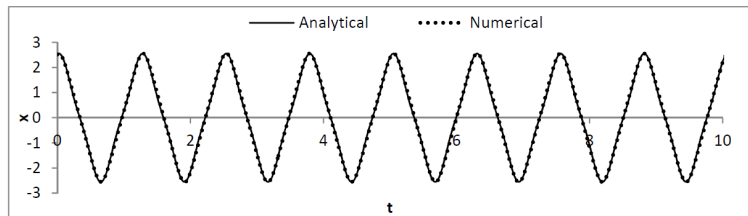
**Figure 1**: Comparison between the results obtained by the presented method and a numerical technique when $\omega = 5, \epsilon = 1.0, \alpha_3 = 1, \alpha_5 = 1, \mu = 0.1, E = 10$.
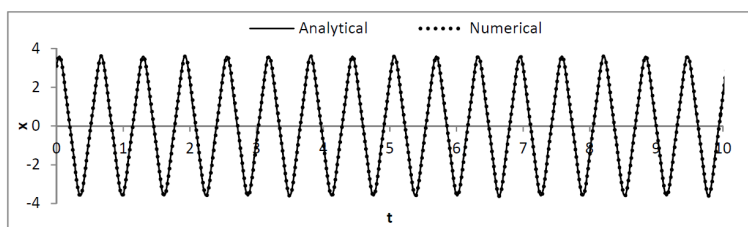


**Figure 2**: Comparison between the results obtained by the presented method and a numerical technique when $\omega = 10, \epsilon = 1.0, \alpha_3 = 1, \alpha_5 = 1, \mu = 0.25, E = 20$.
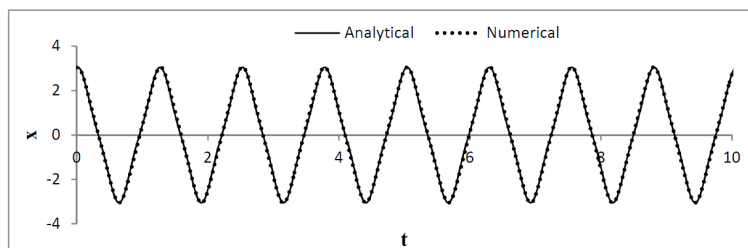


**Figure 3**: Comparison between the results obtained by the presented method and a numerical technique when $\omega = 5, \epsilon = 0.5, \alpha_3 = 1, \alpha_5 = 1, \mu = 0.05, E = 10$.
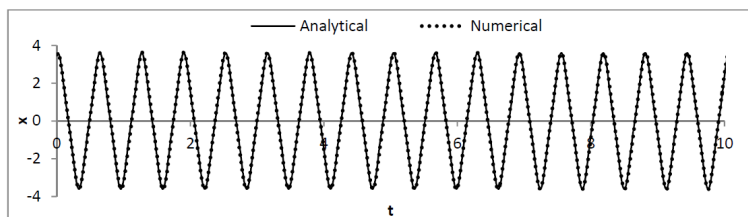


**Figure 4**: Comparison between the results obtained by the presented method and a numerical technique when $\omega = 10, \epsilon = 1.0, \alpha_3 = 1, \alpha_5 = 1, \mu = 0.1, E = 20$.

harmonic balance method. The results obtained by the present method show a good agreement with the numerical results. It is assumed that the proposed method is very effective and convenient for damped forced generalized nonlinear oscillators with strong as well as weak nonlinearities. Our results exhibit acceptable complaince with the solutions computed by the fourth order Runge-Kutta method for several values of systems parameters and significant damping.

## Acknowledgment

## References

[1] J. A. Wickert. Non-linear vibration of a traveling tensioned beam. *International Journal of Non-Linear Mechanics* **27** (1992) 503–517.

[2] A. H. Nayfeh. *Introduction to Perturbation Techniques*. Wiley, New York, 1981.

[3] M. Fooladi, S. R. Abaspour, A. Kimiaeifar and M. Rahimpour. On the analytical solution of Kirchhoff simplified Model for beam by using of homotopy analysis method. *World Applied Sciences Journal* **6** (2009) 297–302.

[4] S. J. Liao. *The proposed homotopy analysis technique for the solution of nonlinear problems*. Ph.D. Thesis, Shanghai Jiao Tong University, 1992.

[5] Y. Wu and J. H. He. Homotopy perturbation method for nonlinear oscillators with coordinate dependent mass. *Results in Physics* **10** (2018) 270–271.

[6] M. A. Uddin, M. A. Alom and M. W. Ullah. An analytical approximate technique for solving a certain type of fourth order strongly nonlinear oscillatory differential system with small damping. *Far East Journal of Mathematical Sciences* **67** (1) (2012) 59–72.

[7] C. U. Ghosh and M. A. Uddin. Analytical technique for damped nonlinear oscillators having generalized rational power restoring force. *Far East Journal of Mathematical Sciences* **130** (1) (2021) 25–41.

[8] M. A. Wazwaz. The variational iteration method: A reliable analytic tool for solving linear and nonlinear wave equations. *Computers and Mathematics with Applications* **54** (2007) 926–932.

[9] J. H. He. Some asymptotic methods for strongly nonlinear equations. *International Journal Modern Physics* **B 20** (2006) 1141–1199.

[10] R. E. Mickens. A generalization of the method of harmonic balance. *Journal of Sound and Vibration* **111** (1986) 515–518.

[11] K. Y. Sze, S. H. Chen and J. L. Huang. The incremental harmonic balance method for nonlinear vibration of axially moving beams. *Journal of Sound and Vibration* **281** (2005) 611–626.

[12] A. S. M. Z. Hasan, M. S. Rahman, Y. Y. Lee and A. Y. T. Leung. Multi-level residue harmonic balance solution for the nonlinear natural frequency of axially loaded beams with an internal hinge. *Mechanics of Advanced Materials and Structures* **24** (13) (2017) 1074–1085.

[13] Y. Y. Lee. Analytic solution for nonlinear multimode beam vibration using a modified harmonic balance approach and vietas substitution. *Shock and Vibration* (2016) Article ID: 3462643.

[14] A. H. Nayfeh. *Perturbation Method.* John Wiley and Sons, New York, 1973.

[15] A. H. Nayfeh and D.T. Mook.*Nonlinear oscillations.* John Wiley and Sons, New York, 1979.

[16] N. N. Krylov and N. N. Bogoliubov.*Introduction to Nonlinear Mechanics.* Princeton University Press, New Jersey, 1947.

[17] M. S. Alam. A unified Krylov-Bogoliubov-Mitropolskii method for solving nth order nonlinear systems. *Journal of the Franklin Institute* **399** (2) (2002) 239–248.

[18] M. S. Alam, M. A. K. Azad and M. A. Hoque. A general Struble's technique for solving an *nth* order weakly nonlinear differential system with damping. *International Journal of Nonlinear Mechanics* **41** (2006) 905–918.

[19] M. A. Razzak and M. H. U. Molla. A Simple Analytical Technique to Investigate Nonlinear Oscillations of an Elastic Two Degrees of Freedom Pendulum. *Nonlinear Dynamics and Systems Theory* **15** (4) (2015) 409–417.

[20] S. E. Jones. Remarks on the perturbation process for certain conservative systems. *International Journal of Non-Linear Mechanics* **13** (1978) 125–128.

[21] Y. K. Cheung, S. H. Chen and S. L. Lau. A modified Lindstedt-Poincare method for certain strongly nonlinear oscillators *International Journal of Non-Linear Mechanics* **26** (1991) 367–78.

[22] M. S. Alam, I. A. Yeasmin and M. S. Ahamed. Generalization of the modified Lindstedt-Poincare method for solving some strongly nonlinear oscillators. *Ain Shams Engineering Journal* **10** (1) (2019) 195–201.

[23] M. S. Rahman, M. E. Haque and S. S. Shanta. Harmonic balance solution of nonlinear differential equation (non-conservative). *Journal of Advances in Vibration Engineering* **9** (4) (2010) 345–356.

[24] S. L. Lau and Y. K. Cheung. Amplitude incremental variational principle for nonlinear structural vibrations. *Journal of Applied Mechanics* **48** (1981) 959–964.

[25] L. Azrar, R. Benamar and R. G. White. A semi-analytical approach to the nonlinear dynamic response problem of beams at large vibration amplitudes, Part II: multimode approach to the steady state forced periodic response. *Journal of Sound and Vibration* **255** (1) (2002) 1–4.

[26] M. S. Rahman and Y. Y. Lee. New modified multi-level residue harmonic balance method for solving nonlinearly vibrating double-beam problem. *Journal of Sound and Vibration* **6** (2017) 295–327.

[27] Y. Wu. The harmonic balance method for Yao-Cheng oscillator. *Journal of Low Frequency Noise Vibration and Active Control* **38** (2019) 1716–1718.

[28] U. V. Wagner and L. Lentz. On the detection of artifacts in harmonic balance solutions of nonlinear oscillators. *Applied Mathematical Modeling* **65** (2019) 408–414.

[29] D. Younesian, H. Askari, Z. Saadatnia and M. K. Yazdi. Frequency analysis of strongly nonlinear generalized Duffing oscillators using He's frequency amplitude formulation and He's energy balance method. *Computers and Mathematics with Applications* **59** (2010) 3222–3228.

[30] M. A. Uddin, M. W. Ullah and R. S. Bipasha. An approximate analytical technique for solving second order strongly nonlinear generalized Duffing equation with small damping. *Journal of Bangladesh Academy of Sciences* **39** (1) (2015) 103–114.

[31] H. Rafieipour, A. Lotfavar and A. Masroori. Analytical approximate solution for nonlinear vibration of microelectro mechanical system using He's frequency amplitude formulation. *IJST, Transactions of Mechanical Engineering* **37(M2)** (2013) 83–90.

[32] M. M. F. Karahan and M. Pakdemirli. Free and forced vibrations of the strongly nonlinear cubic-quintic Duffing oscillators.*Zeitschriftfr Naturforschung A* **72**(1) (2017) 59-69.

[33] M. W. Ullah, M. S. Rahman and M. A. Uddin. A modified harmonic balance method for solving forced vibration problems with strong nonlinearity.*Journal of Low Frequency Noise, Vibration and Active Control* **40(1)** (2021) DOI: 10.1177/1461348420923433.

[34] M. S. Rahman, A. S. M. Z. Hasan and I. A. Yeasmin. Modified multi-level residue harmonic balance method for solving nonlinear vibration problem of beam resting on nonlinear elastic foundation. *Journal of Applied and Computational Mechanics* **5** (4) (2019) 627–638.

[35] I. A. Yeasmin, N. Sharif, M. S. Rahman and M. S. Alam. Analytical technique for solving the quadratic nonlinear oscillator.*Results in Physics* **18** (2020) Article No. 103303.

[36] A. K. Cheib, V. E. Puzyrov and N. V. Savchenko. Analysis of the Dynamics of a Two-Degree-of-Freedom Nonlinear Mechanical System under Harmonic Excitation. *Nonlinear Dynamics and Systems Theory* **20** (2) (2020) 168–178.

# Contents of Volume 21, 2021

Volume 21                     Number 3                     2021

Volume 21                      Number 4                      2021

Volume 21                      Number 5                      2021